# Three Dimensional Optofluidic Devices for Manipulation of Particles and Cells

Anusha Keloth

A dissertation submitted for the degree of Doctor of Philosophy

School of Engineering and Physical Sciences

Heriot-Watt University

January 2017

# ABSTRACT

Optical forces offer a powerful tool for manipulating single cells noninvasively. Integration of optical functions within microfluidic devices provides a new freedom for manipulating and studying biological samples at the micro scale. In the pursuit to realise such microfluidic devices with integrated optical components, Ultrafast Laser Inscription (ULI) fabrication technology shows great potential. The uniqueness and versatility of the technique in rapid prototyping of 3D complex microfluidic and optical elements as well as the ability to perform one step integration of these elements provides exciting opportunities in fabricating novel devices for biophotonics applications. The work described in this thesis details the development of three dimensional optofluidic devices that can be used for biophotonics applications, in particular for performing cell manipulation and particle separation.

Firstly, the potential of optical forces to manipulate cells and particles in ULI microfluidic channels is investigated. The ability to controllably displace particles within a ULI microchannel using a waveguide positioned orthogonal to it is explored in detail. We then prototype a more complex 3D device with multiple functionalities in which a 3D optofluidic device containing a complex microchannel network and waveguides was used for further investigations into optical manipulation and particle separation. The microfluidic channel network and the waveguides within the device possess the capability to manipulate the injected sample fluid through hydrodynamic focusing and optically manipulate the individual particles, respectively. This geometry provided a more efficient way of investigating optical manipulation within the device. Finally, work towards developing a fully optimised 3D cell separator device is presented. Initial functional validation was performed by investigating the capability of the device to route particles through different outlet channels using optical forces. A proof of concept study demonstrates the potential of the device to use for cell separation based on the size of the cells. It was shown that both passive and active cell separation is possible using this device.

*To my parents and brother*

# Acknowledgments

Firstly, I would like to express my sincere gratitude to my PhD supervisors Dr. Lynn Paterson and Prof. Ajoy K. Kar for their guidance and constant support throughout my PhD. Their motivation and encouragement helped me in all time of research and writing of this thesis.

I also express my sincere thanks to Dr. Melanie Jimenez for helping me with many of the experiments in this thesis and for her valuable support and motivation. I would also like to thank the present and past members of Nonlinear Optics Group – Nitin, James, Mark, Adam, George, Fiona, Ashleigh, John and Graeme for all their support and help. In particular, Dr. Debaditya Choudhury for the training he provided me in ultrafast laser inscription and the insightful discussions throughout the duration of my studies.

I am also thankful to Prof. Gerard Markx, Jochen and Dr Michael Winson for their suggestions and valuable inputs.  I would also like to thank Judit, Krystena, Katarzyna and Allende for providing biological samples and Isabella for helping me with the tweezers experiment.

I am thankful to all my friends Rose, Rishad, Cristtel, Hari, Vikram, Nirosh, Ximing, Magda, Aurora, Gillian for their friendship and encouragement. Special thanks to Shraddha for being there always with a word of encouragement or listening ears. I would like to express my heartfelt thanks to Linda for her moral support and care throughout my stay in Edinburgh.

I would like to extend my thanks to my friends and family back home for all their support over the years. Last and most importantly I would like to thank my parents for their unconditional love and faith in me.

# Publications by the author

## Journal articles by the author

1. **A.Keloth**, M. Jimenez, A. K. Kar, and L. Paterson ''Particle separation in a 3D optofluidic device'', Under preparation.

2. **A.Keloth**, M. Jimenez, A. K. Kar, and L. Paterson ''Passive and active cell sorting in femtosecond laser fabricated 3D optofluidic device'', Under preparation.

## Conference papers and posters by the author

1. **A. Keloth**, M. Jimenez, L. Paterson, G. H. Markx and A. K. Kar "Femtosecond laser fabricated integrated chip for manipulation of single cells".Proc. SPIE Int. Soc. Opt 9705, Eng.Microfluidics, BioMEMS, and Medical Microsystems XIV, 97050K, doi:10.1117/12.2212719, 2016, Oral Presentation. Presented by A. K. Kar.

2. **A. Keloth**, L. Paterson, G. Markx & A. K. Kar, Three-dimensional optofluidic device for isolating microbes. Proc. SPIE Int. Soc. Opt. Eng.Microfluidics, BioMEMS, and Medical Microsystems XIII, 93200Z, DOI::10.1117/12.2078852, 2015, Oral Presentation.

3. **A. Keloth**, L. Paterson, G. H. Markx and A. K. Kar, ''Single microbial cell manipulation in a three dimensional microfluidic chip'' PIERS 2015, Prague 7th July 2015, Oral Presentation.

4. **A. Keloth**, L. Paterson, A.K. Kar, G. H. Markx "Isolation of single microorganisms using optical micromanipulation technology" Biophotonics: Tools and Techniques Meeting, Dundee September 2015, Poster presentation.

5. **A. Keloth**, M. Jimenez, L. Paterson, A.K. Kar, G. H. Markx "Manipulation of single cells in a femtosecond laser fabricated three dimensional microfluidic device". Advances in photonic tools and techniques for the life sciences, PHOTONEX 2015, Poster presentation.

# TABLE OF CONTENTS

# LISTS OF FIGURES

# LISTS OF ABBREVIATIONS

| | |
|---|---|
| ULI | Ultrafast Laser Inscription |
| OT | Optical Tweezer |
| 3D | Three Dimensional |
| 2D | Two Dimensional |
| PDMS | Polydimethylsiloxane |
| HF | Hydrofluoric Acid |
| TWG | Transverse Writing Geometry |
| LWG | Longitudinal Writing geometry |
| NA | Numerical Aperture |
| FACS | Fluorescence Activated Cell Sorter |
| NIR | Near Infrared |
| KOH | Potassium Hydroxide |
| PEEK | Polyetheretherketone |
| DI | Deionised |

# Chapter 1

# Introduction: Optical Manipulation in Optofluidic Devices

## 1.1   Introduction

Cells are the fundamental unit of all living organisms, capable of proliferating, differentiating and interacting with their micro environment or with other cells. Being the building blocks of life, the study of different structures and functions of cells is considered to be one of the most important areas of biological research. Cell based studies provide deep biological insight into understanding complex systems including tissues, organs and even complete organisms that are composed of cells. For a long time, it was assumed that no variability exists between individual cells of a particular type and was considered to be 'identical'. Based on this assumption, most cell based biological examination is performed on group of cells and the analysis is made taking an averaged response from the whole group of cell. However, evidences from the studies on behaviour of single cells, it has become clear that this assumption is incorrect and variability exists between individual cells of even same kind. Thus population based biological analysis could lead to misleading information as a consequence of the cell to cell variation [1]. This has put great attention on the study of individual cells that offers to overcome the fundamental limitations inherent in measurement of bulk cell population. An accurate and in-depth understanding of the cellular behaviour at single cell level provides scientific basis for cell biology, drug development and disease diagnostics.

Single cell based studies are of great importance in both eukaryotic and prokaryotic cellular research especially in cancer research, stem cell biology, marine microbiology and microbial biotechnology. Furthermore, single cell analysis is crucial for uncovering the biotechnological applications of marine microorganisms. Marine microorganism exists in huge numbers and presents an almost untapped resource for biotechnological application. However scientific knowledge on marine microbial diversity is limited because vast majority of these microorganisms are unidentified and are  considered as

'unculturable'[2]. One of the main reasons for the low rate of identification is the lack of efficient isolation techniques for isolating microorganisms. Conventional tools and methods for direct isolation of single cells are, on the whole, labour-intensive, time consuming and puts high demand on skills of the operator. Today, one of the main challenges faced by microbiologist is to develop strategies to isolate and cultivate the uncultured majority of microorganisms. There is thus a great demand for technologies that offers high through-put, enhance the speed, and accuracy of cell isolation. The greater demand for new and efficient isolation can only be expected to be met by tools that work at the same scale as cells, i.e. by using micromanipulation technologies. Single cell studies remains as a ''hot topic of research'' and more emphasis has now given for developing robust and high throughput techniques allowing single cell based studies.

## 1.2   Micromanipulation of cells in optofluidic devices

Manipulation of biological particles in small volumes of the order of micro and nanolitre has paramount importance in cell biology to better understanding living systems. One of the main challenges in cellular-based biological studies is to move, separate or perform the analysis on single cells without losing the viability and biological functionality of cells. To address these challenges and to have a detailed understanding of cell biology several micro-scale manipulation techniques has been developed [3].

The understanding of cellular structure and the path to observe smaller worlds was made possible by the invention of microscope. It was, Robert Hooke a Physicist and microscopist first coined the term cells in 1665, for describing the units in plants tissue as it appeared under the microscope.  The initial finding by Robert Hooke was then followed by other observations that provided a more clear definition, that cell is the structural and functional unit of life. With improved microscopic techniques by early 1900's, scientists were able to extract more internal details within the cells. At the earlier stage ultraviolet microscopes and phase contrast microscopes were developed and used for observing transparent biological particles and these microscopes were later commercialised. The advanced microscopic techniques and improved staining

techniques then offered more detailed analysis of cellular and intercellular processes and components at real time [4]. An example for this is fluorescence microscopy that has been widely used in the field of biology for studying the dynamic cellular events [5]. Sophisticated methods are still being developed in the field of microscopy for subcellular and cellular level studies. Light possess a passive role in these imaging techniques, providing invaluable information about the cellular processes at microscopic scale. Light has not only influenced imaging techniques, but also is used to manipulate objects at submicron scale by exerting controllable force on the object. The speculations about the concept of light exerting a pressure, was made by the famous astronomer Johannes Kepler, in 17th century [6]. He observed that the tail of a comet is pushed away from sun at all the time and he attributed this repulsion to some sort of solar pressure. Scientific developments over several years then proved that transfer of momentum from light to matter results in physical motion, giving theoretical confirmation to Kepler's observations on radiation pressure. These key observations opened up new possibilities for development of optical manipulation technology based on the concept that force exerted by light on particle can be used to manipulate the particle. The invention of lasers by the mid of 20th century stimulated the research in the field of optical manipulation technology allowing the non-invasive manipulation of microscopic particles. The pioneering work in the field of laser based optical manipulation was by Arthur Ashkin who demonstrated that a weakly focused laser beam is sufficient to move particle along the beam axis, and through the beam centre [7]. Later on, in 1987 Ashkin and his co-workers, demonstrated a single beam gradient force optical trap also called ''optical tweezers'' (OT) [8] and employed this in a wide range of experiments including manipulation of cold atoms, viruses and bacteria. These fundamental studies resulted in a rapid and consistent growth in the field of optical manipulation with a great impact in physics, chemistry and biology with its greatest use in biophysics.

In recent years, efforts have been focused on performing biological experiments with very small volume of samples of the order of microliters, for achieving high sensitivity, resolution and a better understanding of cellular processes. The emergence of a new field, Microfluidics in 1980's offered the potential to deal with microliter volumes of samples. The need for new instrumentation for performing analyte analysis at micron scale level attracted biologists' attention towards microfluidic-based research.

Microfluidic systems possess several advantages such as low sample volume usage (reducing the consumption of sample), short processing time, low cost and flexibility in design. In addition, several microfluidic systems can be processed in parallel resulting in high throughput and allows implementation of several functions on the same platform. The early stage applications of microfluidic systems were in molecular analysis, biodefence, molecular biology and microelectronics [9]. With the advance in fabrication technology, it became possible to fabricate microfluidic prototype devices capable of testing new ideas in short time scales and offered possibilities for the study of chemical, biological and physical cellular and molecular process. Various cell manipulation techniques can now be incorporated within microfluidic systems which has gained significant attention in cell biology studies, clinical research and biomedical engineering. The cell manipulation techniques that have been developed are based on applying forces to particles or cells in the microfluidic channels. These forces include optical, magnetic, electric and mechanical forces, possess the ability to precisely control and manipulate cells and analyse the information at single cell level [4].

Among the different manipulation techniques, optical-based methods enable precise control and manipulation of particles noninvasively without causing any contamination and thus they find wide use in manipulating biological species. Because of these advantages there is an increasing interest in applying optical forces for micromanipulation of small particles and cells in microfluidic devices. OT serves as a delicate optical tool for manipulating biological particles. Being a powerful micromanipulation tool, OT have been used for handling objects in microfluidic systems. With a great impact in biotechnological research, this has paved a way for the realisation of microfluidic cell sorters [10] and flow cytometers [11]. In spite of the advantages of OT, however, the use of OT with microfluidic systems presents some criticalities because of the bulk optical setup and complicated optical alignments. In addition to this, it requires labour intensive and time consuming procedure to localise individual cells. An immediate solution for overcoming these limitations is to combine the optical and microfluidic circuits with a fully integrated approach to develop optofluidic systems. 'Optofluidics' refers to a class of system synthesised by synergetic integration of optical and fluidic components into a single substrate. The term 'Optofluidics' was introduced in 2004, to represent a newly formed research initiative supported by the U.S Department of Defence [12]. Since then, optofluidics has emerged

as a rapidly growing field of research. A good understanding of fluid behaviour at the micron scale level and the compatibility of using fluids with optical devices has enabled the researcher's to generate new optofluidic devices that offers high efficiency, accuracy and improved sensitivity in measurements Optofluidics has evolved substantially in last few years with growing interest in inter- disciplinary research and application of photonic devices to the life sciences [12, 13]. With an increasing interest in single cell studies, optofluidics offers a unique platform for rapid, high throughput, non-contact single cell analysis under a controlled cellular microenvironment. The integration capability of optofluidic devices allows the realisation of compact multifunctional optofluidic systems as illustrated in figure1.1.
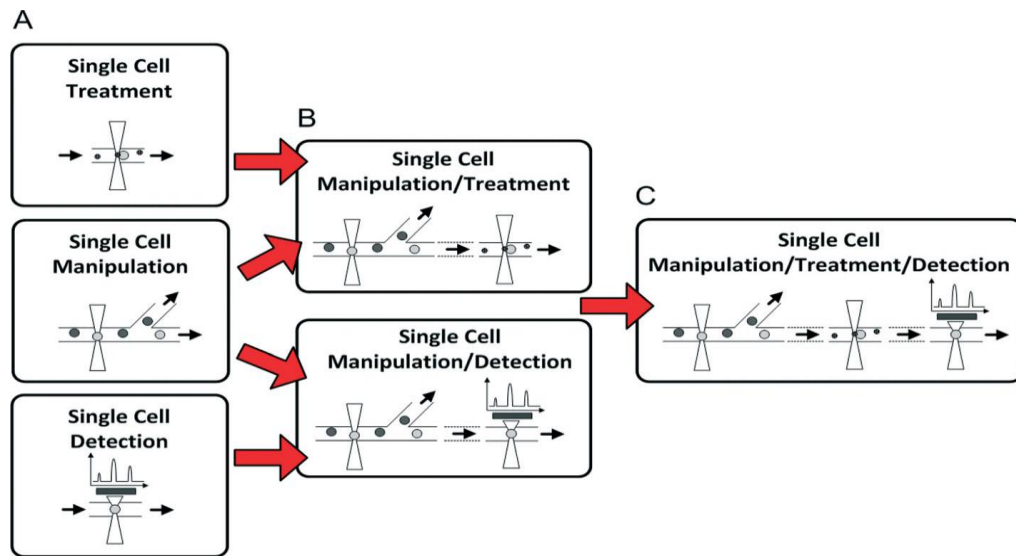


Figure 1.1 Optofluidic techniques for single-cell analysis. a) Single cell manipulation, treatment and detection performed in different devices. b) Microfluidic platforms integrate the single cell treatment or detection scheme after single cell manipulation. c) Microfluidic platforms capable of systematically performing single cell manipulation, treatment, and detection. Taken from [14].

The figure 1.1a represents three different optofluidic system for performing cell treatment, manipulation and detection. The figure 1.1b represents an integrated system capable of performing multiple functions such as manipulation and treatment or manipulation and detection in single system. Finally the figure 1.1c illustrates optofluidic platform with all the functionalities integrated in to it. The ability to precisely control and manipulate cells in conjunction with optical manipulation allows

performing cellular assays at single cell level. Thus optofluidics serves as a powerful tool for optical manipulation of biological particles.

## 1.3 Microfabrication of optofluidic devices

Optofluidic devices are commonly fabricated using microfluidic fabrication technology into which photonic components are embedded. Technological advances in device fabrication have made it possible to build miniaturised devices or chips with integrated multifunctional components in it. A wide variety of microfabrication techniques have been developed in past few decades, for improving chip functionalities, efficiencies and reducing the cost of production.

Early microfluidics systems were fabricated in glass and silicon using lithography. These techniques were derived from silicon microelectronics, which were well established in semiconductor industry. By early 1990s lithographic techniques were well developed, enabling fabrication of micron sized channel networks on the surface of silicon [15]. An efficient evolution in silicon-based fabrication technique offered the ability to fabricate monolithically integrated microsystems. However, some of the drawbacks such as optically opacity of devices, high cost of material and the requirement of clean room facilities preclude it from research requiring fast growth in prototyping and for use in biological or medical applications where optical interrogations are needed. In subsequent years a broad range of optofluidic device fabrication techniques have been developed, involving variety of process steps and materials. There has been a recent thrust in manufacturing microfluidic systems using polymeric materials, which can overcome the shortcomings of traditional microfabrication technology. Polymer material includes polydimethylsiloxane (PDMS), polymethylmethacrylate (PMMA), polycarbonate (PC) and polystyrene (PS). Amongst these, PDMS is the most widely used polymer material for fabricating microfluidic and optofluidic devices since PDMS can be cast against a suitable mould with high fidelity. In addition, they are optical transparent, the biocompatible material is inexpensive and the fabrication procedure is simple [16]. Development of soft lithography in PDMS was one of the most important contributions towards microfabrication technology. The technique has the capability for fabricating prototypes in a short period of time at low cost of fabrication [17]. Soft lithography technique has been increasingly used with PDMS for fabricating biochips because of these advantages and the simplicity. The

technique has been demonstrated to use for fabricating complex microstructures and optical components [18]. However, some of the drawbacks in devices containing microstructures and optical components include solubility in many common solvents, material damage upon tightly focussed irradiation and auto fluorescence at certain wavelengths. These drawbacks limit the use of polymeric materials for optofluidic applications [19]. Several other microfabrication techniques including micro-injection moulding, hot embossing and UV laser ablation with mask patterning have been explored over the past years in response to the demand to enhance the functionalities of the microfluidic devices [20]. These above mentioned techniques have been used on a wide range of materials, including semiconductors, polymers, glass and more recently paper [16], allowing production of complex microfluidic and optofluidic devices. However all of these techniques enable only fabrication of microstructures on the surface of the substrate and thus a subsequent bonding step is required to isolate the device features from the environment. The additional bonding step can cause imperfections that lead to leakage of liquid samples and clogging of the microchannel. Bonding issues become more severe when fabricating complex three dimensional (3D) structures, which involves stacking and bonding of multiple layers, since failure in one of the bonding layer affects the performance of whole device.

Over the past decade, a new fabrication technology has been developed based on the nonlinear interaction of femtosecond laser pulses with transparent material. The technique is referred to as Ultrafast Laser Inscription (ULI), which is capable of directly forming 3D microstructures and optical components within glass substrates. ULI involves irradiation of femtosecond laser pulses of the order ~ 50 fs to 500 fs within the bulk transparent material that result in localised modification of the material. The technique possesses the ability to alter the local refractive index of the material, allowing fabrication of optical waveguides [21] and other photonics components [22, 23]. The process also has the ability to selectively enhance the local chemical etching rate of the laser modified region, enabling the formation of 3D microfluidic structures [24]. In the recent past ULI has been widely used for fabrication and integration of optical and fluidic components into a single substrate. Femtosecond laser fabrication technology has proven to be a powerful tool for multifunctional integration in monolithic substrate for fabricating various optofluidic devices, in a single irradiation

step with subsequent chemical etching [25, 26]. The salient advantages of ULI over other established microfabrication techniques for fabricating optofluidic devices are; direct and easy integration of multifunctional components, enables rapid prototyping, provides higher accuracy, does not require clean room facilities for fabrication, it is a 3D direct writing technique and the technique offers great freedom of device design allowing realisation of novel geometries. These advantages have opened up new areas of research for fabricating optofluidic devices using ULI for biological or biomedical applications. The use of ULI for fabricating optofluidic devices has already proven to be successful in several bio-photonics applications, especially for single cell detection and analysis [27].

## 1.4    Femtosecond laser fabricated devices for manipulating cells

Conventional techniques for handling and sorting cells includes use of optical tweezers and FACS machines. Optical tweezers allows precise control and transportation of cells and FACS machines are widely used in biological research labs for high throughput cell sorting. Despite the advantages, these machines are bulky and need skilled operators to use them, limiting their use for several applications. The emergence of microfluidic research and the advent of cost effective fabrication techniques has allowed the realisation of microfluidic platforms with integrated functionalities capable of  handling and sorting cells.  The unique ability of femtosecond laser writing along with selective chemical etching to simultaneously create fluidic and optical functions into one single substrate has been utilized by several groups [28-30], and in this thesis, to fabricate various optofluidic devices for working with biological samples. This thesis presents different geometries of integrated optofluidic systems fabricated using ULI for manipulating particles and cells and presents a 3D optofluidic device which is capable of routing cells into required outlet when subjected to optical forces. The device presented promises to isolate cells with the precision of optical tweezers but with a higher throughput than tweezers. In addition, it allows us to work with smaller volumes of samples which is not possible with FACS machines. The following section discusses some examples of applications of ULI fabricated optofluidic devices used for single cell studies.

A simple example of monolithic integration of waveguides and a fluidic channel using ULI is a cell stretcher, fabricated in fused silica to use for optical trapping and stretching of single cells [29], as shown in figure 1.2. The device consists of a ULI-fabricated microfluidic channel with square cross section and optical waveguides that are positioned opposite to each other, orthogonal to the microfluidic channel. Waveguide writing and pre-etching irradiation was done in a single irradiation step, ensuring precise positioning of waveguides with respect to the channel. The monolithic chip is connected to the external fluidic circuit through capillary tubes and inscribed waveguides are coupled to a laser source using optical fibres.
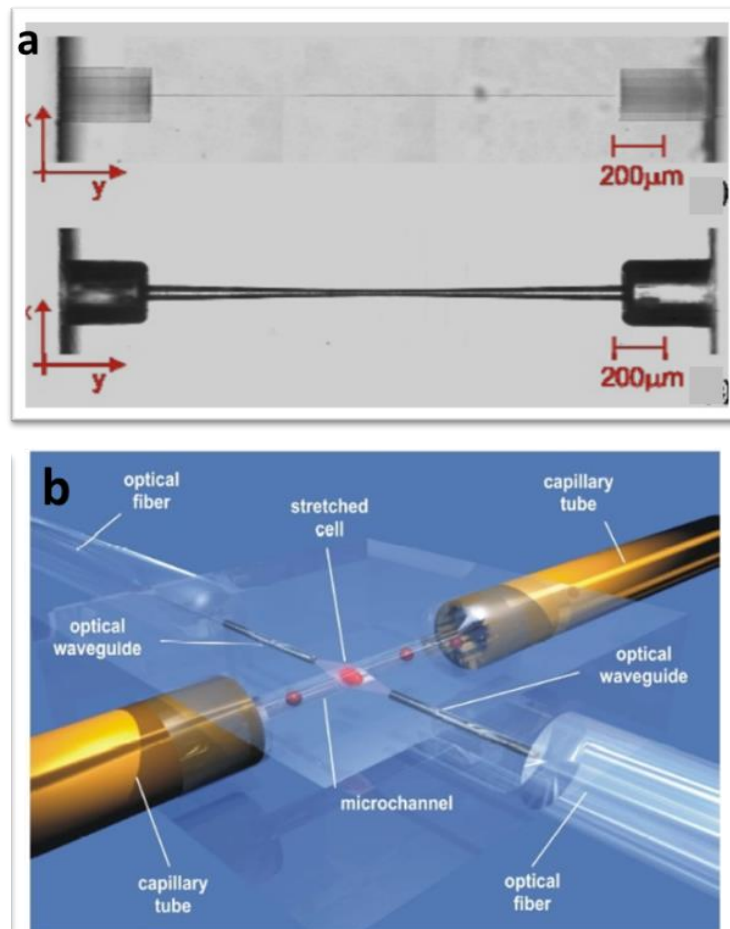


Figure 1.2 a) Picture of the fabricated microchannel after chemical etching b) 3D rendering of the monolithic optical stretcher fabricated by femtosecond laser micromachining. The cells flowing in the microchannel are trapped and stretched using the dual beam trap created by the optical waveguides. Connections to capillaries and optical fibres are also shown. Taken from [29].

The device functionality was experimentally tested by trapping and stretching red blood cells (RBCs) and was monitored using a transmission microscope. Optical trapping and stretching of RBCs are obtained by means of two counter propagating beams coming from two integrated optical waveguides orthogonal to the microfluidic channel, as shown in figure 1.2 b. Trapping and stretching were successfully achieved, with an increase in size up to 20% of its initial size. However, the curvature and roughness of the cells resulted in a limitation in the accurate analysis of cells.

Another effective application of optofluidic system is its use as cell sorter. A glass substrate based optofluidic device was successfully demonstrated to detect RBCs via two detection approaches [27]. The femtosecond laser processing is utilised to fabricate circular channels with a tapering cross section, with diameter tapering from ~100 µm at the entrance/exit ports and ~10 µm at the flow neck, as can be seen in figure 1.3. The tapering cross section of the channel ensures a uniform detection configuration for all cells. Transverse and longitudinal optical waveguides that are both parallel and normal to the top surface of the glass substrate are integrated in to the device, orthogonal to the microfluidic channel.

The optical detection of RBCs are performed via two methods, the first approach is a passive optic detection which involves sensing the intensity change of a waveguide-delivered He–Ne laser light (632.8 nm) induced by the refractive index difference caused by a cell flowing in the channel. The second approach is based on fluorescent emission detection, which involves detection of fluorescence emission from a dyed RBC excited by Ar laser light (488 nm) delivered by the optical waveguide. The fabricated optofluidic system was able to detect up to 23 particles per second, whereas commercial flow cytometers allows counting up to 1000 particles per second. Even though the operation range of this device is lower than commercial flow cytometers, it offers the potential to extend the range of counting efficiency by incorporating unique geometries, tuning of detection electric circuit and by particle speed calibration.
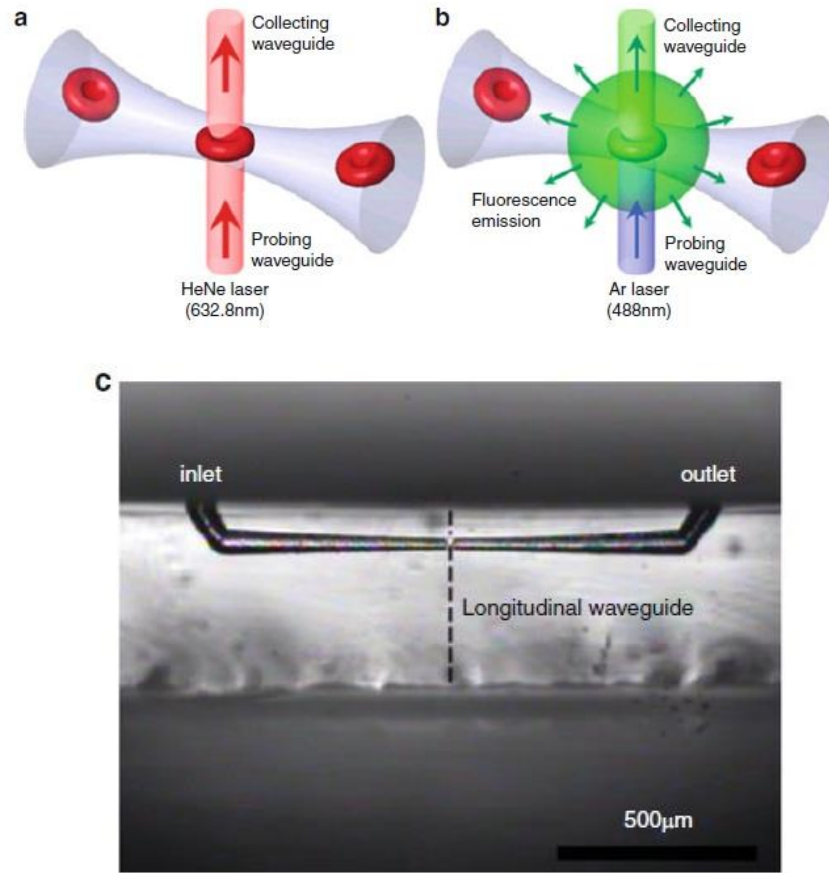
Figure 1.3 a) Schematic illustration of cell detection experiment using transmission intensity change and b) using fluorescence emission, c) Optical transmission image of an integrated optofluidic device fabricated for detecting single cells. Taken from [27].

A fully integrated fluorescence activated cell sorter fabricated using ULI microfabrication technology, which is capable of sorting single cells with optical forces, on the basis of their fluorescence has been demonstrated [28] . This device consists of two input channels merging at a central section, where the fluorescence investigations and sorting are performed, two output channels, and waveguides positioned orthogonal to the central section, as shown in figure 1.4.
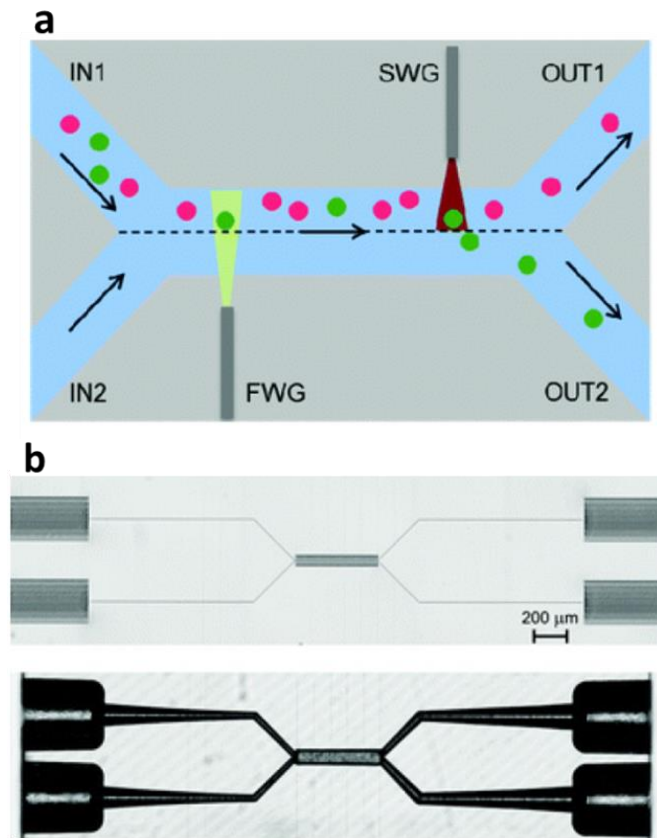
Figure 1.4 a) Schematic diagram of the cell sorting working principle. Green particles represent fluorescent ones, and red particles represent non fluorescent ones. FWG: 'fluorescence waveguide' used to excite the fluorescence of the flowing cells; SWG: 'sorting waveguide' used to apply the optical force during the sorting process, b) Microscope image of the femtosecond laser irradiation pattern to form the integrated optical sorter and c) Same structure shown in (b) after 5 h of chemical etching in 20% aqueous solution of HF. Taken from [28] .

The fluorescent marked cells flowing through the channel are excited using a fluorescent waveguides (FWG). The fluorescence signal is then used as a trigger to switch on an external laser source coupled to the sorting waveguide (SWG), so as to push the target cell in to the other half of the channel for collection. The fluorescence activated cell sorting capability of this device was used for sorting a cell sample constituted of human transformed fibroblast transfected with plasmid encoding the enhanced green fluorescent protein.

Most recently, femtosecond laser processing was exploited to fabricate complicated 3D microfluidic networks within a fused silica substrate. An example for this is the fabrication of a monolithic cell counter capable of 3D hydrodynamic focusing and high

efficiency cell counting [31]. The hydrodynamic focusing function of the device is implemented with the aid of a sheath flow, to confine the sample flow in to narrow stream as shown in figure 1.5a.
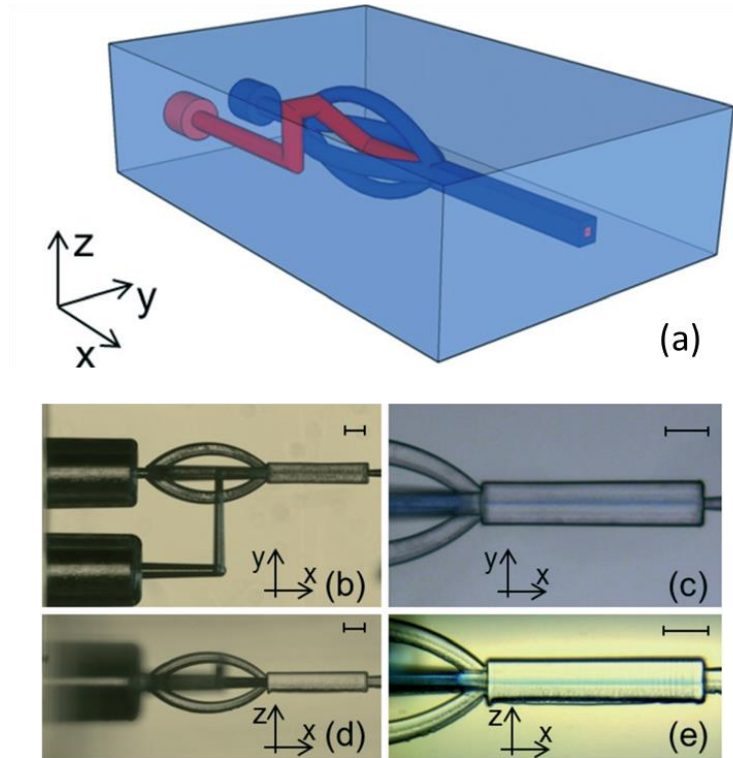


Figure 1.5 a) Schematic representation of 3D hydrodynamic focusing. Blue and red coloured channels represent the sheath and sample fluids flowing through the respective channels. b) Top and d) side microscope images of the fabricated device. c) Top and e) side views of the flow confinement in the horizontal and vertical directions achieved with a ratio between sample and sheath pressures of 0.55. Taken from [31].

The hydrodynamic focusing of sample flow in both vertical and horizontal plane was validated, and is as shown in figure 1.5c and e. The confined flow is visualised using blue coloured dye as the sample and distilled water as sheath flow. The minimum width of 10 µm for the confined flow was achieved in both horizontal and vertical directions, at a sample/sheath flow pressure ratio of 0.55. By further integration of optical waveguides into the system, a monolithic cell counter is constructed which is capable of counting up to 5000 particles per second. The combination of improved particle confinement in the detection region and integrated optical waveguides are highly desirable for single particle analysis, microfluidic flow cytometers and fluorescent activated cell sorting applications.

## 1.5   Thesis outline

The development of miniaturised, three dimensional optofluidic devices for achieving high efficiency manipulation of cells, thereby allowing to isolate, separate or sort cells at single cell resolution serves as the motivation of the work described in this thesis. The work presented in the thesis explores the versatility of ULI fabrication technology to develop novel optofluidic devices for fulfilling the goal of the work which could potentially be used in biological laboratories. Chapter 2 introduces the ULI fabrication technology. The materials and methods involved in fabricating and validating the optofluidic devices are detailed in chapter 3. Chapter 4 and 5 explain the progression in the development process towards the realisation of the high throughput optofluidic system. The chapters of this thesis are outlined as follows.

**Chapter 2** gives an introduction to technology of ultrafast laser inscription (ULI). The underlying nonlinear mechanism of ULI and consequent modification regimes are discussed.  The fabrication capability of ULI along with different inscription parameters for achieving high quality fabrication results are discussed in this chapter.

**Chapter 3** presents the materials and methods used for the experiments described in this thesis. The femtosecond laser inscription setup used for the fabrication of optofluidic devices in the subsequent chapters is detailed. The parameter consideration for achieving optimised values for writing waveguides and enhancing selective etching is detailed. The chapter also discusses the experimental setup used for performing different experiments with the optofluidic devices. The chapter also details the biological cells and other particles used as samples for the different experiments in this study.

**Chapter 4** gives an introduction on using optical force as a manipulation tool. Particle and cell manipulation in optofluidic device is investigated with detailed discussion on the device fabrication and validation process.  The first half of the chapter details the investigations on the potential of using optical scattering force to control and manipulate particles using simple optofluidic geometry. The second half of the chapter details a more complex 3D optofluidic device for particle manipulation. Novel geometric features of the device allows to hydrodynamically focus the particles and cells in to

narrow stream and optically manipulate the particle passing through the manipulation region within the device.

**Chapter 5** presents the work done toward developing a 3D optofluidic device that can be used for separating, sorting and isolating cells, exploring the versatility of ULI technology. The device design along with the fabrication and validation details is presented in this chapter. The potential of the device to route cells to required outlets by combining the hydrodynamic flow focussing and optical manipulation technique shows the capability of the proposed geometry to use as cell sorter.

**Chapter 6** discusses the conclusions achieved from the work presented in the thesis and the future scope of the work presented in this thesis.

## 1.6 Summary

Optofluidic systems create a powerful tool for manipulating and analysing single cells. The salient characteristics of ULI technology have proven it to be a powerful microfabrication technology for fabricating optofluidic devices enabling straightforward integration of fluidic and optical components. The work presented in this thesis explores the capabilities of ULI microfabrication technique to develop novel optofluidic devices for biophotonics applications, in particular for controllably manipulating particles and biological cells within these devices. The development of optofluidic devices incorporating different levels of complexity and demonstration of their functional validation form the main body of the work that will be described in this thesis.

# Chapter 2

# Ultrafast Laser Inscription

## 2.1 Introduction

The invention of the laser is marked as one of the greatest innovations in $20^{th}$ century. Since the demonstration of a working laser by Theodore Maiman [32] over 50 years ago, lasers have been widely used for scientific investigations as well as for industrial applications. The use of lasers for these applications is directly linked to the exceptional properties of laser light, which includes high spatial coherence, low divergence, variable interaction time defined by laser pulse duration and the availability of variety of laser operating at different wavelengths. The combination of all these properties makes laser an invaluable tool in a versatile range of different applications including laser material processing, optical communication and medical research.

The interaction of light with matter before the invention of laser was considered to be linear, with the optical properties of the material system remaining consistent in the presence of light. The invention of lasers however, enabled researchers to study the behaviour of light in optical material at higher irradiances. The observations have clearly demonstrated that the optical properties of material systems depend on the strength of the optical field in a nonlinear manner, giving rise to the field of nonlinear optics. The rapid development in the field of laser technology has led to the studies on different nonlinear phenomena of light matter interaction, many of which are eminently useful. Ultrafast Laser Inscription (ULI) is a technique that relies on such nonlinear phenomena of light matter interaction. One of the most impressive capabilities of ULI is that the nonlinear nature of interaction can lead to material modification, providing a new approach for local modification of transparent dielectrics through nonlinear optical processes.

Davis *et al*. [21], in 1996, demonstrated that by focusing femtosecond pulses within the bulk of transparent glass, refractive index change can be induced beneath the surface of

the substrate. Initial application of ULI was mainly focussed on fabricating devices for optical communication. A number of waveguide based devices including splitters [33], Bragg–waveguides [22] and couplers [23] have been fabricated using ULI. The new opportunities in microstructuring transparent material using ULI was later presented by Marcinkevicius *et al*. [24] by demonstrating the fabrication of microfluidic channel within fused silica by femtosecond laser irradiation followed by etching in hydrofluoric acid. This has broadened the scope of using ULI to fabricate three dimensional photonics devices. In particular, the potential of ULI to integrate optical and fluidic components within same substrate, in a single irradiation step, created new opportunities in the field of optofluidics for the realisation of new functionalities. The technique has now evolved as a powerful tool for fabricating photonics devices offering wide range of applications. This chapter introduces the ULI fabrication technology, including its underlying nonlinear energy transfer mechanism and different structural modification regimes. The fabrication capability of ULI and different inscription parameters for achieving high quality fabrication results are also discussed in this chapter.

## 2.2 Energy absorption mechanism in transparent media

In non-metallic material, at absolute zero, the highest occupied energy level (i.e. valence band) is separated by energy gap $E_g$ from the lowest occupied energy level (i.e. conduction band). If a single photon of light is to promote an electron from valence band to conduction band, the incident photon energy must exceed the band gap energy, $E_g$. However, the band gaps for most dielectric transparent materials are typically much larger than the energy of single photon from an infrared or visible source. Therefore the incident energy from a single photon is not sufficient to promote an electron from the valence band to the conduction band. In this case, nonlinear absorption processes are required to allow the interband transition of valence electrons, which is the key property of ULI. The underlying physical phenomena of ULI can be understood by analysing the absorption process of an intense laser pulse by dielectric transparent material.

To perform ULI, the substrate material and incident laser wavelength is chosen such that the photon energy is insufficient to promote valence electron to conduction band. Under these circumstances, laser radiation would travel through the material without

being absorbed. If, however, laser irradiation is sufficiently high, nonlinear absorption of incident photons occurs that in turn leads to material ionisation. The peak irradiance to cause such a nonlinear excitation process can be readily achieved by focusing laser pulses with ultrashort pulse duration. These nonlinear excitation mechanisms occur through, nonlinear photoionisation and avalanche ionisation [34, 35].

In nonlinear photoionisation, bound electrons are directly excited to the conduction band by nonlinear absorption of incident photons. Photoionisation can occur through two pathways depending on the laser frequency and intensity; multiphoton ionisation and/or tunnelling ionisation. Multiphoton Ionisation (MPI) occurs when multiple photons from the incident laser field are absorbed simultaneously by a single electron in the valence band, as shown in the figure 2.1a. In order to promote electrons from valence band to conduction band by MPI, the total energy absorbed by electrons from $n$ photons must exceed the bandgap energy $E_g$ i.e.

$$n\hbar v \geq E_g \qquad (2.1)$$

where $\hbar$ is Plank's constant and $v$ is the frequency of laser. MPI is dominant at higher laser frequency and low laser irradiance. The transition to the tunnelling ionisation regime takes place at high irradiances [36]. Ionisation in this case is determined by the electric field strength and is independent of laser radiation frequency.
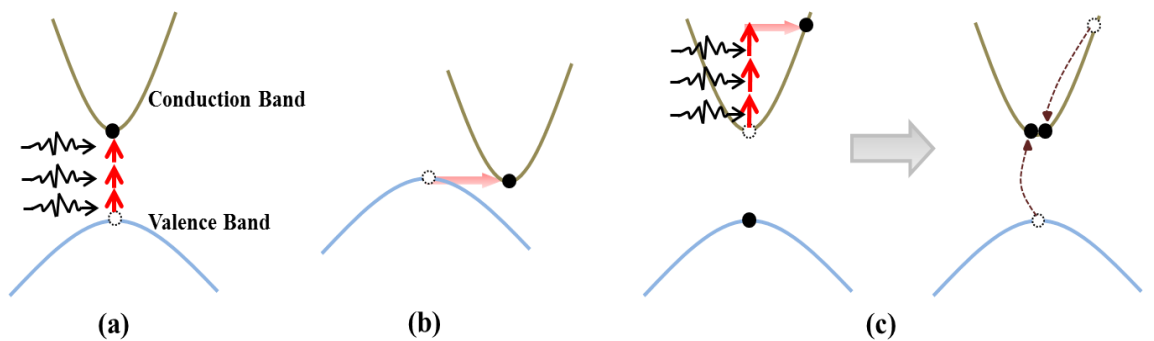


Figure 2.1 Nonlinear Excitation mechanism a) Multiphoton ionisation, b)Tunnelling Ionisation, c) Free carrier absorption followed by Impact Ionisation [37].

The strong field distorts the band structure, reducing the potential barrier between the conduction and valence band, resulting in direct transition of electrons from the valence band to conduction band through quantum tunnelling, as depicted in figure 2.1b. The theoretical outline for the probabilities of occurrence of multiphoton ionisation and tunnelling ionisation was provided in 1965 by Keldysh [36]. The transition between the processes was described in terms of Keldysh parameter, $\gamma$ given by

$$\gamma = \frac{\omega}{e} \sqrt{\frac{m_e c n \epsilon_0 E_g}{I}} \qquad (2.2)$$

where $\omega$ is the laser frequency, $e$ is the fundamental electron charge, $m_e$ is the effective electron mass, $c$ is the speed of light, $n$ is the linear refractive index, $\epsilon_0$ is the permittivity of free space, $I$ is the laser irradiance at the focus and $E_g$ is the bandgap energy. The photoionisation is a multiphoton process for $\gamma > 1.5$ and tunnelling process for $\gamma < 1.5$. For $\gamma \sim 1.5$, an intermediate regime exists which is a combination of multiphoton and tunnelling ionisation.

Depending on the incident laser frequency and irradiance, valence electrons are initially excited to the conduction band through photoionisation. At higher irradiances, an electron already present in the conduction band absorbs photons linearly, moving to higher energy states in the conduction band, as shown in figure 2.1c. After subsequent absorption of photons until the energy exceeds the conduction band minimum by more than the band gap energy, the electron can then collisionally ionise another bound electron in the valence band. The collisional ionisation thus results in two electrons in the conduction band minimum as shown in the figure 2.1c. These two electrons can then undergo free carrier absorption and impact ionisation and the process can repeat causing the increase in electron density in conduction band, under the presence of laser field. This process is referred to as avalanche ionisation. The initial seed electrons required for triggering the avalanche ionisation process are provided by thermally excited impurities or defect states, or by direct photoionisation [35]. When the density of electrons in the conduction band reaches about $10^{29}$ m$^{-3}$ through avalanche ionisation, the electrons behave as plasma with a frequency that is resonant with the laser leading to strong

absorption of incident photons [38]. At this critical density the optical break down is assumed to occur in the material.

## 2.3  Energy Transfer and Damage Mechanism

Following the initial generation of free electron plasma through nonlinear absorption, the deposited energy is transferred to the lattice through electron phonon coupling, leading to permanent modification of the focal volume of the material. The mechanism that leads to the structural change in the material largely depends on the pulse duration of the incident laser. The material damage caused by femtosecond (fs) laser pulses is different from that caused by pulses of picosecond (ps) duration [38]. For longer laser pulses with pulse durations ranging from picosecond (ps) to nanosecond (ns), energy transfer from electrons to the lattice occurs on the time scale of the pulse duration. Thermal effects become more predominant at this time scale and energy is transferred to the lattice through thermal diffusion. The peak irradiance for longer laser pulses is too low to allow multiphoton ionisation/tunnelling ionisation. The avalanche ionisation process is thus seeded by impurities and defect states present in the focal volume of the laser. A small fluctuation in the number of seed electrons present at the focal volume strongly affects the breakdown process [35]. This dependence of defects and impurities makes the ps laser pulse interaction with the dielectric a non-deterministic process.

On the other hand, for shorter pulses of fs timescale, the nonlinear absorption takes place on a time scale shorter than time taken to transfer energy to the material lattice via electron phonon coupling [34]. For fs laser pulses the peak irradiances are much higher and multiphoton/tunnelling ionisation becomes significant. When the incident laser irradiance exceeds a given threshold, some free electrons are generated in the focal volume by these mechanisms. These electrons act as a seed, for the avalanche ionisation process, resulting in an increase of electron density until the plasma frequency approaches the laser frequency, at which point the material becomes strongly absorbing. The breakdown process in this case is less dependent on the defect in the material, resulting in a deterministic breakdown process [35]. It is therefore clear that fs laser processing allows deposition of energy in a very controlled and deterministic way in the bulk of a material allowing high quality microfabrication.

## 2.4 Fundamental morphology of modification

In 1996 Davis *et al.* [21] demonstrated the ability to induce refractive index changes in glass by focussed femtosecond laser, which opened new possibility of using ULI for writing three dimensional optical circuits in bulk glasses. Later, several studies showed that morphological changes can be induced in the transparent material by femtosecond laser pulses followed by nonlinear absorption and energy transfer to the lattice. The physical mechanism, after energy transfer leading, to structural change of the material is not fully understood. The resulting morphological changes may depend on exposure parameters and material properties. Different exposure parameters include pulse energy, pulse duration, repetition rate and wavelength of the incident laser, and material properties include bandgap, and thermal conductivity of the material. The three regimes of laser induced modification are shown in figure 2.2.
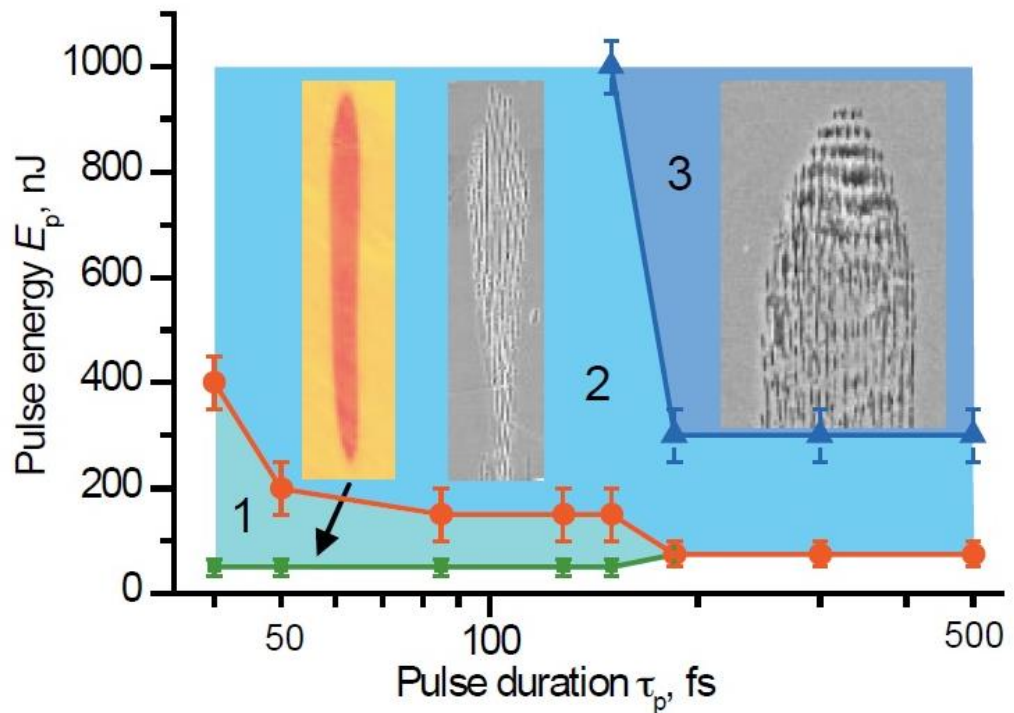


Figure 2.2 Plot of pulse energy versus pulse duration defining three regimes of modification using a NA = 0.65 microscope objective. Regime 1 produces isotropic modification, Regime 2 nanogratings (SEM insert) and Regime 3– complex disrupted region interconnected with nanocracks in the top portion of the modified region (SEM insert). Taken from [39].

Three different kinds of structural changes have been induced in the bulk of material as a result of femtosecond laser material interaction: a) a homogenous modification resulting in refractive index change [21, 40], b) formation of nanograting [41, 42], c) a disruptive modification resulting in the formation of voids [43]. For fused silica, the most interesting material for optofluidic applications, these three modifications can be observed by simply changing the incident laser energy [44]. The three regimes of modification produced in fused silica when interacting with focused femtosecond laser pulses is discussed in the next section.

### 2.4.1    Regime 1: Isotropic refractive index change

At pulse energies slightly above the modification threshold of the material a homogeneous modification in the structure is observed, which is characterised by a similar variation in the refractive index of the material across the modified region. This regime of modification is particularly suitable for waveguide fabrication. The physical origin of such laser induced homogeneous structural changes in the material is not fully understood, however several arguments explaining the underlying mechanism have been proposed over years.

A first possible mechanism for causing an isotropic change in refractive index is thermally induced material densification [45]. In fused silica, density increases when the material is rapidly cooled from high temperatures [46]. Therefore increase in density and change in refractive index at the focal volume is attributed to the local heating at the focal spot followed by quick quenching. Another possible mechanism for laser induced refractive index change is through the formation of colour centres [47]. Several spectroscopic analyses have been performed to study the changes in the molecular structure and formation of colour centres within femtosecond laser irradiated regions. Although the formation of colour centres have been observed in glasses within a femtosecond laser irradiated region, there is no experimental evidence to show a strong correlation between colour centre formation and the induced refractive index change [48]. A third possible mechanism leading to the change in refractive index is through direct photo structural change induced by the femtosecond laser pulses, in which case the density at the focal volume increase due to the rearrangement of the network of chemical bonds [45]. The contribution from the three mechanisms discussed above for

inducing smooth change of refractive index varies with depending on the composition of glass and the femtosecond laser exposure conditions [49], which add complexities to the existing postulates. Therefore, a complete understanding of refractive index modification is not yet achieved.

### 2.4.2 Regime 2: Formation of nanogratings

At a moderate value of laser pulse energy, higher than the value for creating smooth refractive index modification, periodic and self-organised nanograting structures are observed [42]. The first indications of the existence of birefringent refractive index in glass was from the observations on the anisotropic light scattering in femtosecond laser irradiated Ge-doped silica glass as reported by Kazansky *et al.* [50]. In the same year Sudrie *et al.* [41] reported that permanent anisotropic changes of refractive index can be inscribed in fused silica irradiating with femtosecond laser. The occurrence of birefringence was attributed to the formation of self-organised periodic nanograting structures. The formation of these nanogratings were initially interpreted in terms of interference between the incident light field and the electric field of the electron plasma wave. This interference leads to periodic modulation of electron plasma concentration and the structural changes in glass. [51]. In 2006, Taylor *et al.* [52] reported that these periodic nanostructures are found to orient in direction perpendicular to the writing laser polarisation and are separated by $\lambda/2n$, where $\lambda$ is the wavelength of incident laser and $n$ is the refractive index of the medium. Figure 2.3 shows the images to show the evidence of self-organised periodic nanostructures.
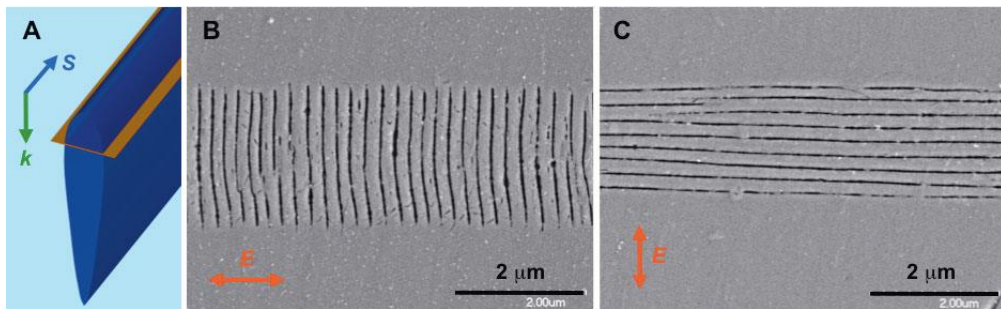


Figure 2.3   SEM images of self-organized periodic nanoplanes. A) Transverse writing direction, k is light propagation direction and s is the writing direction. B) Electric field, E is parallel to writing direction, S. C) E is perpendicular to S. Nominal separation of the grating planes is 250 nm. Taken from [39].

The relative constant spacing between the nanostructures implies a self-replicating phenomenon underlying the nanostructure formation. The orientation of the periodic nanostructures can be optically controlled by changing the angle between electric field vector of the linearly polarised laser beam and the writing direction.

A second postulate explains the formation and orientation of nanostructures in terms of local field enhancements. When femtosecond laser pulses of peak irradiances are focussed inside the bulk material, it leads to plasma formation through multiphotoionisation. Any inhomogeneity in the plasma formation will lead to local field enhancements, resulting in the formation of nanoplasma. The nanoplasmas then lead to the structural changes that are embossed in the material [52]. The physical mechanism underlying nanoplasma formation is based on the transient nanoplasmonic model. Figure 2.4 represents the formation of self-aligned nanoplanes.
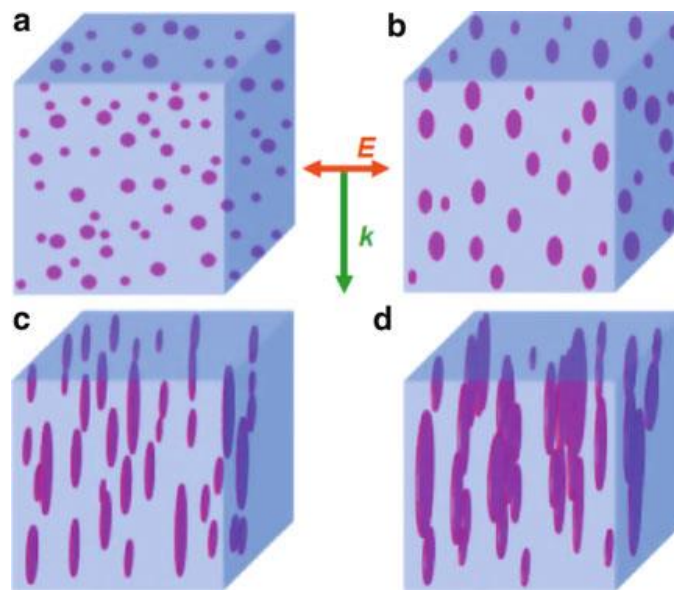


Figure 2.4 Pictorial representation of the evolution of nanoplasmas into nanoplanes explaining the formation of nanoplanes aligned perpendicular to the writing direction. Taken from [39].

After irradiation with ultrashort pulses, hot spots as shown in figure 2.4a, are produced at the focal volume due to the localised inhomogeneous nonlinear multiphoton absorption process. These hot spots can evolve in to spherically shaped nanoplasmas, as depicted in figure 2.4b over several laser pulses due to a memory effect [53]. The existence of memory in the material could arise from defects present in the material or

colour centres. This memory effect can lead to lowering of the bandgap energy which helps to ionise the material on next laser pulse. An asymmetric growth of spherically shaped plasma occurs in a direction perpendicular to the laser polarisation due to the field enhancement at the boundary of plasma, leading to the formation of ellipsoidal shaped plasma as shown in figure 2.4c, and finally grows in to nanoplanes as shown in figure 2.4d.

As mentioned above, it was shown that orientation of these periodic nanoplanes can be controlled optically by changing the angle between the electric field vector of the incident laser beam and writing direction. Preferential hydrofluoric (HF) etching was observed across these laser written tracks, when polarization is perpendicular to the writing direction [54]. This is because nanogratings are formed parallel to the writing directions allowing the HF acid to diffuse easily into the track. The nanogratings formed in the femtosecond laser modified zone in fused silica exhibits high etching selectivity compared to the unmodified region, which is a key parameter determining the potential to fabricate high aspect ratio microchannels for optofluidic applications.

### 2.4.3    Regime 3: Formation of voids

When the incident laser energy is even higher than that needed for formation of nanogratings, disruptive modification occurs resulting in creation of voids. The likely mechanism for creation of voids is attributed to microexplosions that occur inside the material. Energy from the incident femtosecond laser transfers to the material though nonlinear photoionisation. At peak irradiances, the energy deposition creates high temperature and pressure at the focal volume leading to ejection of material from centre and forced into the surroundings. This results in the formation of structures consisting of voids [55]. Such voids can be served as 3D optical memories as shown in the figure 2.5 and photonics crystal structures [56].
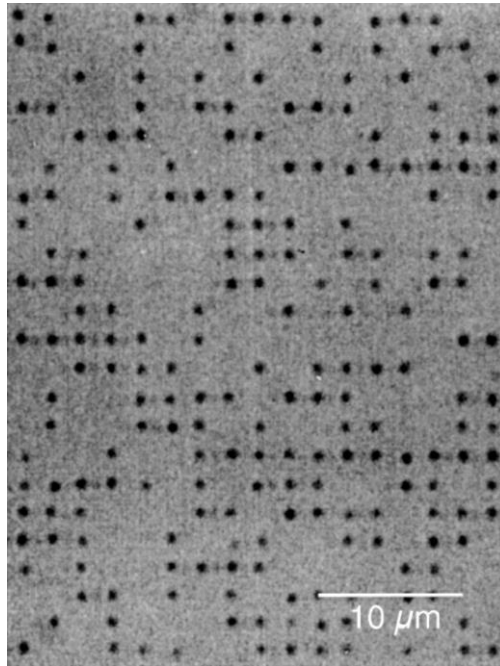
Figure 2.5 Binary data pattern stored inside fused silica with 2 µm bit spacing, photographed with an optical microscope using transmitted light. Taken from [55].

## 2.5 Control parameters of ULI process

The preceding sections discussed in this chapter highlight the potential of ULI in fabricating photonic and fluidic components by inducing a variety of structural modifications inside a transparent material. Optimal fabrication of these components can be achieved by control of a variety of inscription parameters associated with the inscription laser as well as exposure conditions. A desired high-quality laser micro processing result for specific materials can be achieved by choosing the correct laser operating parameters. A brief explanation of the key parameters that must be considered throughout the fabrication process is discussed in the following section.

### 2.5.1 Laser parameters

Different laser parameters associated with femtosecond laser processing includes laser pulse wavelength, laser energy, pulse repetition rate, translation speed, pulse duration, and focusing optics.

*Pulse Wavelength*

The pulse wavelength of the inscription laser determines the order of multiphoton process in femtosecond laser processing. The number of photons required to overcome the bandgap of the substrate material for efficient energy deposition has a direct dependence on the laser wavelength for each target substrate.

*Pulse Energy*

The incident laser pulse energy is another key laser parameter, as it directly determines the amount of energy deposited at the focal volume. A detailed discussion of different modification regimes in fused silica formed with varying the energy of the incident fs laser pulses was discussed in section 2.4. Control of the incident laser pulse energy enables the desired material modification.

*Pulse Repetition Rate*

The pulse repetition rate of the incident laser has direct influence on the heat accumulation process and thus is one of the most important laser parameters. For relatively low laser repetition rate, each pulse interacts with cold material. In this regime, the spatial distribution of the modified region is mostly defined by the spatial distribution of plasma induced by each pulse and the effect of heat dissipation out of the focal volume is negligible. For higher repetition rates heat accumulation and dissipation plays a key role in defining the spatial distribution of the modified region [57]. In this regime, the second pulse is incident before heat absorbed from the first pulse diffuses away, resulting in accumulation of heat at the focal volume. The material undergoes melting as long as the pulses arrive. Once the series of pulses have left the focal volume, heat diffuses out of the focal region equally in all directions. This causes an increase in the size of the modified region, with a more symmetric cross section. Therefore heat accumulation and diffusion plays a crucial role in determining the cross section of the modified region [58].

*Pulse duration*

The pulse duration of the incident laser beam also influences the material modification in femtosecond laser processing. A detailed discussion on effect of pulse duration on material modification is given in section 2.3. The pulse duration directly determines the

coupling of electron energy to the surrounding lattice. The selection of pulse duration of the inscription laser depends on the nonlinearity of the material. For materials with nonlinear refractive index $n_2$ value similar to fused silica, ultrashort laser pulses of width ~hundred fs are optimal for inducing homogenous refractive index and nanogratings.  In contrast to this, in highly nonlinear material that exhibit nonlinear effects such as self-focusing and filamentation, it is shown that laser pulses above ~1ps are needed for inducing refractive index change [59]. The use of longer pulses helps in reducing the peak power for a given pulse energy, thereby avoiding any detrimental nonlinear affects that cause degradation in energy deposition.

### 2.5.2    *Other Exposure Parameters*

*Substrate Translation Velocity*

The velocity at which the substrate is translated is used to alter the laser fluence falling on the substrate, while keeping the pulse energy the same. By increasing the translation speed, the amount of pulse energy deposited at the focal volume decreases, thereby affecting the induced modification. In the single pulse regime, the laser-induced refractive index changes can be controlled via the pulse energy and translation speed. However at high repetition rates, it gets more complex due to thermal accumulation and diffusion effects [60, 61].

*Writing Geometry*

The direction of translation of substrate plays a key role in femtosecond laser processing. The substrate can be translated either along or transverse to the direction of propagation of the writing laser, known as longitudinal and transverse writing geometries respectively, as shown in figure 2.6. The longitudinal writing geometry (LWG), allows writing structures and waveguides with symmetric cross section inherently circular due to the transverse symmetry of the Gaussian beam profile. But the maximum length of the structures and waveguides that can be inscribed with LWG is limited by the working distance of the focusing lens.
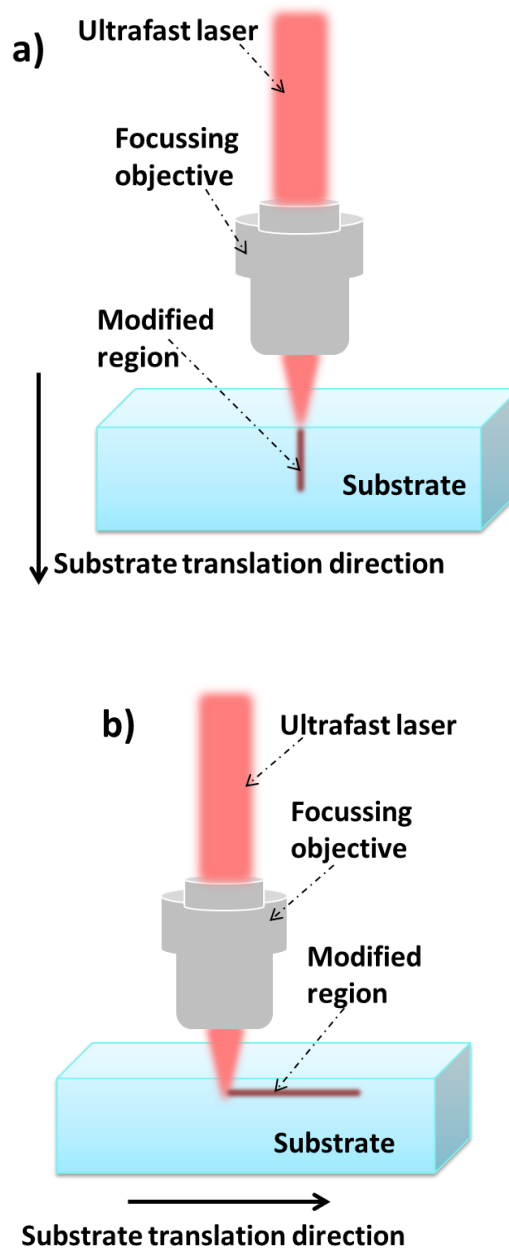
Figure 2.6 Writing geometries used for femtosecond laser writing. a) Longitudinal writing geometry (LWG), where substrate is translated along the incident femtosecond laser b) Transverse writing geometry, where the substrate is translated perpendicular to the indent laser beam.

It has been recently reported that LWG can be improved by the application of Bessel beam instead of Gaussian beam, which can be achieved by incorporating an axicon lens [62]. In contrast with LWG, transverse writing geometry (TWG) enable the inscription of structures without any restriction in length as in LWG, as the sample can be translated over any allowed distance by the translation stage. However, TWG results in highly asymmetric cross sections for any structures inscribed, due to the elongation of

the focal spot in the direction of the incident laser beam. Several beam shaping techniques [63, 64] [65] and use of multiscan approach [66] have been demonstrated to overcome this problem.

*Focusing Optics*

The focusing optics in femtosecond micromachining setup is the focusing objective that determines the spatial extend of modification at the focal volume. For LWG, cross section of the inscribed structure is directly related to the focused beam waist diameter and for TWG, the cross section depends on both confocal parameter and beam waist diameter, given by Equations 2.4 and 2.5, respectively.

$$b = \frac{2\pi n \omega_0^2}{\lambda} \tag{2.4}$$

$$D = 2\omega_0 = \frac{2\lambda}{\pi NA} \tag{2.5}$$

where, $b$ is the confocal parameter, $n$ is the refractive index of the medium, $\lambda$ is the wavelength of the incident laser, $D$ and $\omega_0$ are the focussed beam waist diameter and radius respectively and $NA$ is the numerical aperture of the focusing objective.

## 2.6  Fabrication capabilities of femtosecond laser processing

The versatility of ULI process to alter the optical and chemical properties of glass material provides the possibility of fabricating optical and fluidic components all on a single substrate enabling use for a wide range of applications. The ability to locally enhance the refractive index of the material enables optical waveguides to be written within the material, and the ability to locally enhance the chemical etch rate enables the inscription of 3D hollow structures. These structures can be directly inscribed in the volume of the material by translating the substrate through the laser focus along the desired path. Such waveguides and hollow structures constitute the main building block for constructing miniaturised photonic devices. The following section describes femtosecond laser assisted optical waveguide writing and selective etching for formation of hollow structures.

### 2.6.1    *Femtosecond laser assisted optical waveguide writing*

Optical waveguides can be directly inscribed within transparent material using ULI, by suitably selecting the irradiation conditions, to create refractive index modification at the focal volume. This induced modification can be extended along any 3D path by simply translating the sample, using an xyz translation stage, through the focus. The underlying physical mechanism involving the formation of homogenous refractive index change, the regime well suited to fabricating waveguides was discussed in section 2.4.1. Over the years femtosecond laser processing has been utilised to fabricate buried waveguides in various transparent materials including glass [67], crystalline materials [68, 69] and polymer [70]. However, waveguides written in fused silica have gained more attraction for optofluidic applications. The reason for this is the ability of the fabrication technique to integrate optical and fluidic functions in same substrate with a single exposure.

The careful optimisation of the inscription parameters such as the substrate translation velocity, the pulse energy, the pulse duration, the numerical aperture of the focusing objective and the pulse repetition rate has to be done for fabricating low loss waveguides to use in optofluidic applications. Another key parameter of optical waveguide is the mode profile, which reflects the intensity distribution in a plane perpendicular to the translation direction, when using the transverse writing geometry. The asymmetric cross section of waveguides makes it difficult to achieve single mode propagation of light for optofluidic applications. Several beam shaping methods have been demonstrated to address this issue including astigmatic focusing, slit beam shaping, use of deformable mirror/spatial light modulator and a multiscan technique. In the first three techniques the incident beam is compressed in one direction before it enters the focusing lens so that tight focusing occurs only along the axis of the elliptical incident beam resulting in a symmetric circular cross section. In the multiscan technique, the desired cross section of waveguide is created by scanning the substrate multiple times through beam focus. These methods are described in more detail below.

31

*Astigmatic beam shaping technique*

The first technique that was developed for controlling the waveguide cross section is based on astigmatic shaping of the writing beam [64]. This is achieved by introducing a cylindrical telescope between the fs laser beam and the focusing optics as shown in figure 2.7. The glass sample is placed in an x-y plane, with sample translation along x-axis and beam propagation direction in z-axis. The astigmatism that causes different focusing condition in x and y planes can be tuned to ensure tight focusing in x-z plane that in turn minimises the asymmetry and allows to achieve near symmetric circular cross section waveguides. Furthermore distance between the two cylindrical lenses can be finely tuned to control the astigmatic difference for achieving desired cross section of waveguide.
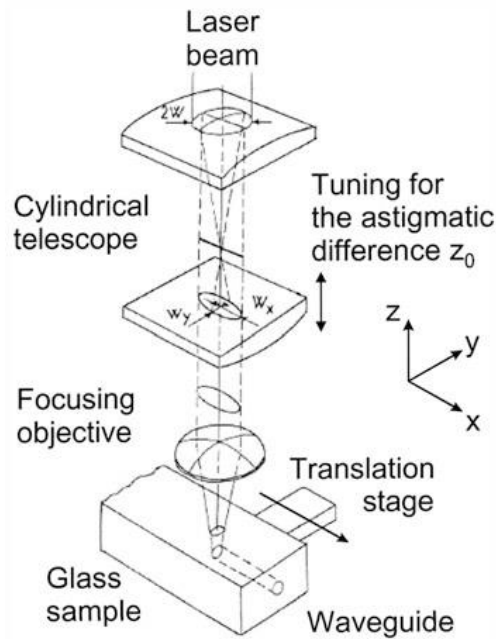


Figure 2.7 Experimental setup for astigmatic beam shaping technique. Taken from [64].

*Slit beam shaping technique*

Slit beam technique utilises a slit aperture inserted before the focusing objective to control the aspect ratio of the focussed beam. The technique was demonstrated to fabricate microfluidic channels with symmetric cross section[71] as well as for shaping the cross section of waveguide [63]. This approach is based on the idea that in TWG,

the beam waist along x and y axis depends on the NA of the focusing objective in the respective axis. Assuming that sample translation is along x axis, a slit aperture place along this axis reduces the NA of focusing in the plane perpendicular to the x axis. Therefore by calibration of slit it is possible to control the shape of focal volume and hence the waveguide symmetry. Due to experimental simplicity this technique has been utilised widely, however the technique is limited in applications were inscribed structure requires bends to be written.

*Waveguide shaping using deformable mirror and SLM*

Instead of using a cylindrical telescope or a slit for shaping the beam, recently active optical elements such as deformable mirrors or Spatial light modulators (SLM) are used for shaping the writing beam. The use of two dimensional deformable mirror allows the spatial profile of the laser beam to be shaped, enabling the asymmetry of the cross section of the inscribed waveguide to be controlled [65]. Deformable mirrors are intended to imitate the function of the slit in slit beam shaping, but with the advantage of using it in inscription of curved structures by adjusting the deformable mirror. Other active optic element that have been explored to use for shaping the writing beam is SLM [72]. The computer controlled SLM placed before the focusing objective can be used to induce astigmatism in the laser wave front and thereby controlling the waveguide cross section.

*Multiscan technique*

The other alternative technique used for controlling the cross section of the structure and waveguides is a multiscan technique. In the multiscan technique the desired cross section of the structure is constructed by scanning the sample multiple times each with an incremental relative to the previous scan, through the laser focus as shown in figure 2.8. Each scan is separated with an offset in the direction perpendicular to both beam and translation directions. The dimension of the waveguide orthogonal to the direction of beam propagation is thus determined by number of scans and separation between each of them. As it defines the cross section of the waveguide, it is considered as a fabrication parameter and has to be investigated when using different materials.
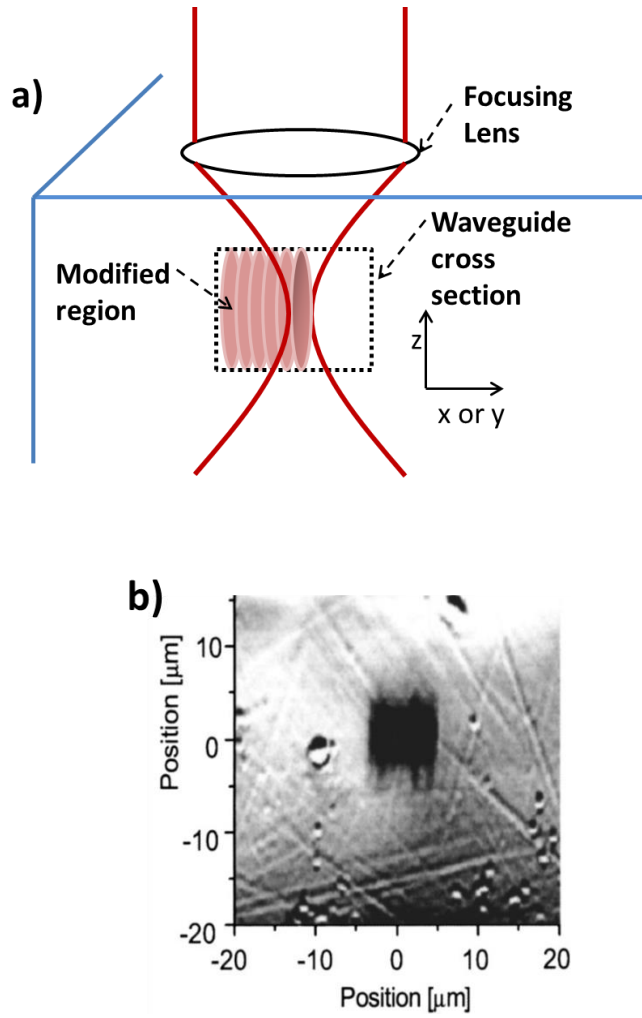
Figure 2.8 a) Pictorial illustration of how multiscan technique can be used to construct desired cross section of waveguide b) Cross section image of the waveguide written using multiscan technique. Taken from [66].

In contrast with the conventional beam shaping methods, the multiscan technique allows control of the cross section and enables fabrication of microstructures with arbitrary shape without involving any complex optics. The microchannel structures and optical waveguides of all the optofluidic devices described in this thesis are written using multiscan technique.

### 2.6.2    *Femtosecond laser assisted selective chemical etching*

The other peculiar characteristic of ULI is the ability to locally alter chemical properties through nonlinear optical effects induced at the focus. At a moderate fluence of the incident laser beam, formation of self-ordered nanograting occurs, that are characterised

by high etching selectivity. The mechanism of nanograting formation with respect to fused silica is discussed in section 2.4.2. During the etching process the nanograting structures acts as a channel for the etchant to diffuse deeply through fused silica, allowing selective removal of the modified region. Femtosecond laser irradiation of fused silica with subsequent selective chemical etching enables the fabrication of desired three dimensional microchannel structures within the bulk of the material.  In 2001 Marcinkevicius *et al.* [24] demonstrated the 3D fabrication of hollow structures inside fused silica  in a two-step process: 1) Direct writing of desired pattern in fused silica by femtosecond laser irradiation, 2) selective etching of the modified region using 5% aqueous solution of hydrofluoric acid  (HF). The choice of a suitable etchant for removing the modified region depends on the chemistry of the substrate. Etching of silica based glasses using HF and HF-containing aqueous solution has been studied and demonstrated over the years [73]. The chemical reaction that takes place during etching of fused silica with HF is given as,

$$SiO_2 + 4HF \rightarrow SiF_4 + 2H_2O \qquad (2.6)$$
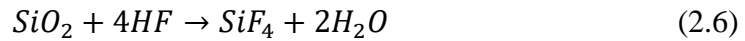
The possibility for fabricating high aspect ratio microchannels and tunnels of arbitrary shape and dimension in fused silica based on the two previously mentioned steps was later demonstrated by [74]. HF etching of the irradiated structures written using various laser parameters has been investigated confirming the high rate for etching. The reason for increased etch rate was attributed to the decrease in Si-O-Si bond angle induced by the internal stress created in the femtosecond laser irradiated region [74].

A second mechanism responsible  for high etching selectivity  was later proposed by Hnatovsky *et al.* [54] . The highly differential etching of the fs laser modified region was attributed to the formation of polarisation dependent self-ordered nanostructures, which enables the etchant to diffuse easily in to the modified region. The dependence of laser polarisation on etch rate was studied in fused silica, which showed a change in the etch rate up to 2 orders of magnitude. The cause for the observed polarisation sensitivity is due to the formation of periodic nanograting structures inside the fs irradiated region. The etch rate is controlled by changing the angle, θ between the electric vector of the fs laser beam and the writing direction, as shown in figure 2.9 [75]
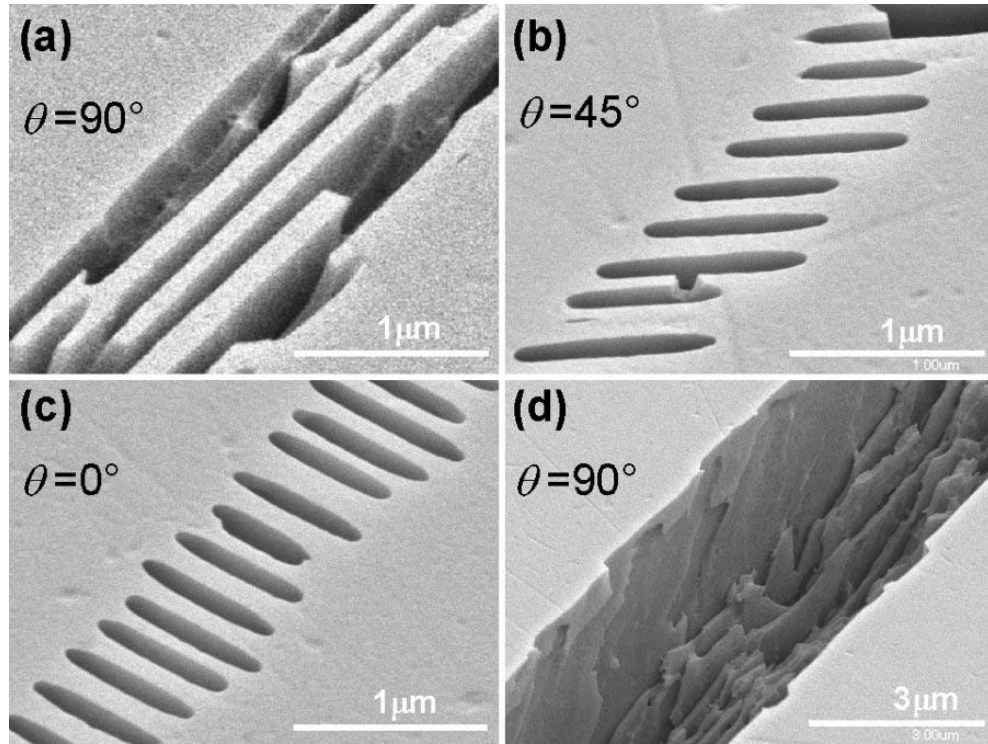
Figure 2.9 (a-c) Orientation of self-ordered nanostructures formed along the writing direction for different θ, where θ is the angle between the electric field vector of the incident laser beam and writing direction at pulse energy, $E_p$ = 300 nJ, a) Nanograting orientation for θ = 90$^0$, b) Nanograting orientation for θ = 45$^0$, c) Nanograting orientation for θ = 0$^0$, and d) Nanogratings written with $E_p$ = 900 nJ and orientation for θ = 90$^0$. The structures were revealed after etching for 20 min in a 0.5 % aqueous solution of HF. Taken from [75].
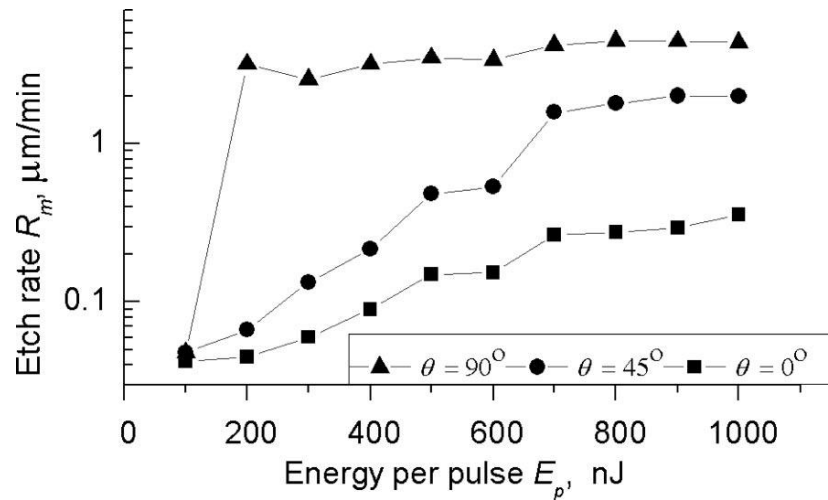


Figure 2.10 Etch rate of femtosecond-laser-modified zones as a function of pulse energy for three different polarisations of the writing beam. Taken from [75].

When grating structures are oriented perpendicular to the writing direction as shown in figure 2.9c, the alternative regions of modified and unmodified regions prevents acid to easily penetrate though the channel, which results in slow etch rate. However, an increased etch rate can be achieved by orienting the nanogratings parallel to the microchannel, allowing the fast diffusion of the acid along the written modification, as shown in figure 2.9a. With an increase in pulse energy $E_p$, the grating structures gradually get destroyed and eventually get substituted by disruptive modification as can be seen in figure 2.9d. The graphical representation of these observations is as shown in figure 2.10.

The use of an alternative etchant Potassium Hydroxide solution (KOH) was later demonstrated for etching laser modified regions in pyrex [76] and silica-based glasses [77]. It was found that the use of KOH acid solution offers higher etching selectivity compared to HF solution enabling fabrication of channels of length 1 cm and width ~60 µm, using a prolonged etching duration of ~60 hr. Despite the longer etching time, KOH offers higher etching selectivity, which shows the potential of using KOH for etching structures with high selectivity requirement.

## 2.7 Summary

The technique of ultrafast laser inscription has been introduced in this chapter. The underlying physical mechanisms of ULI leading to different material modification regimes have been detailed. The potential of ULI induced refractive index change and chemical etch rate modification in fabricating waveguides and microfluidic components have been discussed. Furthermore, the key parameters that must be considered throughout the fabrication process for achieving high quality processing results are discussed in detail. The 3D direct writing capability and successful integration of microfluidic channels and optical waveguides offers a great opportunity for developing complex 3D photonic devices and microfluidic devices with high application potential.

# Chapter 3
# Materials and Methods

## 3.1 Introduction

The incorporation of photonic components in microfluidic systems is a logical path of evolution for microfluidic research. The main reason for this is that the popular detection and manipulation systems such as fluorescence techniques, Raman spectroscopy, surface enhanced Raman spectroscopy (SERS) and optical trapping are photonics in nature, allowing the study of single cells or small volume reactions [13]. With great interest in the single cell manipulation including cell sorting and cell isolation, the work described in this thesis mainly focusses on to the development of novel optofluidic devices capable of performing high throughput manipulation of single cells. Taking advantage of the method simplicity and the 3D capabilities, the technique of ULI has been explored to develop monolithic integrated devices to enable single cell manipulation. Three different optofluidic device geometries consisting of waveguides and microfluidic channel networks have been developed as well as validated in this work, with the aim to improve the throughput of single cell micromanipulation. These devices along with their functional validation have been discussed in detail in the following chapters of this thesis.

This chapter starts with detailing the different steps involved in fabricating the optofluidic devices. The general experimental setup for inscribing basic components of the optofluidic devices is discussed in detail. Furthermore, the parameter consideration for achieving optimised values for writing waveguides and enhancing selective etching is also discussed. A detailed discussion on the general experimental setup that has been used to perform the experiments for validating the performance of the optofluidic devices fabricated using ULI is presented. Finally the cells and other particles used as samples for the different experiments in this study are detailed.

## 3.2 Optofluidic Device Fabrication

The contribution of ULI in fabricating integrated photonic and microfluidic platforms has enabled the realisation of devices with unprecedented capabilities [78, 79]. In particular, optofluidic devices fabricated by ULI are increasingly being used in biological applications, as is discussed in Chapter 1. This section discusses the different steps involved in the fabrication of optofluidic device using ULI. The fabrication process mainly involves two steps. The first step is the inscription of preprogramed 3-D pattern of channel and waveguide in the glass substrate using femtosecond laser pulses. The experimental setup used for this inscription process is discussed in section 3.2.1. The second step is selective chemical etching of the femtosecond irradiated region in HF solution for fabricating 3D hollow microstructures buried within the bulk of fused silica. One of the advantages of ULI is that waveguides and fluidic structures can be inscribed in a single irradiation step, allowing monolithic integration of these components. In addition, it allows the fabrication of desired structures of waveguides and microfluidic networks by suitable translation of the sample through the focus in three dimensions. The 3D capability provides greater freedom in the design and also allows fabrication of more compact designs.

### 3.2.1 ULI setup

The basic ULI experiment setup used for inscribing waveguides and fluidic structures described in this thesis is as shown in figure 3.1. A commercial variable repetition rate Yb-doped master oscillator power amplifier system (IMRA FCPA μjewel D400) is used for delivering $1047\pm10$ nm pulses at a repetition rate of 500 kHz. The linearly polarised laser beam from the laser system is directed to a telescope using mirror M1. The collimated beam from the telescope is then directed by mirrors M2 and M3 to a half wave plate ($\lambda/2$), followed by a polarising beam splitter (PBS), a second half wave plate and a quarter wave plate. The pulses are attenuated by the first half wave plate and the polarisation beam splitter.
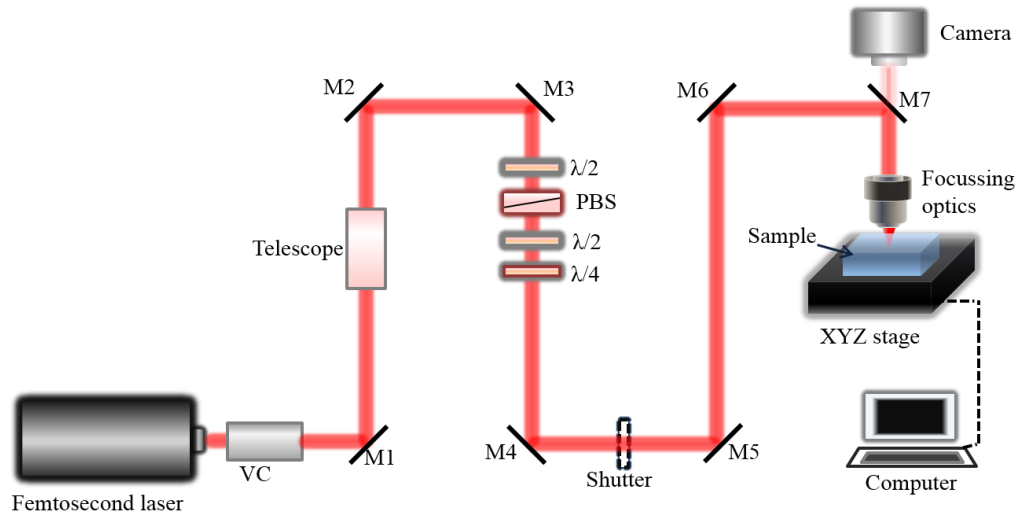
Figure 3.1 The basic experiment setup for ULI. VC: Variable compressor, M1, M2, M3, M4, M5, M6, M7: Mirrors PBS: polarising beam splitter, λ/2: Half wave plate, λ/4: Quarter wave plate.

As discussed in section 2.6.2 of chapter 2, the etch rate of the inscribed microstructures can be altered by varying the angle between the electric field vector of the beam and the writing direction. This is accomplished by passing the beam through a second half wave plate, positioned after the PBS, whereby the polarisation state of the beam is rotated as required for the application. Finally, passing the beam through the quarter wave plate (λ/4) allows a circularly polarised beam to be produced. This enables producing modifications consisting of disordered nanostructures [54], shown to be more favourable for fabricating waveguide structures with low propagation loss. The beam is then directed through the mirror M4, M5, M6 and M7 to the back aperture of the focusing objective and then to the sample. Sample is mounted on to an XYZ air bearing stage (Aerotech, ABL 1000) and the translation of the stage is controlled by Automation 3200 N-view software, whereby the design of the optofluidic prototypes were first programmed and simulated. The shutter placed after M4 in the setup is used to control the ON/OFF state of the laser beam during the laser inscription process. The wave plates and the shutter are also controlled using computer. Suitable translation of the device thus allows writing of desired waveguide and fluidic structures in a single-step irradiation process as the same laser source and focusing conditions are used. The only variation involved in writing the waveguide's and fluidic structures i.e. the incident laser pulse energy can be switched electronically. In this way, a fine control of the

position enabling a precise alignment between the microchannel and waveguides can be achieved. An initial parameter test experiment was performed, for achieving optimised conditions for writing waveguide and microfluidic structures in fused silica, which is discussed in section 3.2.2.

### *3.2.1.1 Material: Fused Silica*

A wide variety of materials including different types of glasses [49, 80], polymers [81] and crystals [68, 82] have been explored for femtosecond laser processing, particularly for fabricating waveguide and microfluidic components with potential application in photonics and biophotonics fields. Among the different materials, glass that offers features such as high transparency, low thermal expansion coefficient, good chemical durability and biocompatibility is considered to be an excellent material as substrate for fabricating microfluidic or optofluidic sensing devices using ULI.

Fused Silica is the most commonly used material for fabricating optofluidic devices, although other glass materials have been explored. To date several optofluidic devices have been developed in fused silica using ULI that are used for a wide range of applications [29], [78], [31]. All the optofluidic devices described in this thesis are fabricated in fused silica (Corning HPFS 7980) substrate. In particular, the choice of fused silica as substrate material adds to the aforementioned advantages a wide range of transmittance from deep ultraviolet through infrared and a very low background fluorescence. In addition to this, the laser induced modification in fused silica can be tailored by varying the incident laser pulse energy allowing writing of optical and fluidic elements in a single irradiation process with high precision using the setup discussed in section 3.2.1. Fused silica also exhibits laser assisted etching that can be controlled by varying the polarisation state of the incident laser pulse [75]. These salient features makes fused silica the most suitable material as a substrate for fabricating the optofluidic devices described in this thesis.

### 3.2.2    *Waveguide and selective etching characterisation and optimisation*

Waveguides and microfluidic structures form the basic elements of the optofluidic devices. Extensive studies on fused silica with respect to microfabrication using ULI have been carried out since the demonstration of optical waveguides [21] and selective

chemical etching [24] . These studies in turn have provided substantial knowledge on characterisation along with optimisation of the parameters for fabricating optical waveguides and microfluidic structures, the building blocks of an optofluidic system, within the bulk of fused silica. This section describes the optimisation of inscription parameters that has been used for obtaining the best waveguide and selective etching results.

In order to determine the best and optimum parameters for fabricating waveguides, it is important to characterise the inscribed waveguide morphology and loss. The cross-sectional shape of the refractive index modification is controlled by using the multiscan technique as discussed in chapter 2. The desired cross section is constructed by scanning the sample through the focus multiple times, each with an incremental movement relative to the previous scan, as presented in figure 2.8, chapter 2. The waveguide cross section is designed to have a cross section of ~4 µm to match with the core diameter of the coupling fibre. The ~4 µm size core was fabricated using 13 fabrication scans with an offset of 0.3 µm. The scan separation is set at a lower value than the beam diameter at the focus to ensure a high degree of overlap between the individual scans. Figure 3.2 shows the cross section of waveguides inscribed in fused silica using multiscan technique.
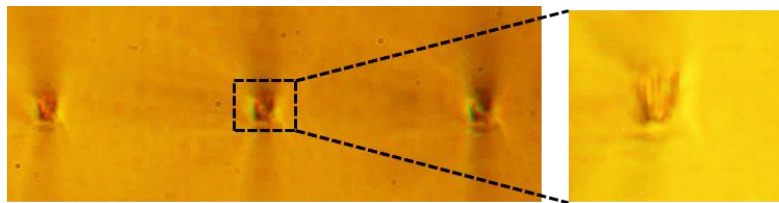


Figure 3.2 Cross section of waveguide in fused silica written using multiscan technique. The waveguide cross section is ~4 µm × 4 µm.

**Processing window for waveguides**

A range of pulse energies from 120 nJ to 180 nJ were used for inscription, focussed at a depth of 300 µm below the surface of the fused silica substrate using 0.4 NA lens. The sample was translated perpendicular to the beam propagation direction at a speed of 2 mm/s and the polarisation was adjusted to be circular [83] to fabricate the waveguides using multiscan technique. The repetition rate of the laser was set at 500 kHz and the

pulse duration was measured to be 430 fs. After the inscription process the end facets of the fabricated waveguides were ground and polished to high optical quality. The guiding properties of these waveguides were inspected from the output facet using a NIR camera while coupling 980 nm laser at the opposite end using fibre butt coupling. From this observation a window of laser pulse energies for writing single mode waveguides were obtained, which is then used for writing more waveguides to estimate the insertion loss.

**Insertion loss characterisation**

Insertion loss (IL) of the waveguide is an important parameter in determining the quality of the inscribed waveguide. It is defined as the loss of the signal induced when placing the waveguide in the beam path. IL comprises of the propagation loss (PL) through the medium and the coupling loss (CL) from the two end facets. Figure 3.3 shows the experiment setup used to measure the IL for the inscribed setup.
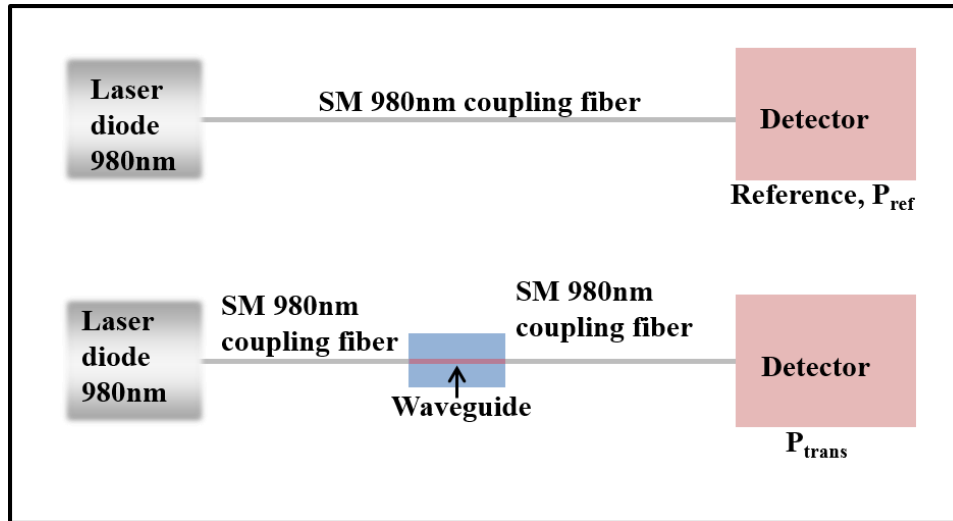


Figure 3.3 Insertion Loss measurement setup.

In order to measure the insertion loss of the inscribed waveguides, two ends of a single mode fibre operating for a wavelength 980 nm was cleaved with one end fusion spliced to a continuous wave (cw) laser operating at a wavelength 980 nm and the other end to a detector. A reference measurement $P_{ref}$ (dB) is then taken by measuring the power propagating through the fibre. The fibre is then broken, cleaved and butt coupled to the end facets of the inscribed waveguide using index matching liquid, to help eliminate the

Fresnel losses. The power transmitted through the inscribed waveguide is then used to calculate $P_{trans}$ (dB). The insertion loss is then defined by the expression,

$$IL \text{ (dB)} = P_{ref} - P_{trans} \qquad (3.1)$$
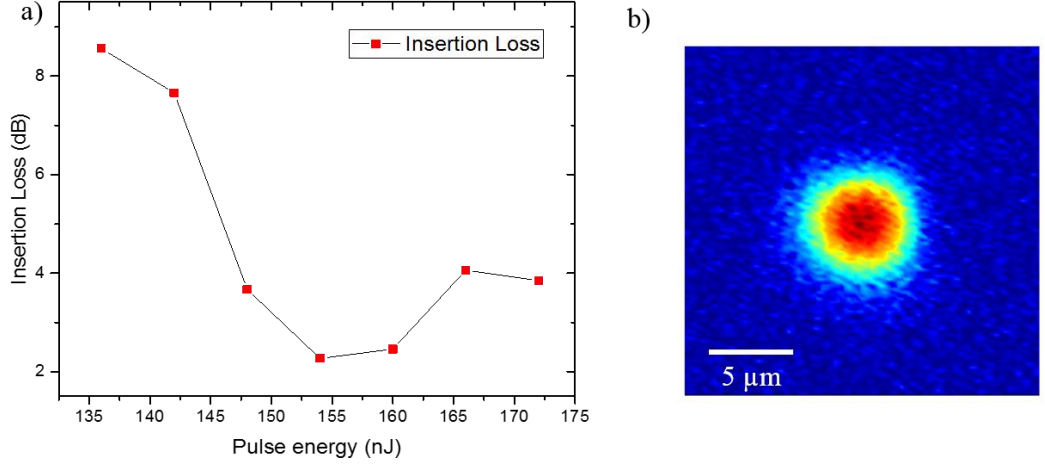


Figure 3.4 a) Insertion Loss for multiscan waveguide at 980 nm. b) Intensity mode profile of the waveguide at 980 nm, written with a pulse energy 154 nJ.

Figure 3.4a shows the IL of a multiscan waveguide fabricated using 13 scans at a translation speed of 2 mm/s. A minimum value for IL of 2.27 dB was obtained using a waveguide inscribed with a laser pulse energy of 154 nJ. A relatively high value for insertion loss of 2.27 dB can be attributed to the presence of nanostructures formed in the modified region when written with a laser pulse energy of 154 nJ and pulse duration of 430 fs, as is discussed in section 2.4. The intensity mode profile of the waveguide at 980 nm is as shown in figure 3.4b. These parameters were adopted for inscribing waveguides in the optofluidic device that was fabricated for demonstrating the manipulation of objects using optical forces within a microfluidic channel in Chapters 4 and 5 to follow.

**Selective etching optimisation**

The second step involved in fabrication of optofluidic devices is preferential etching of the laser modified region. The modified chemical properties of fused silica after fs laser irradiation exhibits high etching selectivity and this allows removal of the modified tracks using etchant such as Hydrofluoric acid (HF). Figure 3.5 schematically illustrates

the etching process for fabrication of 3D microstructures in fused silica glass. As shown in the figure 3.5, after the inscription of desired pattern of microstructure, the chip is immersed in 5-10% HF solution in an ultrasonic bath. The interaction of HF with the laser modified region results in chemical reaction as discussed in section 2.6.2 of Chapter 2 leading to selective removal of the material. The ultrasonic bath helps in significantly enhancing the etch rate by effectively transferring the chemical etchant in to the thin channel.
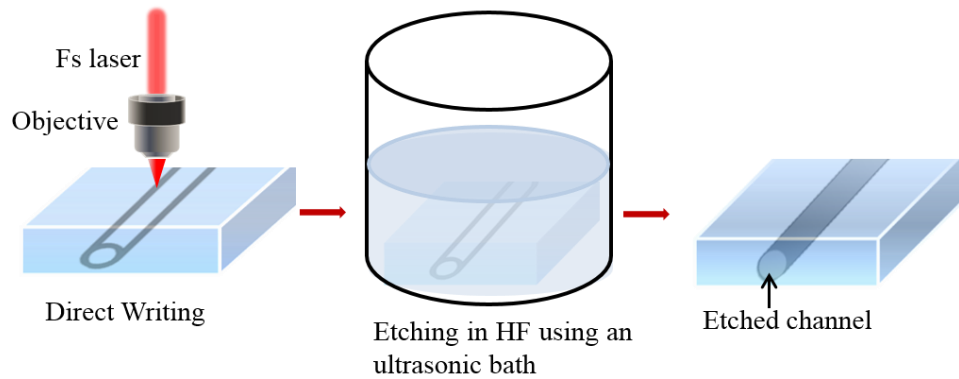


Figure 3.5 Schematic illustration of fs laser direct writing followed by chemical etching in HF.

The optimisation of selective etching is important for fabricating microstructures composed of design variations. Based on the previous knowledge on etching in fused silica available in the research group [84] a parameter acquisition experiment was performed. In doing so, fs laser pulses at a repetition rate of 500 kHz and with duration of 350 fs were focused 1 mm beneath the surface of fused silica substrate. The energy of the incident pulse was varied from 500 nJ to 820 nJ. Single scans were written for each of the pulse energies by translating the sample through the focus for a distance of 3 mm at a translation speed of 1 mm/s. The laser polarisation was maintained perpendicular to the writing direction, allowing writing of nanogratings along the translation direction of the substrate. The end facets of fused silica substrate after the inscription process were ground back enabling direct contact of the etchant with the modified region. The device was then subsequently etched in 5% HF solution in an ultrasonic bath as illustrated in figure 3.5.

The length of the etched region for different pulse energies was evaluated from the optical microscopic image of the partially etched laser tracks, as shown in the figure

3.6a. The etched length was then plotted against the laser pulse energy to determine the best etching results, as shown in figure 3.6b.
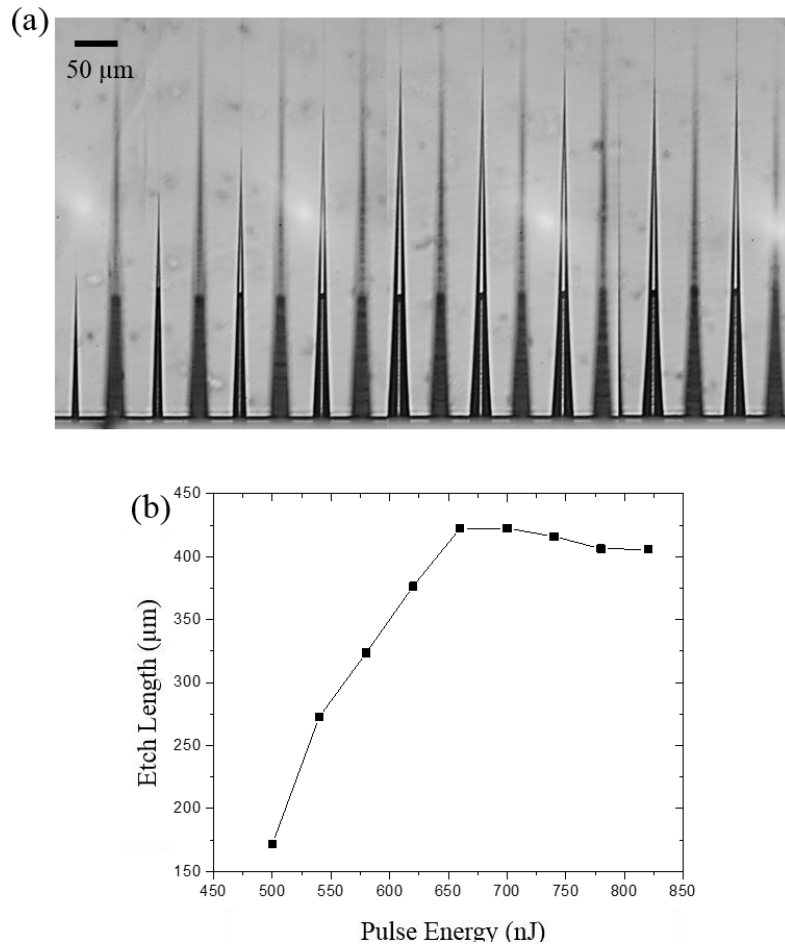


Figure 3.6 a) Optical image of microchannels after etching in HF, b) Etch length of femtosecond laser modified region as a function of incident laser pulse energy. Etching test performed by Mark Mackenzie.

As the acid penetrates deeper into the modified region of the material, it becomes more difficult for fresh acid to reach, resulting in tapered microchannels as shown in figure 3.6a. The relative post etch aspect ratios of microfluidic channels of the devices detailed in this thesis are achieved by etching the microchannels from opposite sides. The etching length was observed to be increasing with pulse energy and reaches a maximum point followed by a saturation regime. A range of pulse energy between 650 nJ and 850 nJ that offered the maximum etched length were later adopted for fabricating the fluidic structures. The all - optical control of etch rate achieved by varying polarisation state of the fs laser pulse has also been utilised in writing complex 3D channel structures of µm precision.

### 3.2.3    *Post etch device*

Fabrication of optofluidic devices with integrated waveguide and microchannel can thus be accomplished by using the ULI setup described in the section 3.2.1 followed by chemical etching step as shown in the figure 3.5. Since the fs irradiation step is performed before the chemical etching process, writing of waveguides for all the optofluidic devices described in this thesis was realised few micrometres before the edge of the chip, in order to avoid the waveguide etching. After the selective chemical etching process, the device end facets were ground and polished to high optical quality for improving the waveguide laser coupling. The devices were then rinsed in de-ionised water followed by acetone for 30 minutes in an ultrasonic bath to remove any residual traces of HF inside the microchannels. Once the devices are fabricated, it is connected to the external fluid circuits for enabling chip to fluid interconnection. In doing so, the fabricated chip was mounted on a translation stage and external capillaries were inserted in to the access holes of the device. Optical microscope was used to ensure that the capillaries were firmly inserted, finally glueing the capillaries using UV – curable resin.

## 3.3    General experimental setup

The basic experimental setup for validating the performances of optofluidic chips is shown in figure 3.7. The device after assembling as discussed in the section 3.2.3 is mounted onto an xyz translation stage. The devices that have been made in this work exploit waveguide delivered light, or transmitted light from an external source, in the devices to probe and manipulate the cells or particles. Two different laser sources have been used for delivering light into the embedded waveguides in the device. In the initial experiments for demonstrating the manipulation of objects using optical forces in an optofluidic device, a cw laser operating at a wavelength of 980 nm (LUMICS) with a maximum output power of 1 W was used to deliver light. In this case the laser to waveguide coupling was enabled by butt coupling one end of a SMF to the waveguide and the other end to the laser diode.
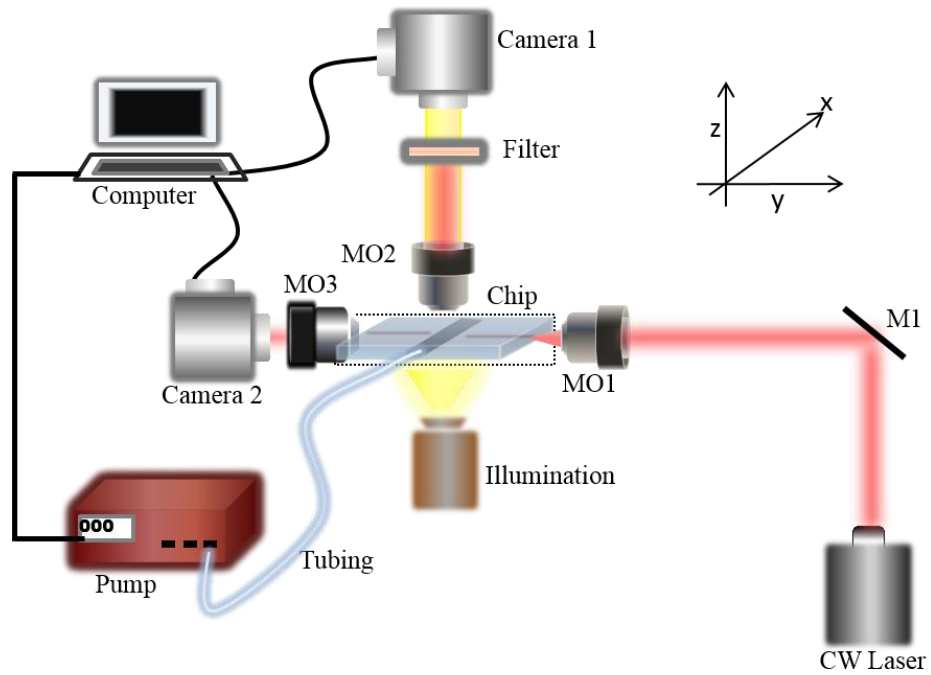
Figure 3.7 General experiment setup experimental setup used for manipulating cells using ULI-manufactured 3D microfluidic devices. MO1 is used for focusing the laser beam in to the embedded waveguide in the device. Device is illuminated from below, MO2 allows coupling out light to camera 1. The band pass filter placed between MO2 and camera1 filters the laser light used for manipulation. Camera 2 is used for monitoring the live performance. MO3 and Camera 2 were used for inspecting the waveguide coupling. Pump, Camera 1 and Camera 2 are controlled by computer.

For further optimisation of the initial results and demonstrating the sorting and isolation capabilities, optofluidic devices with intricate 3D microchannel networks were fabricated. The working principle and device functionality of these devices are discussed in the following chapters. The optical radiation for manipulating objects in these devices was achieved from a cw Nd: YAG laser source (Ventus, Laser Quantum) operating at a wavelength 1064 nm with a maximum output power of 3 W, thus providing a large range of powers. The laser beam was focused on to the facet of the integrated waveguide using a focusing objective. Since glass absorption in the near infrared range is very low, the high powers needed for manipulating the cells can be easily coupled without appreciably heating the chip. In addition the water absorption is lower at the adopted wavelength range providing minimal temperature rise compared to longer wavelengths, allowing cells to remain unperturbed by temperature change [85].

The fluid control within the chip is another important element in the controlled manipulation of cells. The delivery of cells or other particle suspensions to the manipulation region was accomplished by an easy connection to external fluidic circuits. The external fluid circuit mainly consists of a microfluidic pump, capillary tubing of different sizes and micro-adapters and connectors. Based on the requirement of input flow rate ranges, three different pumps including milliGAT (Aquilant Scientific (Presearch)), Syringe pump (Harvard Instruments) and Fluigent flow controller (Fluigent S. A) have been used for achieving a controlled fluid flow in the devices and allowing a high throughput analysis. The chip to pump connections were realised by using PEEK tubing of different inner and outer diameters. Micro adapters and connectors (IDEX health and science (Kinesis)) were used for achieving a leak free connection between tubing of different sizes.

Finally, for monitoring the performance of the device and to acquire images, a detection system, consisting of microscopic objective, filter and camera connected to the computer was used. The chip was illuminated with white light from below. The microscopic objective is used for coupling out the light to camera. The band pass colour filter placed between the objective and the camera was used to filter out the laser light used for manipulation keeping the full spectrum of visible light for the cell imaging. Initial experiments for demonstrating the cell and particle manipulation in the microfluidic channel using optical forces was visualised by mounting the chip on a fluorescent microscope (Nikon Eclipse E600). Live monitoring of the device performance using the setup illustrated in figure 3.7 was accomplished by using CCD cameras including ProgRes CCD SpeedXT core5 (Jenoptik) and Canon EOS 600D enabling fast capturing of images with high resolution. A more compact detection system (including fluorescence excitation) using a USB digital microscope (Dino-Lite Premier AM4113T-GFBW) and a band pass colour filter was also employed for detecting and recording experiments performed with objects emitting green fluorescence above 510 nm as excited by the 480 nm (blue) LED lights of the Dino-Lite microscope. The NIR camera placed after the chip was used to inspect the precise coupling of laser light into the inscribed waveguide at the input facet of the chip. The detailed discussion on the results obtained from each experiment is presented in chapter 4 and 5.

## 3.4 Cells used for experiment

Performance of the all the optofluidic devices were initially validated using polystyrene microspheres of different sizes ranging from 2 μm to 10 μm (Polysterene Latex, Fluorescent Polystyrene Latex MAGSPHERE). In preparation of the sample, microspheres were suspended in deionised water at a desired concentration. A small amount of surfactant was added to the microsphere suspension to stop the beads from sticking on the walls of microfluidic channel. Device performance was also validated to use with biological samples. A list of cell samples used in different experiments carried out in this work has been detailed in the following section.

*Chlorella Vulgaris*

*C. Vulgaris* is a eukaryotic, unicellular green alga found in fresh water environments. These cells are spherical in shape and about 2 μm in diameter. One of the intrinsic properties of *C.Vulgaris* is that the high content of chlorophyll causes autoflourecence. Initial optimisation experiments studies were done using *C. Vulgaris* samples. The cells used in this study were obtained from School of Life Sciences, Heriot Watt University.
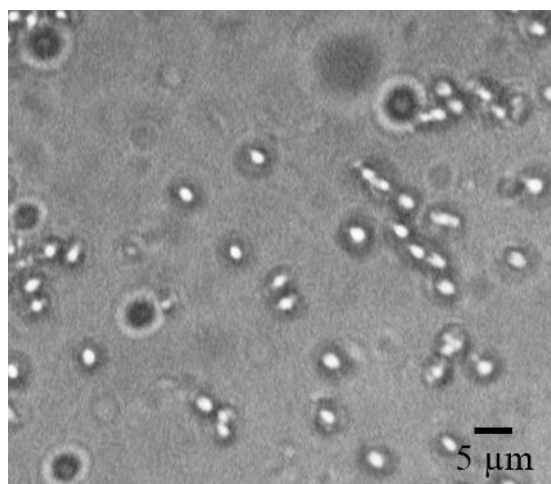


Figure 3.8 Microscopic image of C.Vulgaris cells. Diameter of the cells was calculated as 1.96±.17 μm.

*Saccharomyces cerevisiae*

*S. cerevisiae*, also known as baker's yeast, are single celled fungi, which are widely used for biological studies. Commercially available Baker's yeast of diameter ~ 5μm and spherical in shape were used for the studies.
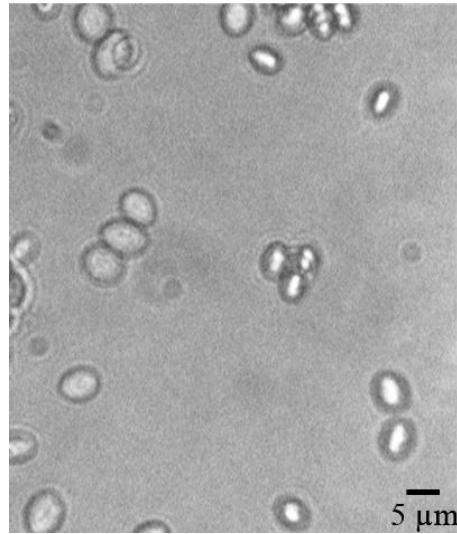
Figure 3.9 Microscopic image of Yeast cells. Diameter of cells was calculated as 5.2±0.63 µm.

### *Escherichia coli (E.coli)*

*E.coli*, rod shaped bacteria commonly found in microenvironments of lower intestinal tract of mammals. *E.coli* cells expressing green fluorescent protein were obtained from School of Life Sciences.

### *AtT-20*

Cultures of AtT-20 cells were obtained from the Life Science Interface Lab, Heriot Watt University. The diameter of these cells from microscope images was calculated as 13±0.54 µm. These cells were used to validate the sorting functionality of the device discussed in Chapter 5 of this thesis. The cells were stained with a fluorescent marker to enable high quality images when using a fluorescent microscope. The protocol for staining the cells with Calcein, AM, cell- permanent is as follows. Cell staining was performed with the help of Krystena Callaghan, IB3, Heriot Watt University.

Figure 3.10 Microscopic image of AtT20 cells. Diameter of cells was calculated as 13±0.54 µm.

The 1 mg calcein (Molecular Weight 994.87) was solubilised in 0.5 mL DMSO to produce a working stock of 2 mM calcein. A 10% stock solution of pluronic acid F-127 was made by dissolving 1 g of pluronic acid F-127 in 10 mL of DMSO. This was further diluted to 0.05% solution by dissolving 10 µL in 2 mL of versene. Dilution of 10 µL of 2 mM calcein in 2 mL of 0.05% pluronic acid F-127 will give a final concentration of 10 µM calcein stain. 2 mL of this solution was then added to a pellet of cells and was kept in the incubator for 30 minutes. After 30 minutes cells were concentrated by spinning for 3 mins at 0.5 RCF (relative centrifugal force). By doing this, the buffer can be separated and removed. Pellets were then resuspended in 4% PFA (Paraformaldehyde) and incubated for 10-20 minutes to fix the cells. After incubation the cells were spun for 3 mins at 0.05 RCF. For washing out the PFA, cells were resuspended in 2 mL of versene followed by spinning then a final resuspension in versene.

## 3.5   Summary

The material properties of fused silica can be tailored by using femtosecond lasers enabling one to write optical and fluidic components within the bulk of the fused silica. ULI technology allows the combination of these components in to single platform to form complex optofluidic systems. This chapter has presented the different steps

involved in fabricating optofluidic devices in fused silica using ULI. Parameter acquisition experiments performed for achieving optimised values for writing waveguides and enhancing selective etching in fused silica are discussed. These parameters were adopted for fabricating the different optofluidic devices detailed in the following chapters. The experiment setup used for validating the functionality of the devices is presented. Chapter 4 and 5 will discuss the demonstration and performance validation of optofluidic devices that are fabricated using the ULI setup (figure3.1) and validated using the setup (figure 3.7) discussed in this chapter.

# Chapter 4

# Optical Manipulation of Particles in 3D Optofluidic Devices

## 4.1 Introduction

Cell manipulation processes including isolation, separation and sorting of cells are critical for single cell based studies. Consequently great importance has been given to develop efficient techniques that enable these manipulation processes. Several approaches including microfluidics [86, 87], optical tweezers [8] and FACS [88] have been used for manipulating cells at single cell level. Depending on the purpose of study, these techniques are individually used or used in combination with other single –cell analysis. For example, a combination of miniaturised FACS can be built in microfluidic platforms enabling to handle very small amount of sample [28]. Microfluidic  platforms also provide a way for applying variety of force fields to achieve cell manipulation. Examples for this  includes electric [89], optical [11, 90], magnetic [91], and acoustic mechanisms  [92]. Electrokinetic forces for manipulating particles includes electrophoresis and dielectrophoresis based on whether it acts on particles' fixed charge or induced charge respectively. The integration of electrical manipulation techniques with microfluidics offers transportation and manipulation of particles with high controllability and high throughput capability [93]. However, high electric fields could result in biological stress within cells leading to cell damage.  Another method for microparticle manipulation is by integrating acoustic manipulation in to microfluidic systems. Surface acoustic waves can be used to sort cells based on the physical properties of cells such as size and density. Although the technique has shown advantages in simplicity and low power required to manipulate cells, a low accuracy in manipulation of single cells limits its use for single cell based studies [92] . Magnetic manipulation techniques can also be employed with microfluidics for manipulating cells and particles that are functionalised using magnetic labels. However, the need to functionalise cells with magnetic tags could affect the intrinsic cell activity adversely [91]. Of the different manipulation techniques mentioned above, optical techniques that uses optical forces to control and manipulate cells has gained much interest in biological

applications due to their non-invasive and contamination free manipulation abilities and high accuracy.

This chapter details the investigation of particle and cell manipulation in 3D optofluidic devices using optical manipulation techniques. Optical forces, the manipulation tool incorporated into these devices are introduced in this chapter. Two device designs and their functional validations are presented. The first half of the chapter details the demonstration and investigations on the potential of using optical scattering force to control and manipulate particles using a simple optofluidic geometry. The results obtained from these experiments were then utilised in prototyping a more complex 3D optofluidic device for particle manipulation experiments, which is discussed in detail in the second half of the chapter. The progression in the complexity of the device designs to use for single particle isolation and sorting applications is discussed in detail.

## 4.2 Optical force for manipulation of particles and cells in microfluidic device

Since Arthur Ashkin [7] demonstrated the control of microscopic particles using optical forces in 1970, optical forces have been used as a manipulation tool in research fields involving the handling of micron sized particles and cells. Of the several manipulation techniques, optical forces, which offer a non-invasive manipulation tool, are employed in several microfluidic systems for the handling of biological samples within the system. In particular, the application of optical forces has enabled a wide range of tasks including transporting, levitating, sorting [11], rotating [94] and immobilising [95] micron sized particles within microfluidic environment.

Optical forces acting on a transparent dielectric particle located within a gradient of light such as Gaussian beam is illustrated in figure 4.1a and b. Since the diameters of the particles used in this study are larger than the wavelength of the incident light, the ray optics model is suitable to describe the optical force on the particle [96]. Figure 4.1a and b shows a dielectric sphere with refractive index greater than the surrounding medium, immersed in a laser field, whose wavelength is smaller than the diameter of the sphere.

Individual rays of light depicted in the figures as red arrow lines emitted from the laser will undergo reflection and refraction as they interact with the sphere.
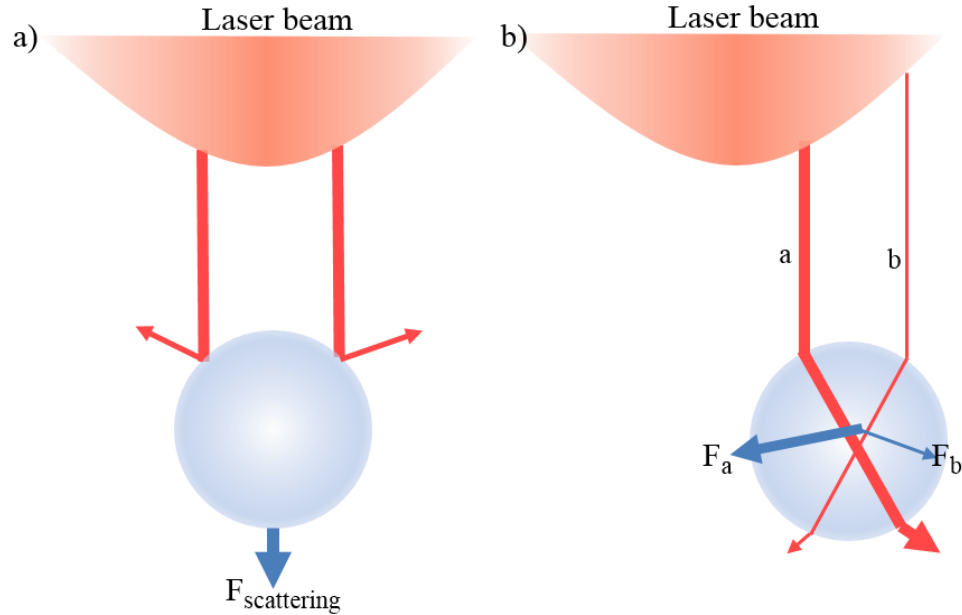


Figure 4.1 Illustration of Optical force arising from a) reflected and b) refracted rays interacting with a particle. Red arrows represents the ray of light and blue arrow lines represents the force vectors.

Since the light beam carries a linear momentum, the reflection and refraction of light by the object results in a change in momentum of the light. Due to conservation of linear momentum, the reflection of rays results in the sphere gaining momentum in the opposite direction giving rise to a net force know as scattering force ($F_{scattering}$) along the direction of propagation of the beam as shown in figure 4.1a. The refraction of rays of different intensities represented as rays a and b in figure 4.1b, results in a total momentum change causing a net force that draws the object towards the most intense region of the beam in a collimated beam. Considering all the symmetrical pairs of rays falling on the sphere and applying ray analysis to each, the net effect of laser on the particle can be understood in terms of two different forces: one scattering force and the other gradient force. While the scattering force acts on the particle, pushing the particle along the propagation direction of the incident laser beam, gradient force acts to move the particle towards the region of highest intensity.

Optical manipulation generally involves making use of the gradient or scattering force for controlling and manipulating particles. The gradient force based technique is mainly

employed in optical tweezers (OT) for trapping and moving particles and cells in three dimensions. This is achieved by generating a large intensity gradient at the focal point of the beam using a high numerical aperture (NA) lens. OT based manipulation has been used with microfluidic devices, to transport the trapped object to desired location in the device [11]. Although OT can manipulate single particles, their use in combination with microfluidic systems has certain limitations involving bulk optical systems and complicated alignment of optics.

The scattering force obtained from a parallel or loosely focused laser beam enables to control the axial motion of particle. Theoretical investigations on 'cross-type' optical particle separation carried out by Kim *et al.* [97] has demonstrated that the displacement of a particle caused by the optical scattering force depends on the particle's size. This has been employed in microfluidic devices for size based particle and cell separations through displacing them to different trajectories along the propagation direction of beam [98]. The application of optical scattering forces can be readily integrated with microfluidic platforms, enabling an easy operation of the system. One example for this is an optofluidic cell sorter device demonstrated by Bragheri *et al.* [28] capable of sorting single cells on the basis of their fluorescence, using the optical scattering forces from a laser beam. The integrated waveguides within the device is used to deliver the optical force for deflecting the cells and for delivering the fluorescence excitation signal. Such integrated devices offer great potential to use for cell manipulation. With a high degree of freedom in cell manipulation, scattering force has been applied in a wide variety of optofluidic device designs for manipulating cells.

### 4.2.1 *Theoretical investigation of optical force acting on particle flowing in microfluidic device*

A theoretical model for optical forces acting on a particle can be described using electromagnetic wave theory or ray optics model. The electromagnetic wave approach is applied when particle size is smaller than the wavelength of the illuminating light whereas, the ray optic approach is used for particles larger than the wavelength of the light [99]. Since the size of the particles used in the current study is larger than the wavelength of illuminating light, the ray optics approach can be used for describing the optical force acting on a particle. In order to investigate the optical force acting on

particle flowing in an optofluidic system as shown in figure 4.2, we use the theoretical model presented by Kim *et al*. [97] which is derived based on the ray optic model.
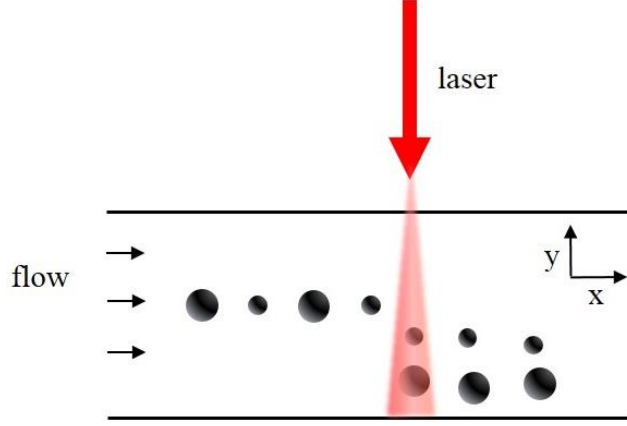


Figure 4.2 Illustration of lateral displacement of particles flowing in a microfluidic channel when subjected to optical force. Adapted from [100].

Particles flowing within the microfluidic channel are irradiated in a direction perpendicular to the fluid flow. In the theoretical model by Kim *et al.* [97], it was assumed that the width of the laser beam and the distribution of optical forces, which varies with the particle position, is constant. Assuming that the laser beam width is larger than particle size, the effect of the gradient component of the optical force is ignored. For a spatially averaged constant scattering force *F* given by,

$$F = \frac{n_0 P}{c} \left(\frac{r}{\omega_0}\right)^2 Q \sqrt{\frac{\pi}{2}} \, erf\sqrt{2} \qquad (4.1)$$

the lateral displacement *Z* of a particle flowing within the channel when subjected to optical force is given by,

$$Z = \frac{n_0 P}{3\pi\mu U c} \frac{r}{\omega_0} Q \sqrt{\frac{\pi}{2}} \, erf\sqrt{2} \qquad (4.2)$$

where, $n_0$ is the refractive index of the medium, $P$ is the applied laser power, $c$ is the speed of light in vacuum, $r$ is the radius of the particle, $\omega_0$ is the laser beam width, $Q$ is

the dimensionless parameter that depends on the refractive index of the particle and medium, $\mu$ is the viscosity of the fluid, $U$ is the uniform fluid velocity and $erf$ denotes the error function. Eq. (4.2) indicates that the lateral displacement of the particle increases with increase in incident laser power and decreases with increase in flow velocity and laser beam width. The given model has been used by researchers to predict the lateral displacement of particles using optical force within a microfluidic channel [98, 100]. The assumptions made in the theoretical model such as having a constant beam width for the laser interacting with the particle and uniform velocity for the fluid flow does not totally agree with the optofluidic system used in the present studies as represented in figure 4.2. Therefore lateral displacement data may not agree as closely as you would like with theory. However the theoretical model allows to predict the change in lateral displacement of the particle subjecting to change in different parameters including laser power $P$, radius of particle $r$, fluid velocity $U$, and laser beam width $\omega_0$. The direct dependence of lateral displacement on radius, $r$, of the particle suggests that larger particles can be displaced longer distance with same laser power along the beam axis. The effect of laser power, particle velocity and particle size have been experimentally evaluated and discussed in the following sections. A comparative analysis of the experimental data with the theoretical model is also presented.

## 4.3    Demonstration of optical manipulation in ULI fabricated optofluidic device

The following sections details the experimental investigations on using optical scattering force to control and manipulate particles within a ULI and chemically etched optofluidic device. The fabrication and validation of the 3D device is detailed. The role of laser power and particle velocity in controllably displacing the particle within the microfluidic channel has been investigated using this device. The results obtained from these experiments were then utilised in designing a more complex 3D optofluidic device for particle manipulation experiments, which is discussed in detail in sections 4.5 and 4.6.

### 4.3.1   Device design

The design of the optofluidic device for studying and evaluating the use of optical scattering forces from the output of a waveguide to manipulate microorganisms and

particles within a microfluidic channel is as shown in figure 4.3. The device is designed to have a straight microfluidic channel connecting the inlet and outlet which are located at the two end facets of the substrate. The waveguide is positioned orthogonally to the channel. The straight channel constitutes the path along which the sample flows and the waveguide will deliver the laser light from a CW laser diode into the channel. The inlet and outlet ports act as access holes, which facilitates the chip to external fluid connection through capillary tubing. The diameters of these ports are thus designed to match the outer diameter of the capillary tubing. The design is such that sample fluid containing particle or cell population can be injected through the inlet with a controlled flow. As a particle or cell flows past the waveguide, the optical scattering force from a laser beam exiting the optical waveguide can be used to push the particle along the direction of propagation of the incident beam, perpendicular to the flow, and so displace a single cell from its original trajectory.
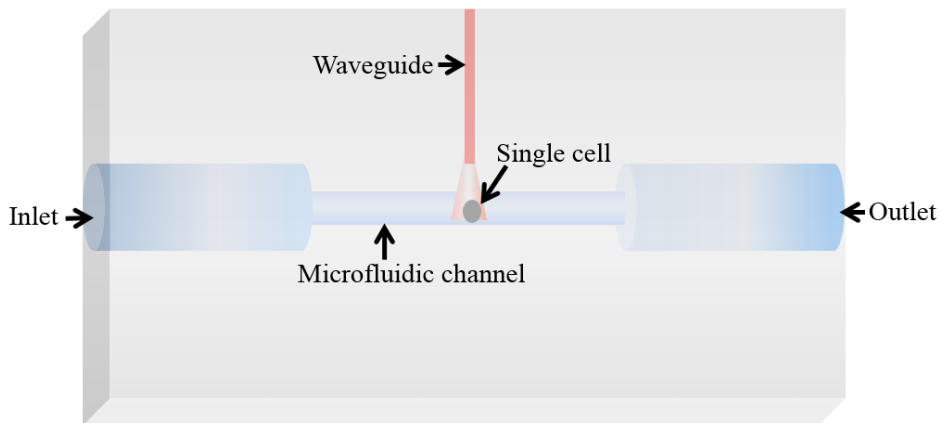


Figure 4.3 Design of the Optofluidic device (Not to scale). Cells can be injected into fluidic channel through the inlet. Waveguide positioned orthogonal to the fluidic channel is used to deliver the optical force for manipulating cells flowing past the waveguide.

### 4.3.2   Device fabrication

The preprogramed pattern of the 3D design was inscribed within fused silica substrate using the ULI setup described in figure 3.1 in Chapter 3.  The choice of laser parameters for fabricating low loss waveguides and microfluidic structures were accomplished by performing a laser parameter scan as discussed in Chapter 2. Microfluidic structures and

waveguides were written using a commercial femtosecond laser system (Satsuma, Amplitude Systems) operating at a wavelength 1047 nm delivering femtosecond pulses at a repetition rate of 500 kHz with a pulse width of 430 fs. The laser pulses are focused inside the fused silica substrate using a ×20, 0.4 NA microscopic objective. The inscription was performed using transverse writing geometry, where the sample is translated perpendicular to the beam propagation direction with a sample translation speed ranging from 0.5 mm/s to 5 mm/s. In order to fabricate the microfluidic channel, multiscan irradiation of the focused femtosecond laser with pulse energy of 550 nJ at a translation speed of 5 mm/s with a scan interval of 0.4 µm was used.  To enhance the etching rate of the laser modified track, beam polarization direction was perpendicular to sample translation. The inlet and outlet of diameter 360 µm and length 1 mm are written at the end facets by irradiating multiple circles with same radii and with a pitch of 0.5 µm. This allows the hydrofluoric acid to flow through the two end facets thereby allowing the etching process to start progressively from the end faces. The inlet and outlet diameters are designed to match the outer diameter of the polyetheretherketone (PEEK) tubes (Upchurch Scientific Tubing).

Figure 4.4 shows the top view images of the device (a) before and (b) after etching taken using Canon DS126181 camera attached to the microscope (Leitz Ergolux). The optical waveguides were directly inscribed in the sample using multiscan technique, in the same femtosecond laser irradiation step for microchannel fabrication. The waveguides were optimised for low loss at 980 nm and written 300 µm below the surface and positioned orthogonally to the microfluidic channel. An insertion loss of 2.27 dB/cm was measured for a waveguide written with pulse energy of 170 nJ and scan speed of 2 mm/s.  After the inscription process, the chip was immersed in an ultrasonic bath containing 10% HF for 5 hrs to etch the device.  A cross section of $60 \times 76$ µm was obtained for the straight channel after etching process.
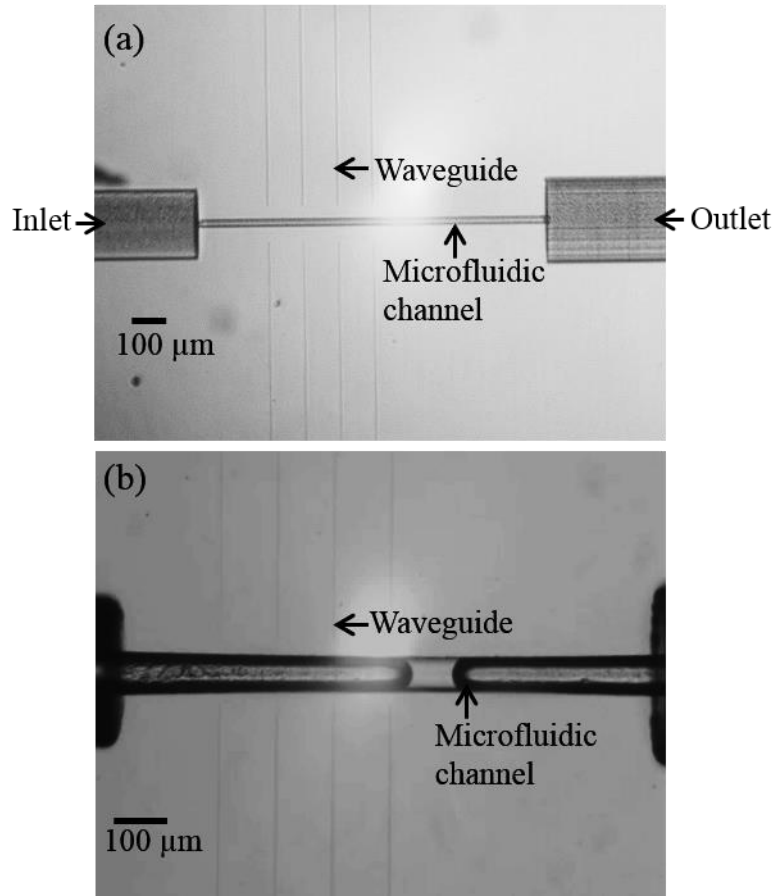
Figure 4.4 Top view microscopic images of the device, a) after inscription of waveguides and microfluidic structures, b) after chemical etching.

After the etching and cleaning process, the end of the waveguides were polished to optical quality and finally bonded to the single mode fibre. The chip to external fluid connection was achieved by inserting PEEK tubes of outer diameter 360 μm into the inlet and outlet ports. The tubing is glued and fixed to the chip using UV curable resin. A CW diode laser with an output power of up to 500 mW operating at 980 nm is coupled through a single mode optical fibre to the laser-inscribed waveguide. Figure 4.4 shows the microscopic image taken using plugable USB-2 Micro- 200 x USB microscope, of the operational optofluidic device with the inlet and outlet attached to PEEK tubing and an optical fibre coupled to the ULI waveguide.

As shown in figure 4.5b, for precise positioning and coupling of the fibre to the waveguides, the fibre is firstly glued into a V-groove using UV curable resin, then butt

coupled to the facet of the inscribed waveguide. The cross sectional view of V-groove with the SMF placed in the groove is as shown in figure 4.5a.
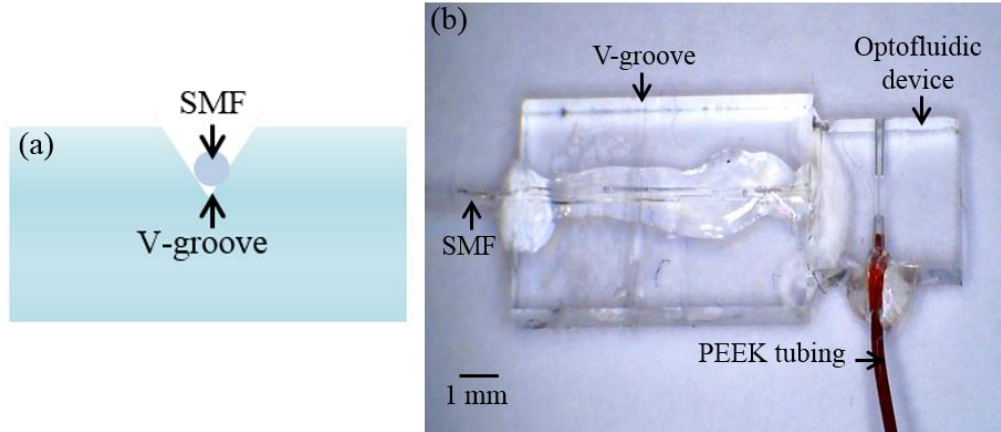


Figure 4.5 a) Schematic illustration of the cross sectional view of V-groove with SMF placed in the V-groove (Not to scale). b) Optofluidic device with inlet sealed with PEEK tubing and waveguide coupled to single mode fibre (SMF).

The V-groove is fabricated on the surface of fused silica also using ULI and chemical etching. The inlet PEEK tube is connected to milliGAT microfluidic pump (Aquilant Scientific (Presearch)), enabling control of the fluid flow through the microfluidic channel. The chip is mounted on a fluorescent microscope (Nikon Eclipse E600) to investigate the device performance.

### 4.3.3   *Experiment, Results and Discussions*

The experimental results that demonstrate the use of the optical scattering force to control and manipulate single particles in a population, within a flow, are discussed in this section.

To validate the performance of the device, fluorescent polystyrene microspheres of 2 μm diameter (Polysciences) were pumped in to the chip with a controlled flow rate. The sample was filtered with a syringe filter before pumping in to the device to avoid any dust particles and particle clusters blocking the channel. Due to the small dimensions of the microfluidic channel, the fluid flow through the device can be characterised using laminar flow.

Since no turbulence occurs at such small scale, the laminar flow provides a means by which particle can be transported in a relatively predictable manner through microchannels. Thus, particles inside the channel are thought to follow a specific stream line (data not shown). Figure 4.6 shows the distribution of 2 µm particles across the width of the microfluidic channel. Under the laminar flow conditions, with no external forces particles were randomly distributed across the width of the channel, as shown in the figure 4.6.
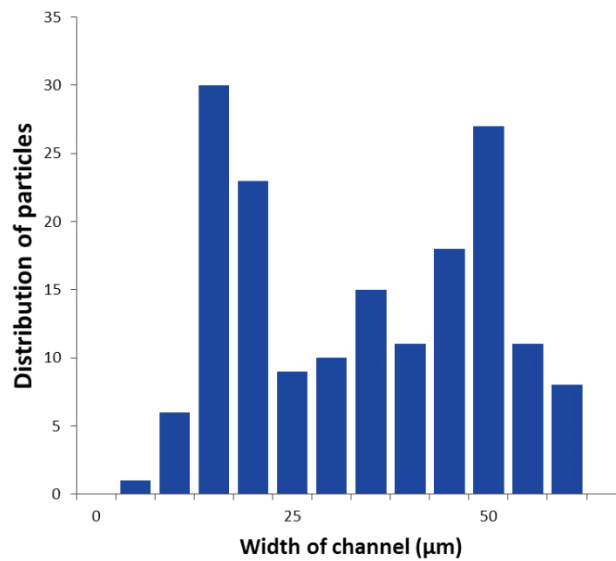


Figure 4.6 Histogram plot showing the distribution of particle within the straight channel.

In straight channel with a rectangular cross section, it was previously shown that the randomly distributed microparticles flowing at sufficiently high velocities migrate to two equilibrium positions centered at the long face of the channel as a result of the lateral lift forces [101]. The key parameters for confining particles to equilibrium positions includes channel dimensions and aspect ratio, particle diameter and flow rate. The lengths of the channels required for focusing to an equilibrium position varies for different particle sizes. For a 2 µm particle flowing at a high velocity, the critical channel length required for focusing is of the order of 10 cm [102]. In the experiment from figure 4.5 and the following experiments using the straight microfluidic channel device, the particles are flowing at relatively lower velocity. In addition, the channel length is ~1mm. As the length and flow rates used do not meet the criteria for focusing,

a random distribution of particles across the channel width (figure 4.6) and height can be expected.

We aimed to study the effect of laser power on the lateral displacement of cells and microspheres out of their flow and along the axis of the incident beam, and how different flow velocities in the channel affected this result. The optical deflection of individual particles was achieved by coupling the embedded waveguides to a 975 nm laser diode with maximum power of 500 mW. When particles flow past the waveguide, the scattering force induced by the laser beam pushes the particle along the propagation direction of the incident beam. The validation test for different laser powers and flow velocities were performed and recorded for further data analysis. Figure 4.7a shows the graphical representation of the lateral displacement of 2 µm polystyrene beads caused by different laser input powers for a given particle velocity of 33 µm/s and b for different particle velocities with a laser power = ~ 250 mW. The presented data is only for particles which were flowing within ±10 µm from the centre of the channel across the width.

The experimental data for lateral displacement of particles is compared with the theoretical predictions derived from Eq. (4.2) and is presented in figure 4.7a and b. Numerical analysis of lateral displacements was performed for particles flowing with velocity, $U = 33$ µm/s subjected to different laser powers with the fixed conditions, refractive index of medium water $n_0 = 1.33$, viscosity of water, $\mu = 10^{-3}$ Nsm$^{-1}$ and for $Q = 0.033$. The laser beam radius $\omega_0$ at the centre region of the channel was calculated by estimating the divergence angle from the inscribed waveguide. For a single mode waveguide with core radius 2.5 µm, assuming that the V-number is 2.405, the numerical aperture of the waveguide is estimated as 0.149. The divergence angle is then calculated using the equation,

$$NA = n \sin \theta \qquad (4.3)$$

where refractive index $n$ of the medium (glass) is 1.45. From Eq (4.3), the divergence angle $\theta$ is obtained as 5.89º. Accounting for the refraction at the glass water interface, where refractive index of the water is 1.33, we estimated the width of the laser beam. In the theoretical model the beam is assumed to be of constant width, but in this experiment it diverges. To take this into account we calculated the beam width for the

65

centre of the channel where the particles are focused and also calculate the width ±10 um from the channel centre, to take into account particles flowing within this region. The laser beam radius at the centre of the channel was calculated to be 8.9 µm. At +10 µm from the centre of the channel it was calculated to be 10.1 µm and at -10 µm the beam radius was calculated to be 7.8 µm. The standard deviation in average displacement for different $\omega_0$ is represented as error bar in the theoretical model as shown in figure 4.7a and b.
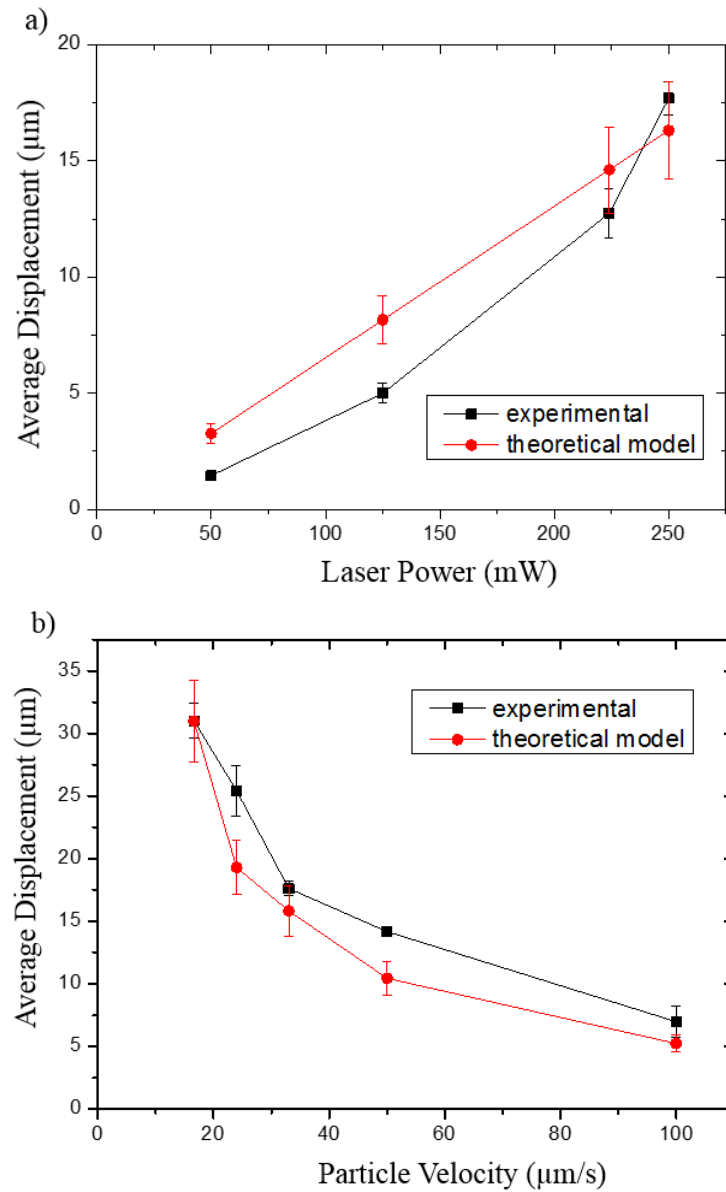


Figure 4.7 Lateral displacement of 2 µm fluorescent beads, a) for different incident laser power but a constant particle velocity of 33 µm/s, b) for different particle velocities but a constant laser power of 250 mW. Error bars represent the standard deviation in average displacement of particles.

As can be seen from the figure 4.7a, particles flowing with a velocity of 33 µm/s are displaced along the direction of propagation of the incident beam. The displacement is found to increase with the laser power which is in good agreement with the expression in Eq. (4.2). The experimental measurements of the lateral displacement of particles are in reasonable agreement with the theoretical predictions. The slight variation from the predicted values are due to the change in laser beam width of the diverging beam (as the model assumes a collimated beam) as well as the error in estimation of laser power at the channel. In addition, as we would expect, the lateral displacement of particles is found to be decreasing with an increase in particle velocity. Figure 4.7b presents the comparison between the experimental and theoretical measurements of lateral displacement of particles flowing at different velocities, at a given power in the channel of $P = ~ 250$ mW. The measured displacements are in reasonable agreement with the theoretical analysis. An increase in the flow velocity reduces the length of time the particle stay in the optical manipulation region resulting in decrease in the displacement of particle. These results suggest that the lateral displacement of the particle can be controlled by changing the incident laser power as well as the flow velocities. Also the results confirm that the velocities of particles can be increased to the desired value, provided that the incident laser power is proportionally increased.

After investigating the functioning of the device with fluorescent polystyrene beads, microalgae (*Chlorella vulgaris*) cells of 2 µm diameter, were introduced into the channel. The deflection of individual cells travelling at different flow velocities was monitored for constant laser output power. Figure 4.7(a, b) is a sequence of images from the fluorescent microscope showing deflection of microalga out of the path of their original trajectories and along the waveguide beam propagation direction (perpendicular to the flow). Figure 4.8a shows a cell moving with a flow velocity of ~5 µm/s which was found to deflect ~41 µm along the beam propagation direction, on applying a beam with laser output power of ~ 250 mW. In figure 4.8b, using the same beam power, a deflection of only ~ 4 µm was observed for a cell flowing with a velocity of ~100 µm/s. The distance that cells were displaced from their path was measured for different flow velocities of the cells and several beam powers. In total tens of cells were measured in this experiment and as expected the slower flow rates and larger beam powers resulted in larger deflections from the cell's original path. Thus by controlling the laser output power and flow velocities, *Chlorella vulgaris* microalgae flowing through the

microfluidic channel could be controllably displaced in the direction of beam propagation from the flowing stream line into a new path within the same flow.
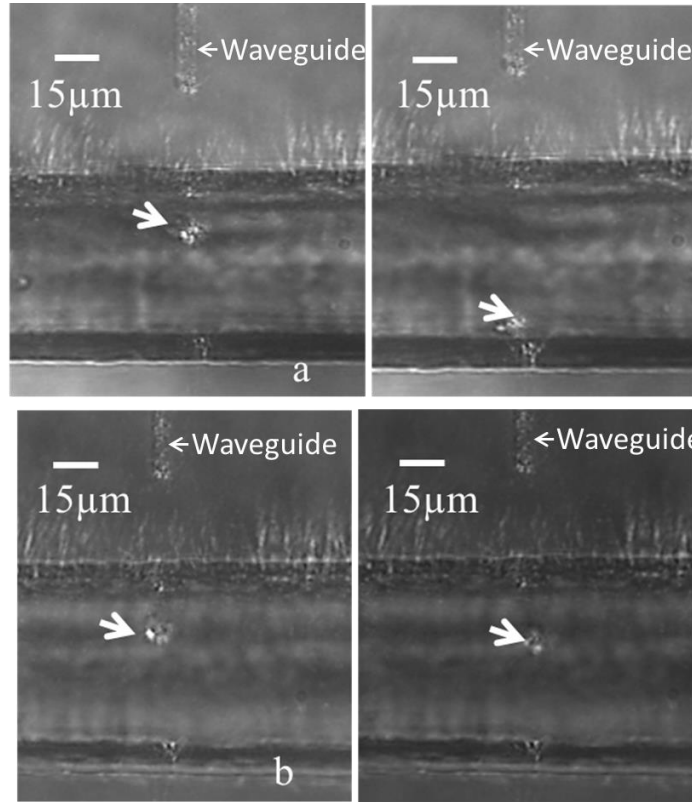


Figure 4.8  Snapshot image showing deflection of alga cell in direction of beam propagation by optical scattering force. a) Cell flowing with a velocity 5 μm/s deflected a distance of ~41 μm.b) Cell flowing with a velocity 100 μm/s deflected a distance of ~4 μm.

A comparative analysis on deflection of algae and polystyrene also shows that at same incident laser power and particle velocity, polystyrene beads are found to displace more compared to algae cells. The reason for this is lower refractive indices of cells compared to beads, resulting in a comparatively lower optical force on cells [95].

The objective of the study, to demonstrate the control and manipulation of micron sized particles using optical force was achieved using this 3D optofluidic device. The preliminary results obtained from the investigations have provided very useful information on the effect of laser power and flow velocities for controllably displacing micron sized particle within microfluidic channel. The scattered distribution of particle and cells across the width and height of the channel resulted in a limited number of

particles passing through the beam that emerges from the waveguide. The particles and cells flowing close to channel walls were also found to stick to the channel walls, significantly increasing the risk of clogging the channel. To overcome these limitations a more complex 3D device capable of confining the particle in to a narrow stream was designed for improving the selectivity and efficiency of manipulation. The design, fabrication and validation details of the device are discussed in the following section.

## 4.4  Hydrodynamic focusing in microfluidics system

From the investigations on manipulation of micron sized particles in microfluidic channel discussed in the previous sections, it is clear that the integrated devices with optical and microfluidic components provides a favourable platform for manipulating particles, but an issue to be addressed is to ensure all particles or cells pass the beam to ensure efficient deflection (when the optical scattering force is to be used), or analysis (if an optical signal is to be excited or detected). To ensure a higher efficiency in single cell manipulation it is important that the optofluidic system should allow one particle at a time to flow through the detection or manipulation region. This can be accomplished by sequentially arranging the particles in a confined volume and controlling the flow of this volume through the optical interrogation region. One of the approaches that can be employed for confining the particle is by making the channels as small as the particle size, of the order of a few micrometres. The disadvantage of reducing the channel dimension is that it will increase the risk of clogging the channels by particles, or damage to the particles. Another approach that can be implemented in microfluidic system for particle confinement is hydrodynamic flow focusing of the sample flow in to a narrow stream. In general, hydrodynamic focusing is a technique in which focusing of a sample fluid is achieved in a channel using a sheath flow at relative flow rates. Figure 4.9 shows the schematic illustration of hydrodynamic flow focusing.
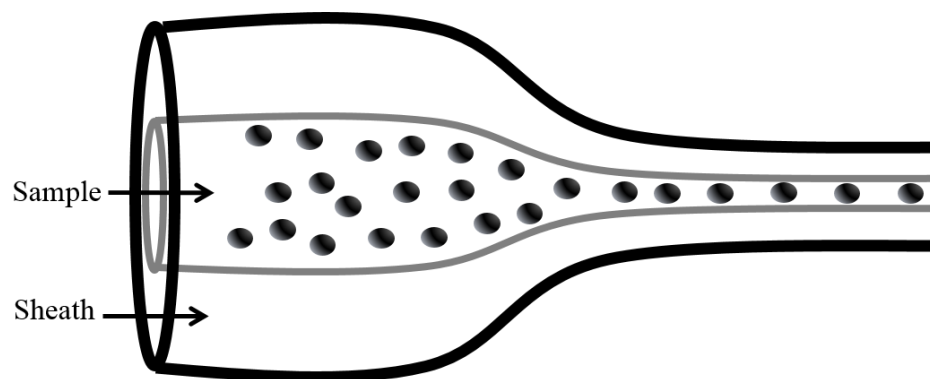
Figure 4.9 Schematic illustration of Hydrodynamic flow focusing.

The fluidics system consists of a centre core region, through which the sample fluid is injected. This centre core is enclosed by a sheath fluid which is injected to the system at a slightly higher flow rate relative to the sample flow rate. As the sheath fluid moves faster than the sample fluid, it creates a massive drag effect that in turn causes narrowing of the centre core region allowing the creation of a single file of particles, as shown in figure 4.9. This technique is employed in flow cytometry as a way to deliver the sample (containing suspended cells) to the optical detection system in an appropriate form, enabling high speed and high throughput counting, analysis (cytometer) or sorting (FACS) of the cells [103]. Over the past decade, hydrodynamic focusing techniques have been successfully employed in microfluidic devices opening new opportunities for developing novel particle /fluid control and manipulation schemes. Such microsystems are effectively used in a wide variety of applications such as microfluidic based flow cytometers for cell/particle sorting and counting [104], microparticle productions [105] and bubble or droplet generation [106] .

In conventional 2D flow focusing techniques, sheath flows from two inlet channels on both sides of the sample inlet are used to confine the sample stream horizontally around the centre of the channel  [107]. In this case, particles are localised in to a small volume with minimal interaction between the sample and the channel walls. Although this geometry allows the positioning of a small volume of the sample through the detection region, a random spread of particles across the vertical direction (across the channel height) results in a significant number of undetected particles. In addition, as the sample is not completely isolated from the channel wall, there exists risk for the cell or particles to become attached to the channel walls, causing difficulties in measurements. 3D flow

focusing techniques, on the other hand, enable confinement of particles in both horizontal and vertical directions, thereby overcoming limitations possessed by 2D flow focusing. In general, 3D flow focusing of sample fluid can be achieved by injecting the sample in to a coaxial flowing sheath fluid, in such a way that the sample fluid is enclosed by the sheath from all around. By maintaining a relative flow rate between sample and sheath fluids, confinement of sample fluid in the vertical and horizontal directions occurs. Goranovic *et al.* in 2001 [108], demonstrated the implementation of 3D flow focusing in microfluidic system using a chimney like structure enabling 3D sheathing. Later in 2004 Sundararajan *et al.* [109] demonstrated 3D flow focusing in a PDMS device, fabricated using micromolding methods. In subsequent years various other 3D designs and geometries of microfluidic channel networks were implemented and fabricated in a variety of material using different fabrication techniques and used in various applications [110-112]. Although these techniques are efficiently tested to be used for different applications, the fabrication techniques to implement 3D functionalities in these devices involve complicated and multistep fabrication procedures. In addition, for detecting or counting particles flowing through the microchannel, an external optical system is used in conjunction with the flow focusing system, which requires precise alignment. Most recently Paie *et al.* [31] utilised the direct 3D writing capability of ULI and selective chemical etching to fabricate a complex 3D microfluidic channel network that can implement hydrodynamic focusing. The monolithic device, fabricated in fused silica consisting of integrated waveguides and 3D flow focusing, was demonstrated to use as an integrated cell counter. In the present study for optical manipulation of particles and cells, we adopted the device design for three dimensional flow focusing from Paie *et al.* [31] as shown in the figure 1.5 of chapter 1. The waveguide inscribed within the Paie's device is used for detecting particles flowing past the laser coupled waveguide, thereby enabling counting of the number of cells. The embedded waveguide within our device is used for delivering laser light to optically manipulate the cells flowing within the focused sample flow. In addition, the channel dimensions as well the sample inlet channel geometry of our device is different from the device as shown in figure 1.5. The detailed discussion of the channel geometry of the device and optimisation of the device to use for manipulation and separation of cells and particles is discussed in the following sections.

## 4.5 Integrated optofluidic device for 3D hydrodynamic focusing and optical manipulation

The direct writing capability and method simplicity of ULI fabrication technology has been utilised to fabricate complex 3D microchannel structures for implementing hydrodynamic flow focusing [31]. Moreover the ability to integrate waveguide structures to these microfluidic systems promises to offer a favourable platform for single particle manipulation with improved efficiency. This section details the design fabrication and validation of a compact, 3D, optofluidic device that presents a new route for particle and cell manipulation using optical scattering force. The 3D flow focusing capability of the device was investigated by analysing the confinement of focussed flow in the horizontal and vertical directions. After this device characterisation, a detailed analysis on the manipulation of focused particles using optical radiation from a laser source coupled to an embedded waveguide has been performed. Furthermore, size based particle sorting and single cell isolation potential of the device has been investigated and presented in section 4.6.

### 4.5.1 Device design and working principle

Figure 4.10 represents the design of our proposed device. A network of appropriately designed microfluidic channels and optical waveguides constitutes the main components of the device. The three dimensional microchannel networks within the device are designed to implement hydrodynamic focusing of the sample fluid, which forms the key functionality of the device. The waveguide in the device is used for delivering the laser beam to manipulate the particles or cells passing through the channel. The sheath and sample inlet channels of the device constitute the path for sheath and sample fluids, respectively. The sheath inlet channel is split in to two horizontal and two vertical curved channels depicted as H1, H2, V1 and V2, respectively in figure 4.10. The sample inlet channel is designed to meet at the junction were the curved inlet sheath channels meets the outlet channel. The connection from the intersection point of curved channels to the sample inlet channel is achieved by using an angled channel.
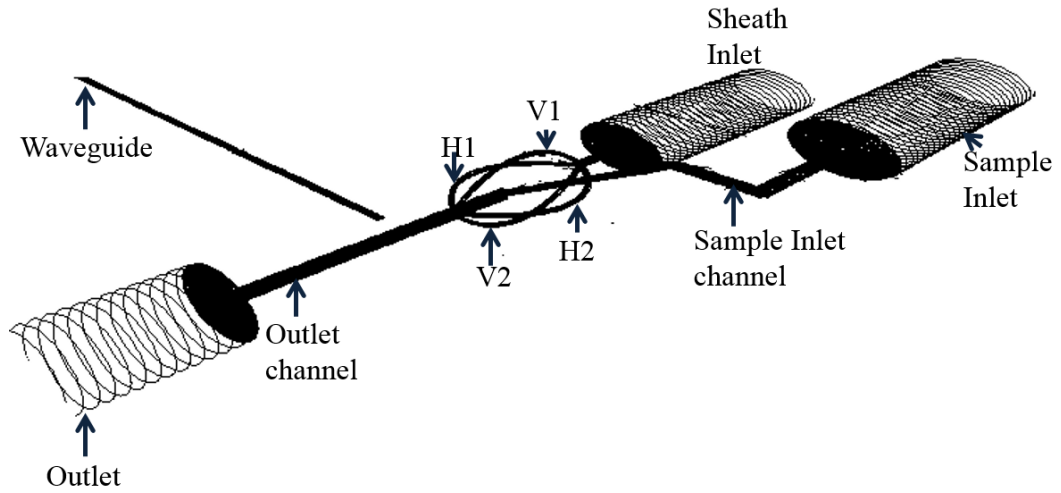
Figure 4.10 Schematic illustration of the laser trajectory of the device design plotted using N-plot software (not to scale). Sample fluid and sheath fluids are injected into the respective channels through sample and sheath inlets. H1 and H2 represent the horizontal, curved, sheath channels. V1 and V2 represent the vertical, curved, sheath channels. Outlet channel constitutes the path for the focused sample flow enclosed by sheath fluid. Waveguides are position orthogonal to the main outlet channel.

The 3D flow focusing of the sample fluid is achieved using the four lateral flows coming from the curved, sheath, inlet channels, by precisely controlling the sample and sheath fluid flows. The width of the focused sample at the outlet channel can be tuned by controlling the relative flow rates of sheath and sample fluids. In this way the suspension of particles or cells injected through the sample inlet can be sequentially arranged and aligned with the integrated optical manipulation system, ensuring an increased efficiency in manipulation and accuracy in the measurements.

### 4.5.2   Device fabrication

The device fabrication was carried out using the ULI setup discussed in Chapter 3. The first step involved in fabrication is the inscription of preprogrammed 3-D pattern of the device design, shown in figure 4.9, within the fused silica substrate using femtosecond laser pulses. This was achieved using a commercial variable repetition rate Yb-doped master oscillator power amplifier system (IMRA FCPA µ-jewel D400) delivering 1047±10 nm pulses at a repetition rate of 500 kHz. A 0.4 NA (aspheric objective) has been used to focus 356 fs laser pulses within the substrate. The accurate translation of the sample through the laser focus using the automated XYZ air bearing translation

stage allowed us to precisely write the 3D microfluidic channel network structures and waveguides as discussed in the device design in section 4.5.1.

A 3D frame with dimension of $6 \times 4.8 \times 2$ mm was laser written at the bottom surface of a 2 mm thick fused silica sample. The inlet and outlet ports of length 1.3 mm and diameter of 360 μm were written at the end facets by irradiating multiple circles of same radii with a pitch of 0.5 μm using laser pulse energy of 680 nJ. The 3D modification for all the microfluidic channel structures was achieved by modifying the outline of the structure. The base of the channel was written by scanning the laser focus along a rectangular path of desired length and width followed by a multiscan rastering of the bottom surface with a scan offset of 0.4 μm between each scan. After the multiscan rastering of the bottom surface, the laser focus spot was scanned along through multiple rectangular planes, each with an incremental movement until the top surface of the channel was reached. The top surface was then written using multiscan technique with a scan interval of 0.4 μm. The 3D curved inlet structures were also modified using same method. All the microfluidic channel structures were written using 680 nJ laser pulse energy at a sample translation speed of 1 mm/s. The polarisation state of the inscription laser was perpendicular to the sample translation direction so as to enhance the chemical etch rate.

The waveguides were written perpendicular to the outlet channel using multiscan technique with laser pulse energy of 234 nJ and translation speed of 1.5 mm/s. The femtosecond irradiation of the 3D pattern was then followed by selective chemical etching process in hydrofluoric acid (HF) leading to the preferential removal of the laser modified tracks to produce microfluidic structures. The device was immersed in 10% HF diluted in DI water for ~10 hours. The end facets of the etched device were polished and then cleaned using mixture of acetone and IPA using to remove the residual HF. Figure 4.11 shows the scale of the fabricated optofluidic device.

Figure 4.11 Optofluidic device in fused silica: Dimension $6 \times 4.8 \times 2$ mm. The chip dimension compared with 5 pence coin.

Figure 4.12 (a, b) shows the side and top and side view optical microscope images of the device, respectively. The sheath inlet port, H1and H2 inlets, outlet channel and the outlet port were fabricated 500 µm beneath the top surface. The sample inlet ports as well as the sample inlet channel were written 1 mm beneath the surface. An easy connection between sample inlet channel and the outlet channel was achieved by an angled channel. Figure 4.12c shows the magnified view of the outlet region. The outlet channel of cross section $75 \times 135$ µm and waveguides written perpendicular to the outlet channel together constitute the particle manipulation region of the device. The distance between waveguide end facet and channel centre is ~50 µm.

As shown in the figure several waveguides were written at different depths across the outlet channel. This offered flexibility in using different waveguides for manipulation depending on position of flow focusing in vertical direction, ensuring higher accuracy in manipulation. Figure 4.12d shows the top view image and cross sectional view of the horizontal and vertical inlets. These channels possess almost symmetric cross sections with width $71 \pm 1.8$ µm and height of $106 \pm 4.5$ µm.
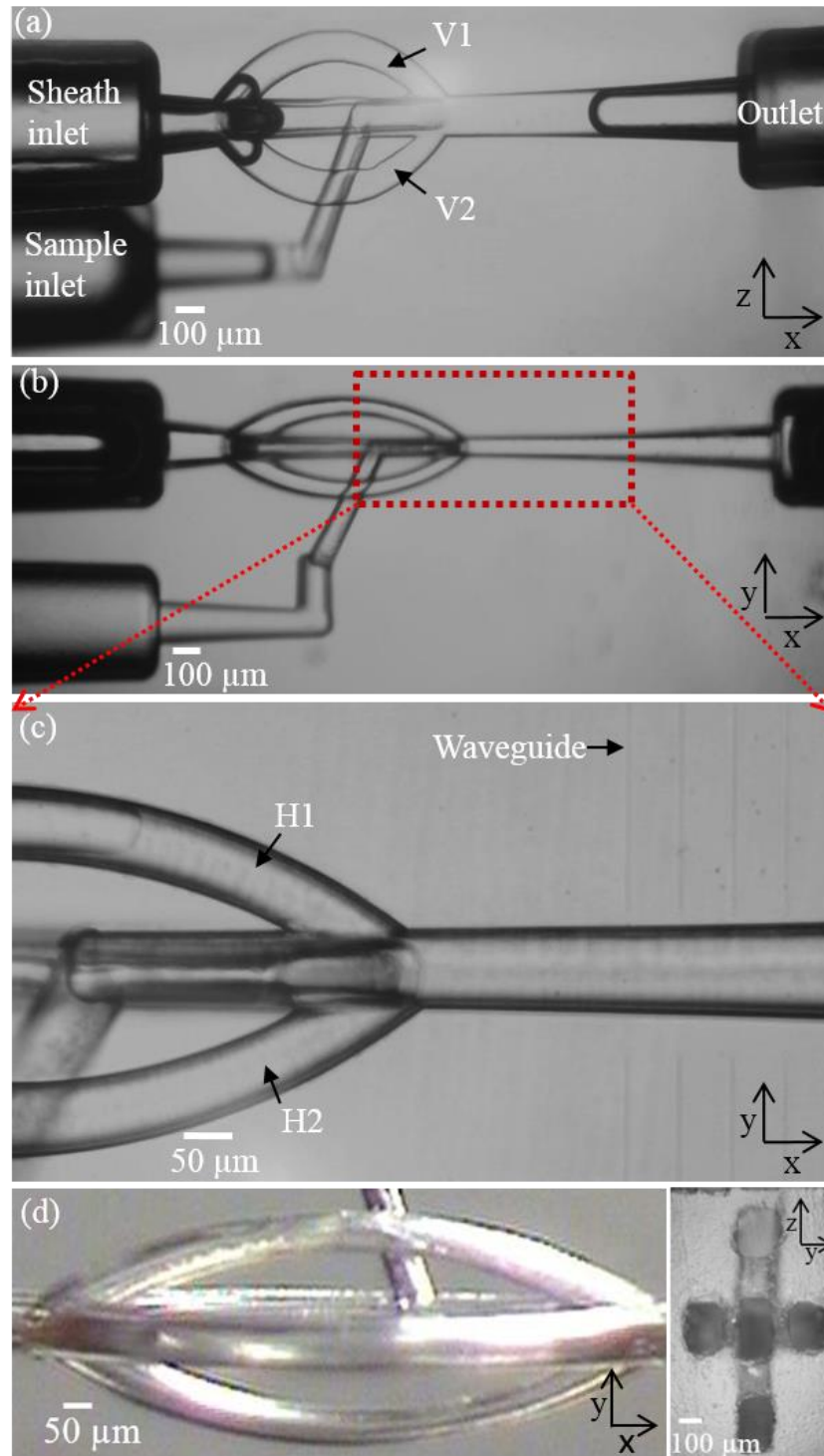
Figure 4.12 Microscopic images of the fabricated device, a) Side view image, b) Top view image, c) top view image showing waveguides and outlet channel that constitute the manipulation region. d) Left hand side; Top view of the sheath inlet and right hand side; the cross sectional view of the sheath inlet. H1, H2, V1 and V2 represent the horizontal and vertical sheath inlets respectively and the centre channel is the cross section of sample inlet.

## 4.6 Experiment, Results and Discussion

This section details the different experiments performed using the device including flow focusing characterisation and the manipulation of particles and cells within the focused flow using optical scattering force. The results obtained from these experiments along with the potential of the results to use such a device for single cell manipulation are discussed in detail. All the experiments were performed using the setup detailed in section 3.3 of chapter 3.

The 3D hydrodynamic focusing capability of the device was first demonstrated by monitoring the flow in the outlet channel. The control of sheath and sample fluid flow was achieved using syringe pump (Harvard Instruments) and pressure driven pump (Fluigent, Measflow). The syringe pump was utilised in experiments to initially demonstrate flow focusing and studies on how the width of focused flow could be controlled with respect to input flow rate ratios. The chip to pump connection was realized by using PEEK tubing's (IDEX Health & Science). The confinement of the sample flow was visualised using a CCD camera (ProgRes CCD SpeedXT core5, Jenoptik). The discussion of the results obtained from the flow focusing validation experiment is detailed in section 4.6.1. After demonstrating hydrodynamic flow focusing in the device, experiment to demonstrate the optical manipulation of micron sized particles flowing in the sample flow was performed. For manipulating individual particles, the laser beam from a cw Nd:YAG laser source (Ventus, Laser Quantum) operating at a wavelength 1064 nm with a maximum output power of 3W was coupled on to the embedded waveguide. A pressure driven pump enabled control of the flow inside the chip at a very low rate. The live monitoring of the experiment was performed by using Canon EOS 600D. For further analysis, the videos of the experiments were recorded and trajectories of particles within the microfluidic channel were tracked using MATLAB (MathWorks).

### 4.6.1 Demonstration and characterisation of 2D and 3D flow focusing in the device

The 2D and 3D hydrodynamic focusing performance of the device was validated using polystyrene microspheres, coloured dye and cells through visualizing the focusing from top and side facet of the device as represented in figure 4.13 and figure 4.14.

(a)



(b)
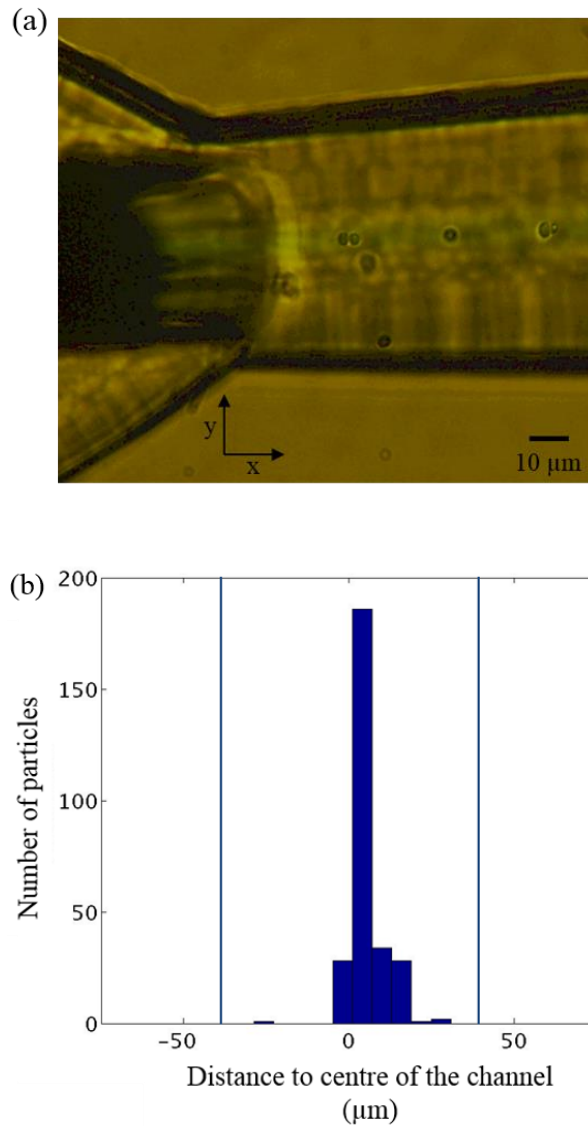


Figure 4.13 Validation of confinement of sample fluid. a) yeast cells and blue dye along the horizontal plane, b) Distribution of yeast cells with respect to the distance from channel centre. Blue line represents the channel wall across the horizontal plane.

Figure 4.13 a represents the horizontal focusing of cells and dye. To achieve this, sample fluid consisting of *Saccharomyces cerevisiae* (Baker's yeast) suspended in DI water was injected through the sample inlet of the device. For better visibility of the width of the focused flow, a blue coloured dye was mixed with the sample suspension. DI water served as sheath fluid for confining the sample fluid. A focused flow of yeast cells and dye was achieved in horizontal and vertical planes by maintaining the relative sheath to sample input pressure ratio as 5:2 mBar. For the same input pressure ratio, a width of the focused flow along the horizontal plane of 7 µm was obtained.

Figure 4.13b presents the distribution of yeast cells in horizontal plane with respect to the distance from channel centre
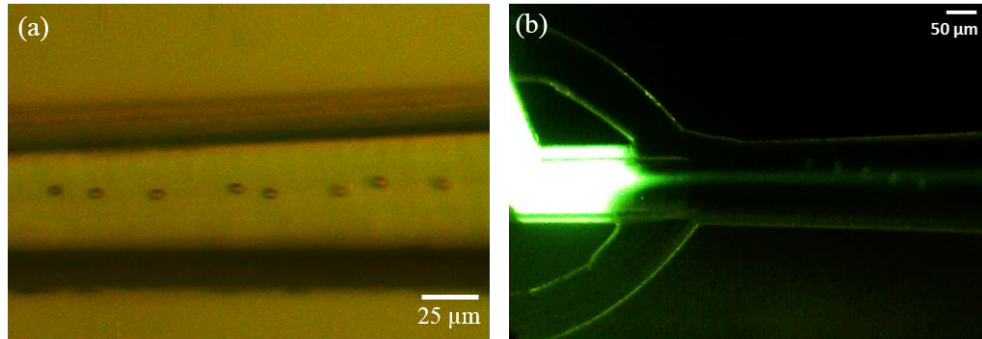


Figure 4.14 Flow focusing a) 5 µm spheres in horizontal plane, b) Fluorescent dye in vertical plane,

Figure 4.14 a and b shows the confinement of 5 µm polystyrene beads and fluorescence dye in horizontal and vertical planes, respectively, using DI water as sheath fluid. A focused sample flow of 12 µm was achieved along the vertical plane at a relative sheath to sample input pressure ratio 5:2 mBar. The flow focussing images along with the distribution plot of particles confirms that the presented geometry for flow focusing is efficient in confining particles in to a small volume. An effective manipulation of particles flowing in the confined flow can be achieved by coupling laser light into the embedded waveguide which is in same plane as the confined flow along the vertical axis, thereby adding to the manipulation capability by using optical forces.

A study on control of the width of focused flow with respect to the change in relative flow rate ratios was performed. To do so, blue coloured dye diluted in DI water was injected at the sample inlet using a syringe pump and DI water at the sheath inlet was injected using a second syringe pump. The sheath flow rate was kept at a constant flow rate of 5 µL/min. The width of the focused dye was then measured at the outlet channel for four different sample flow rates ranging from 9 µL/min to 1 µL/min. The control of fluid and sheath flows was using two syringe pumps.

In order to predict the width of the hydrodynamically focused sample stream along the horizontal plane squeezed by neighbouring sheath flows, the theoretical model proposed by Lee *et al.*[113] based on conservation of mass, was used. It is assumed that the fluid

flow is Newtonian. Due to the laminar nature of flow the diffusion and mixing effects between focused sample flow and the sheath flows are ignored. For a microfluidic system as shown in figure 4.15,
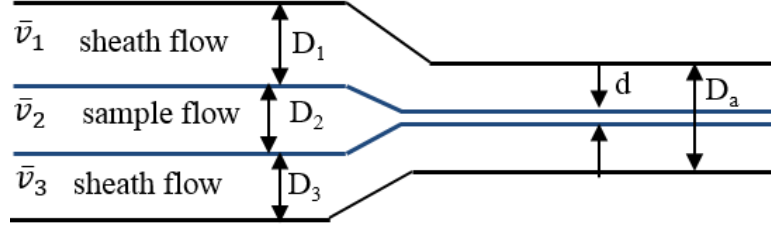


Figure 4.15 Schematic representation of focused sample flow confined by coaxial sheath flow.

The width of the focused stream $d$ is given by,

$$d = \frac{\rho_a D_a}{1.5\left(\rho_1 \frac{\bar{v}_1 D_1}{\bar{v}_2 D_2} + \rho_2 + \rho_3 \frac{\bar{v}_3 D_3}{\bar{v}_2 D_2}\right)} \qquad (4.4)$$

where $d$ is the width of the focused sample stream, $\rho_a$ is the average fluid density in the outlet channel, $\rho_1$, $\rho_3$ and $\rho_2$ are the densities of fluids in two sheath inlets and sample inlet channels respectively. $D_a, D_1,$ $D_3$ and $D_2$ are the width of outlet channel, two sheath inlet channels and sample channel, respectively. $\bar{v}_1, \bar{v}_3$ and $\bar{v}_2$ are the fluid velocities at the two sheath and sample inlet channel, respectively (figure 4.15). The Eq. (4.4) suggests that the width of the focused sample flow decreases with increase in relative sheath to sample flow rates.

As the fluids in the two sheath and sample inlets are water, the densities are $\rho_1$, $\rho_3$ and $\rho_2 = 1000$ kg/m$^3$. The width of the outlet, two sheath inlet channels and sample inlet channel are $D_a = 75$ μm, $D_1 = 71$ μm, $D_3 = 71$μm and $D_2 = 76$ μm, respectively. Considering a nearly symmetric cross section for sheath inlet channels, flow velocities are $\bar{v}_1 = \bar{v}_3 = 2.8$ mm/s. The value for the width of the focussed flow was predicted by substituting these values into Eq. (4.4) for different sample flow velocities $\bar{v}_2$.
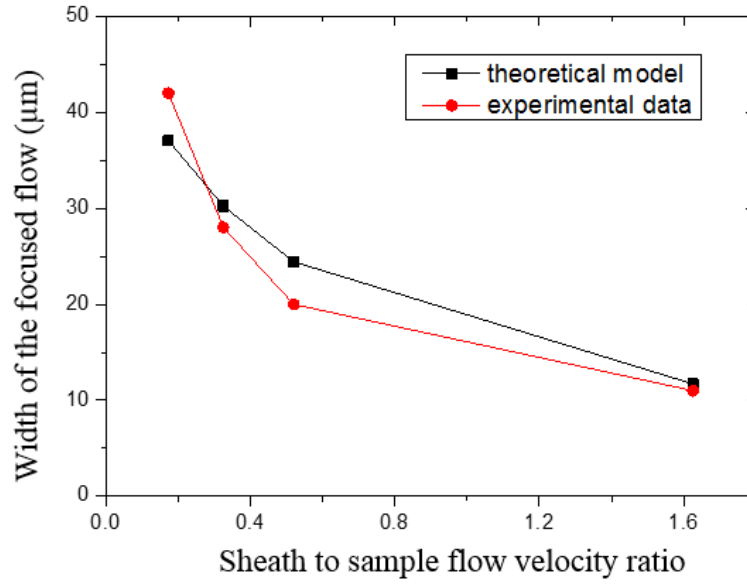
Figure 4.16 Plot showing the change in width of focused flow with respect to relative input flow rate ratios.

Figure 4.16 shows the comparison of experimental measurement and theoretical prediction of change in width of the focused flow with respect to different sheath to sample flow velocity ratios. As expected the width of the focussed flow decreases with increase in the sheath to sample flow rate ratios. The predicted values of focusing width agrees reasonably with the experimental data. Furthermore the trend is consistent with the predicted results derived from Eq. (4.4). A precise control of the inlet sample and sheath fluid flow rates can thus be used to alter the width of the focused flow, promising for use for single cell based studies and when the cells must be well aligned with the integrated waveguide.

In pressure driven microflows through a rectangular microchannel, the relationship between pressure and flow velocities is given by,

$$\Delta P = \frac{12 \eta L v}{H^2} \qquad (4.5)$$

where $\Delta P$ is the pressure drop between the two ends of the channel, $L$ is the length of the channel, $H$ is the height of the channel, $\eta$ is the viscosity and $v$ is the average flow velocity. For zero pressure at the outlet channel of the device, the flow velocity of the particle varies proportionally with pressure at the inlet channel. Therefore when using a

pressure driven flow for the studies with the flow focusing device, a similar trend for variation in focussed flow width as shown in figure 4.16 can be expected with a change in relative sheath and sample input pressure ratios.

### 4.6.2 Manipulation of particles and cells within the device

After confirming the flow focusing capability and related performance of the device in 3D, the device was used for investigating the optical manipulation of micron sized particle using optical force. For these experiments, 5 and 10 um spherical polystyrene beads suspended in DI water were injected through the sample inlet of the device and DI water through the sheath inlet. By maintaining a relative sheath to sample inlet pressure ratio of 5:2 mBar, particles were focused in to a narrow stream, with focusing width = 3.9±2 µm. Optical radiation from the laser was then used to manipulate the focused particles flowing past the laser-coupled waveguide. Investigations on the deflection of particles from the focused flow into the sheath flow for different applied laser power was performed. Videos of the experiments were recorded and used for further analysis. The estimation of insertion loss introduced by the waveguide was done after performing all the validation experiments using the device. The device was cut along the microchannel axis and the transmitted power was directly measured using a power meter. A total insertion loss of 1.76 dB was measured at 1064 nm wavelength.

The videos of the experiment recorded using Canon camera (EOS 600D) at a rate of 50 frames per second were processed using Matlab to extract information on the particle trajectories within the channel and for measuring their respective velocities. The trajectories of particles within the focused flow, i.e before deviation and after deviation caused by optical force were tracked. These tracking results were later used to quantify the average displacements of the particles caused by 5 different laser powers. The Matlab program for tracking the trajectories of the particles was written by Melanie Jimenez (Glasgow University).
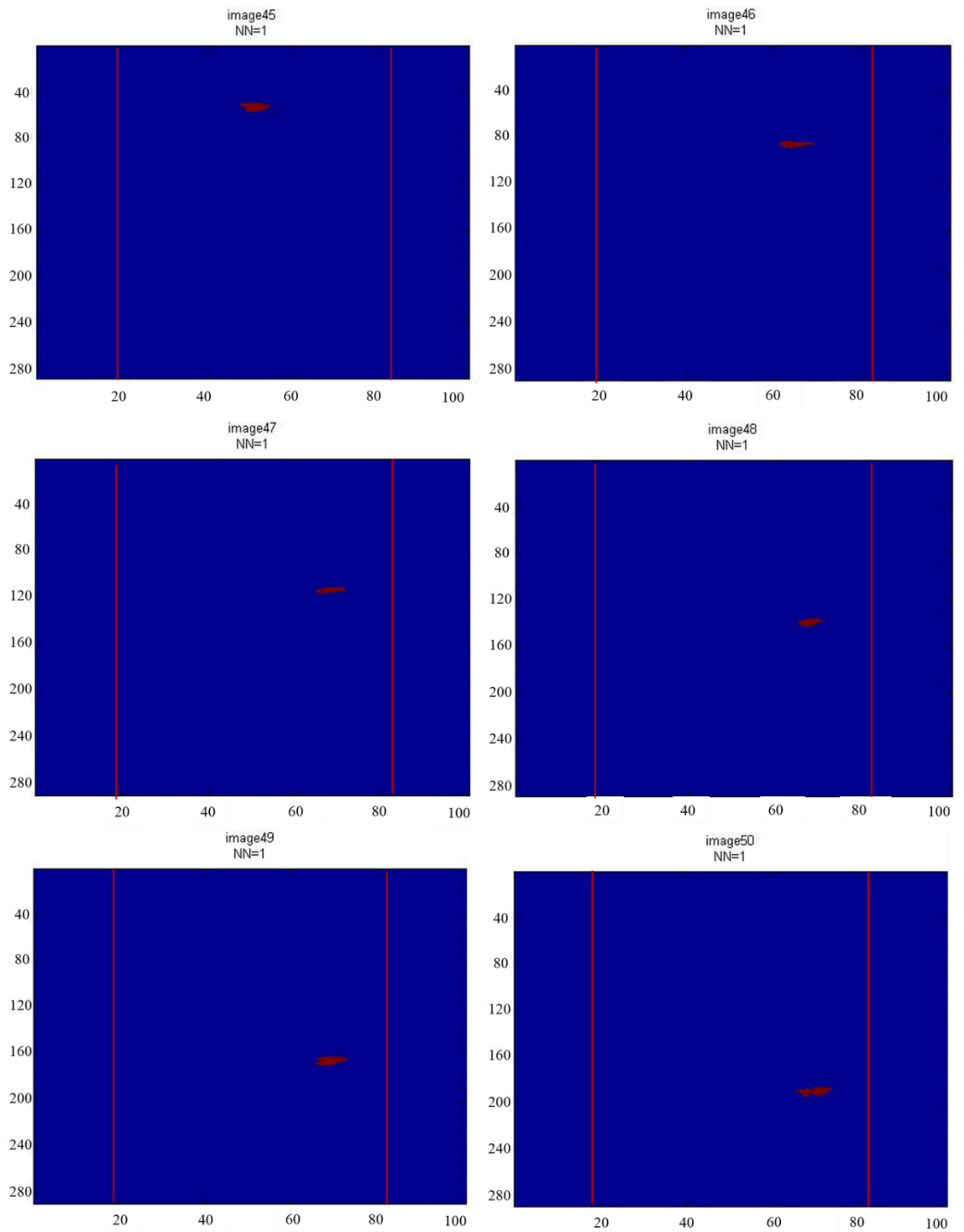
Figure 4.17 Sequence of images indicating the positions of the particle as they move along the microfluidic channel. The axes are the position of particle in micrometers. NN indicates the number of objects being detected. The red line represents the channel walls across the horizontal plane.

Particle trajectories were estimatedby locating single particles in each frame of a recorded video (50 fps). The detection of particles was performed by appropriate thresholding defining the grey level difference between the particle and the surrounding background to binarise the recorded image (0 corresponding to noise and 1 to a pixel with a grey level greated than the defined threshold) and detecting coonected 1-valued pixels using the function *bwlabel* in Matlab.

In order to limit the detection of noise (defined as detected objects that are not particles), a second threshold on the area of detected objects has also been used in accordance to the particle size used for the experiments. After detection, particles are tracked from frame to frame using the open-source particle tracking software proposed by John C. Crocker and Eric R. Weeks [114]. Figure 4.17 shows the sequence of images with positions of particle detected in each frame from image number 45 to 50. The parameter NN is an indication of the number of objects being detected. As shown in the figure, as the particle moves along the channel, the respective position of detected particle is tracked and then linked in to particle velocities using the recording rate of the video.

### *4.6.2.1 Results and Discussion*

This section discusses the results obtained from different experiments performed for validating the optical manipulation of particles using the device. The extracted Matlab data from the videos was used to plot the relation between the average displacements of the particle from the sample to the sheath flow with respect to the incident laser power.

Figure 4.18 shows the trajectories of 5 micron sized particles with the laser off and laser on for an applied power in the channel of 1.5 W. The superposition of trajectories of 34 individual particles when laser ON and 15 particles when lasers OFF are presented in the plot. As shown in the plot, in the absence of optical forces the particles follow a straight trajectory and are confined in a narrow stream with a width of ~ 6 µm. When a laser power of 1.5 W was applied, the particles in the confined flow that are flowing past the laser coupled waveguide were displaced from their original trajectory to the sheath flow. An average displacement of 21.6±4 µm was achieved considering 34

particles, and using applied laser power of 1.5 W. The velocity of the particles was kept constant at 1.4±0.27 mm/s, with a sheath: sample pressure ratio of 5:2 mBar.
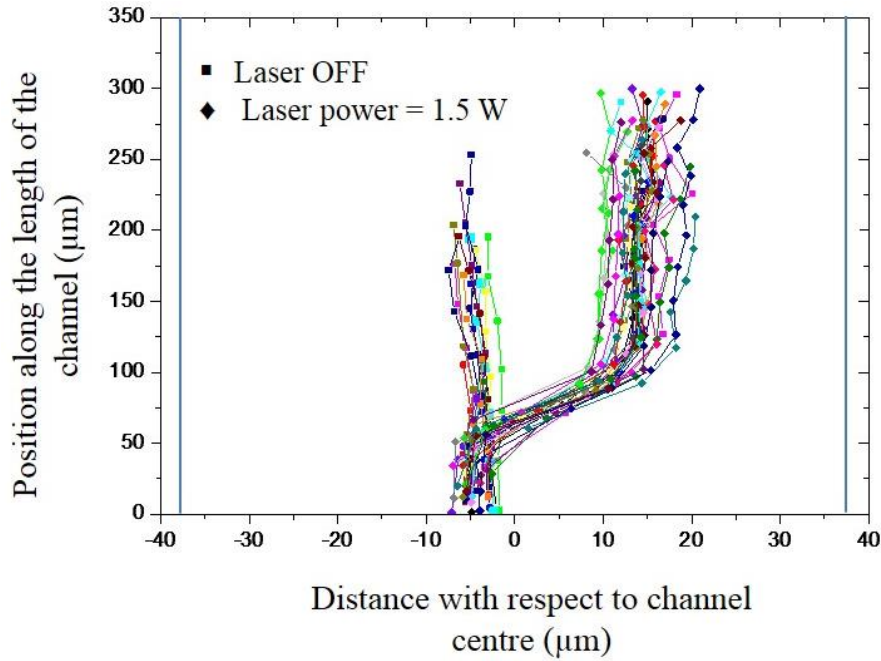


Figure 4.18 Plot showing the trajectories of 5 µm particles flowing in a confined flow at the outlet channel, when laser is off and when laser is on at 1.5 W, Blue line represents the channel wall along the x-y plane.

When laser was ON, all the particles flowing in the confined stream were found to displace into the sheath flow within a range between $y_1$ and $y_2$ along the length of channel. This indicates that the waveguide is positioned between $y_1$ and $y_2$. Therefore an estimation of the interaction length of laser at the centre of the microfluidic channel was performed by taking the difference in position of particles at $y_1$ and $y_2$ in figure 4.19. The interaction length of laser with the particles focused in the sample stream was obtained as, $y_2 - y_1 = 19.9$ µm. Theoretical estimation of beam width was also performed by evaluating the divergence angle of the beam emerging from the end of the waveguide passing through glass and then water. Laser beam width of 19.05±0.8 µm was calculated at the region where particles are confined across the width of the channel as discussed in section 4.3.3. The estimated interaction length of the laser with the particles from experimental data in figure 4.19, and the calculated laser beam width at that position are in close agreement.
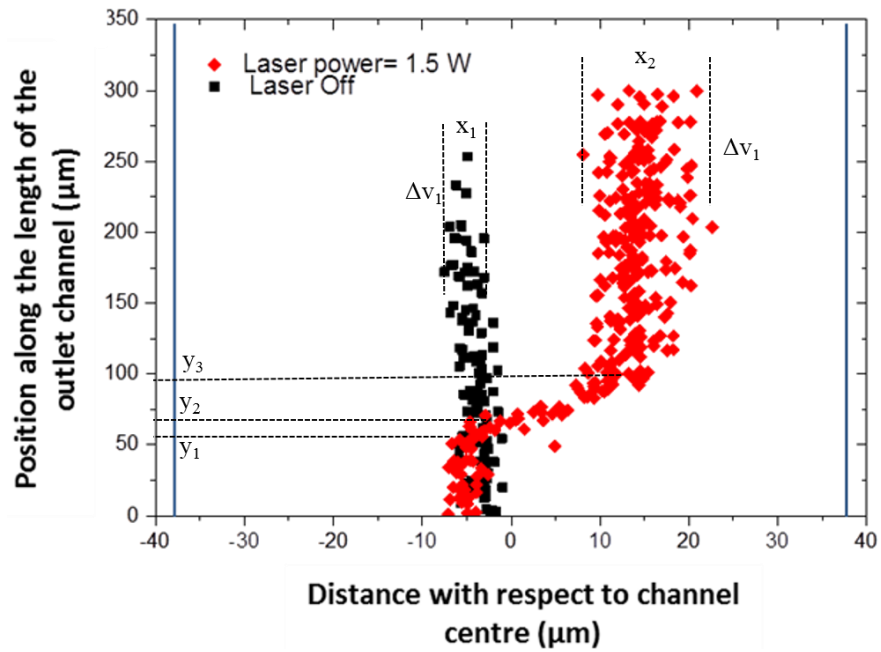
Figure 4.19 Plot showing distribution of 5 µm particles. $y_1$ and $y_2$ represents the positions of the particles along y-axis within which the particles were found to be displaced along the beam axis. $y_3$ represents the position when particles are out of the laser interaction region. $x_1$ and $x_2$ represents the width of the particle distribution flowing at average velocities $\Delta v_1$ and $\Delta v_2$ considering all the particles when laser OFF and ON state respectively.

In addition, the interaction length of the laser with the particles provides experimental information on the divergence angle of the waveguide as well as the numerical aperture of the waveguide. For the experiments mentioned above the distance from waveguide end facet to position were particles are focused is ~ 60 µm. This distance is represented as d in the figure 4.20.
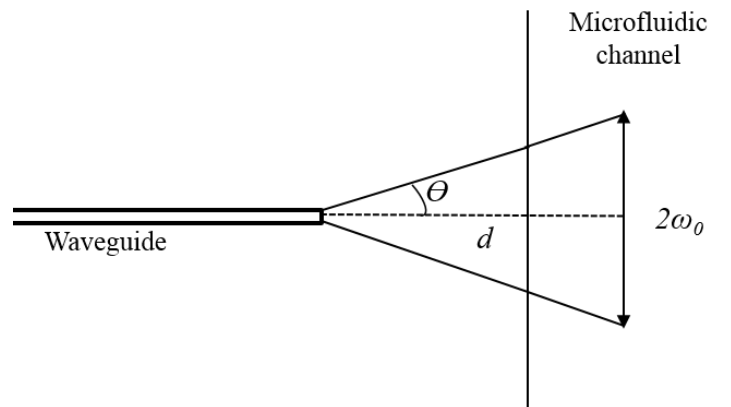


Figure 4.20 Schematic illustration of beam emerging from the laser inscribed waveguide.

For $\omega_0 = 19.9$ µm and $d = 60$ µm the diverging angle, $\Theta = 8.9°$. The numerical aperture of the waveguide NA is given calculated using the Eq. (4.3), where refractive index $n$ of the medium (glass) is 1.45. Substituting the values for $n$ and $\theta$ in Eq. (4.4), the numerical aperture of waveguide was obtained as 0.22. As we haven't accounted for the refraction of beam at the glass water interface, the estimated value of NA using Eq. (4.3) will be slightly higher than the original value of NA of the waveguide.

For the same experimental data in figure 4.19, the width of the distribution of particles in the focused flow and of particles pushed out of the sample flow into the sheath flow along with their respective average velocities were calculated. As shown in figure 4.18, $x_1$ and $x_2$ represents the width of the particle distribution flowing at average velocities $\Delta v_1$ and $\Delta v_2$ when laser OFF and ON state respectively. For laser OFF state, the width of the focused flow $x_1$ is obtained as 5.9 µm. The width $x_2$ for the laterally displaced particles is obtained as 10.7 µm. The particles after displacing into the sheath flow by optical force are distributed at a larger width across the channel in comparison with the distribution when laser OFF. As indicated in Eq. (4.2) the lateral displacement of particle varies inversely with the laser beam width and particle velocity. As the particles are focused within 5.9 µm, the laser beam width seen by the particles flowing at different positions in the focused flow is different as the beam is diverging. In addition, the velocity of particles in the focused flow varies between 1.70 mm/s and 2.06 mm/s. The larger $x_2$ value can therefore be attributed variation in laser beam width as well as flow velocity in the focussed flow, both a result of particle position, resulting in a spread of lateral displacement when subjected to laser power. Furthermore it was observed that the distribution of particles are found to be increasing along the channel length in the sheath flow (figure 4.19) and focused sample flow (data not presented), which can be attributed to the slight increase in width of the channel across the length caused by etching process during fabrication.

From the tracking data produced using Matlab, we also calculated the velocity of the individual particles flowing in the focused flow and the velocity of laterally displaced particles flowing in the sheath flow. The average of these velocities in the focused flow and in the displaced flow are represented as $\Delta v_1$ and $\Delta v_2$, respectively and are

$\Delta v_1 = 1.88 \pm 0.18$ mm/s and $\Delta v_2 = 1.26 \pm 0.18$ mm/s. Figure 4.21 represents the velocity profile of individual particles flowing in the outlet channel of the device.
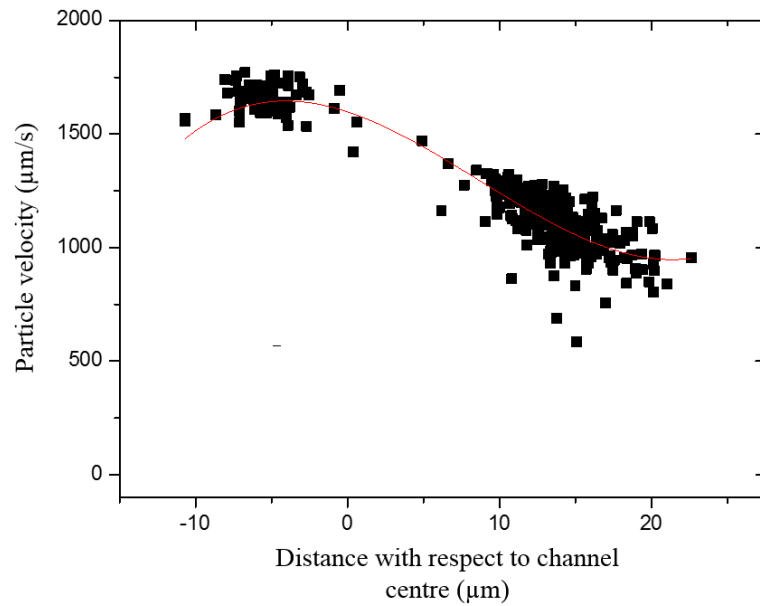


Figure 4.21 Graph showing the velocity profile of individual particles
along the outlet channel of the device.

The distributions of velocities of all the particles flowing in the focused flow and the laterally displaced particles flowing in the sheath flow along the width of the channel is represented in figure 4.20. The experimental data is fitted to a 3$^{rd}$ order polynomial. The velocity profile inside the channel follows a parabolic profile with maximum velocity at the centre region of the channel and a minimum value towards the walls of the channel. The velocity profile thus agrees well with the laminar flow theory.

The experiment for evaluating the lateral displacement was repeated for 5 different laser powers and for 5 and 10 µm particles, with results presented in figure 4.19 a and b. The presented data is considering a total of fifty 5 µm particles and ten 10 µm particles. At a relative sheath to sample inlet pressure of 5:2 mBar, average particle velocity in the focussed flow was measured as 1.4±0.27 mm/s.
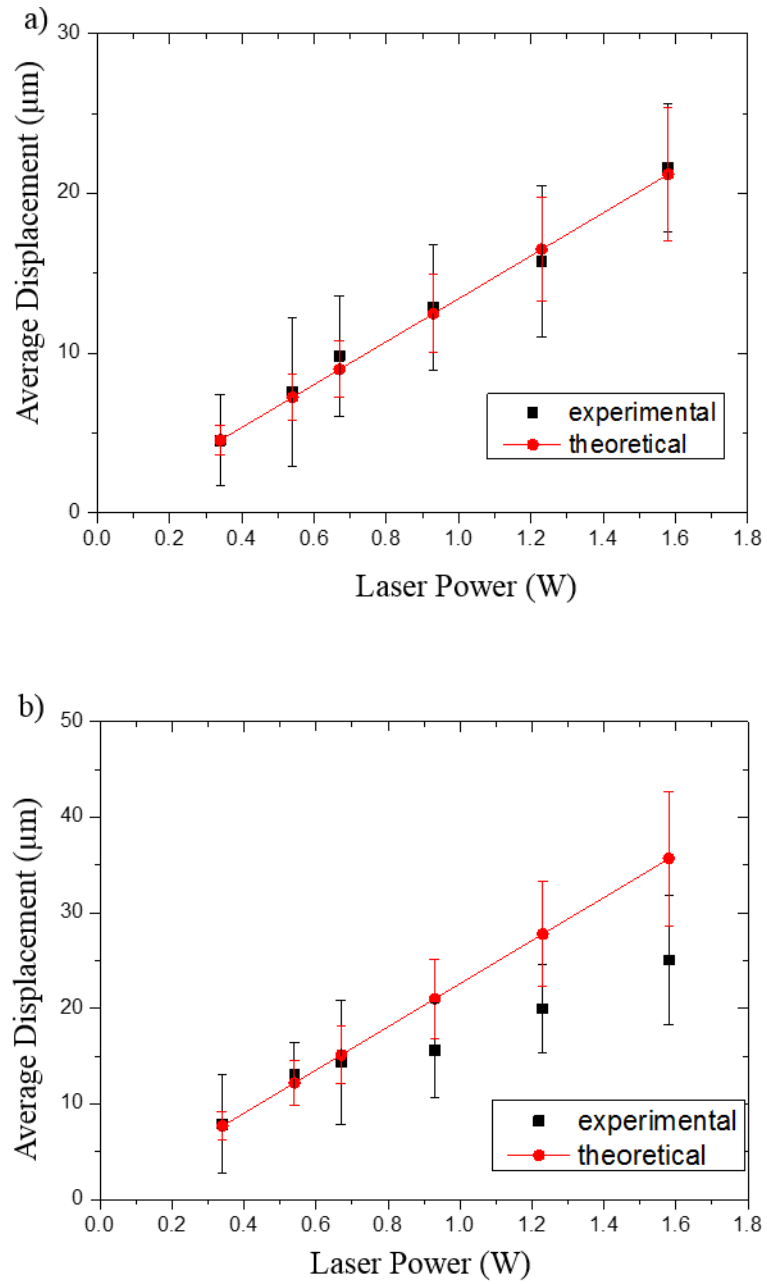
Figure 4.22 Graph showing the average displacement of a) 5 and b) 10 µm particles for different incident laser powers. Error bar for the experimental data represents the standard deviation in displacement of particle. Error bars for theoretical data raPresents the standard deviation in lateral displacement for different velocities.

A linear increase in displacement of the particles was observed for both the particle sizes as the laser power was increased. The theoretical prediction of lateral displacement of the two particle sizes was derived from Eq. (4.2) for fixed conditions, refractive index of the medium (water), $n_0 = 1.33$, viscosity of water, $\mu = 10^{-3}$ Nsm$^{-1}$ and assuming the value for the dimensionless parameter $Q$ as 0.12. We used a different value for $Q$

from the straight channel device, as the present device is different from the straight channel device detailed in section 4.3, and also $Q = 0.12$ has been used previously by Kim *et al*. [100] for predicting the lateral displacements of 5 µm and 10 µm particles in a similar system. For experiments using 5 µm particles, a laser beam radius $\omega_0 = 9$ µm was obtained for at positions were the particles were focused. A laser beam width of $\omega_0 = 10$ µm was obtained at the positions 10 µm particles were focused. The standard deviation in average displacements for $U = 1.4\pm0.27$ mm/s is represented as error bars in theoretical model in figure 4.21a and b.

The experimental measurements and theoretical prediction agrees reasonably with a linear increase of lateral displacement with increase in laser power. A comparison of lateral displacements of 5 µm and 10 µm particles also shows that 10 µm particles are displaced at a larger distance compared to 5 µm particles. This is in good agreement as indicated in Eq. (4.2) which shows that the lateral displacement, $Z$ increases with increase in radius of the particle $r$. The minimum power required to move the 5 µm particles, out of the focused flow was estimated to be ~0.6 W. For 10 µm particles, the minimum power required to push out of the focussed flow was found to be around ~0.5 W. As shown in figure 4.22a and b the particles are laterally displaced at lower power ~0.3 W, however is not enough to push them out of the focussed flow. The results presented here provide insight on the manipulation of particles, confined in a small volume, using optical forces. The ability to displace particles of different size at different distances shows the potential of the geometry of the device combined with the manipulation technique to use for sorting applications based on size of the particle. With incorporation of multiple outlets, this device promises to deliver particles of different size to different outlets and promises to have uses in size based passive cell sorting. The ability of this device to manipulate single particle at a time can be used for isolating single cells, for cell counting and sorting applications.

Photo damage of cells caused by laser exposure is an important issue to be addressed in optical manipulation systems. Several studies on investigation of damage process of cells in optical traps have been reported previously [115, 116]. In the present study we use a diverging beam and for a maximum incident laser power of 1.58 W with a beam width 20 µm incident on a particle flowing with velocity 1.4 mm/s. The time for a

particle pass through the beam propagation area is therefore 0.014 s. According to the studies by Neumann *et al.* [115] no photo damage is observed on this time scale of laser exposure. The optical power density in the laser illumination region is $5 \times 10^5$ W/cm$^2$. The power density in this case is much lower than that used in optical tweezers which is of the order of $10^7$ W/cm$^2$. In addition, the choice of manipulation source with wavelengths in near infrared region provide minimal temperature rise as the water absorption is lower compared to the longer wavelengths, reducing heating [85]. Thus the presented device enables to use for a variety of cell handling functionalities without losing the viability of the cells.

## 4.7   Summary

This chapter has presented two different geometries of integrated optofluidic devices fabricated using ULI and selective chemical etching for investigating the manipulation of particles and cells within these devices. The device detailed in the first half of the chapter demonstrated the use of optical scattering force in controlling and manipulating particles within a straight microfluidic channel at different flow conditions.

The preliminary results from experiments done with this device have provided a good insight on the effect of laser power and flow velocities for controllably displacing microscopic particles within a microfluidic channel. The limitations including the risks of clogging the channel and the increased possibility of not addressing every particle in the sample due to random distribution of particles across the channel however affected the efficiency of manipulation. This has resulted in prototyping a more complex device design that promises to offer improved manipulation and handling of particles, as detailed in the second half of the chapter. The 3D direct writing capability of ULI was utilised to realise this design. The device possesses multifunctional capability that includes the ability to confine particles in to a narrow stream through hydrodynamic focusing and optically manipulate individual particle, all integrated in to a single platform.   Studies on particle and cell manipulation using optical scattering force in this device has helped in realising precise and efficient particle control at single particle level, showing the  potential of the device to be used for miniaturised flow cytometers, cell separators and for single cell based studies.

The application aspects and the advantages of ULI fabrication technique, allows one to visualise the potential of this device for biological applications, by incorporating new modules to the device. We further developed a 3D optofluidic device with extra design features to demonstrate as a cell separator device. Chapter 5 presents the fabrication and validation details of that device.

# Chapter 5

# Towards the Development of a Three Dimensional Miniaturised Cell Separator

## 5.1 Introduction

Effective methods to sort, separate and isolate individual particles from a population of cells have been of critical importance in biological studies and clinical applications. Over the past 40 years flow cytometers and FACS machines have been widely used for performing these tasks [117]. Although conventional bench top flow cytometers and FACS machines provide high throughput analytical capacities and multi-parameter cell sorting [118], they are still bulky, expensive and are mechanically complex. Moreover, they require a larger volume of the order of milliliters of the sample to be analysed. These factors limit the full use of such systems in various biomedical research applications. In particular for applications that require smaller volume sample analysis such as for single-cell based studies. Over the past 20 years, microfluidic based approaches are widely used in order to achieve inexpensive, simpler, portable and easy to operate systems to enable the handling of smaller volumes of sample. The introduction of different particle sorting techniques in to these systems has allowed the realisation of miniaturised flow cytometers and cell separator/sorter.

Miniaturised cell separator devices generally consist of microfluidic channel structures that constitute the path for sample to be analysed, and a sorting or separation region that uses electrical [89], acoustic [92], magnetic [91], optical [28] or mechanical [87] means to divert and collect cells or other particles. Particle or cell separations in these systems are employed based on the user defined parameters including size, refractive index, fluorescence emission and morphology of the object. Of the different cell sorting techniques, optical forces for manipulation are found to be of great interest due to their intrinsic features as discussed in Chapter 1. Hydrodynamic focusing is the other key functionality that is employed in several microfluidic systems for effectively controlling the passage of a sample through the microchannels within the devices. The flow focusing of sample fluid by sheath fluid can be easily achieved by controlling the

relative flow rates of sheath and sample flows allowing single cells or particles to pass through the detection or manipulation region.

In chapter 4, a detailed investigation of integrating the two functionalities of hydrodynamic flow focusing effect and optical manipulation system within the same system to use for particle and cell manipulation applications have been discussed. This chapter presents a miniaturised 3D optofluidic device that can be used for separating, sorting and isolating cells. Section 5.3 introduces the ULI fabricated device followed by the discussion on the device design and working principle in section 5.3. The progression in the device designs for achieving the proposed device functionality is discussed in section 5.5. Section 5.6 presents the device performance validation and section 5.7 summarises the chapter along with discussing the future prospects of the device.

## 5.2   A three dimensional miniaturised cell separator fabricated using ULI

Microfluidic devices incorporating hydrodynamic flow focusing capabilities combined with different manipulation techniques have been reported before [104, 113].   The fabrication procedures for these devices mostly rely on photo or soft lithography techniques [17] which generally involves complicated and multistep processes for developing 3D structures. In addition, the detection systems used in these devices are externally employed which requires careful alignments.

The following section demonstrates a 3D miniaturised cell separator device fabricated in fused silica. The versatility of the ULI fabrication technology to directly write 3D microstructures and waveguides have been utilised to fabricate complex microfluidic structures and waveguides within the device. The device is capable of confining the sample flow in to a narrow stream and laterally displacing particles away from the centre line of the channel. This has been validated using different samples. The device functionality in routing cells and particles in to different outlets using optical force was validated.

## 5.3   Device design and working principle
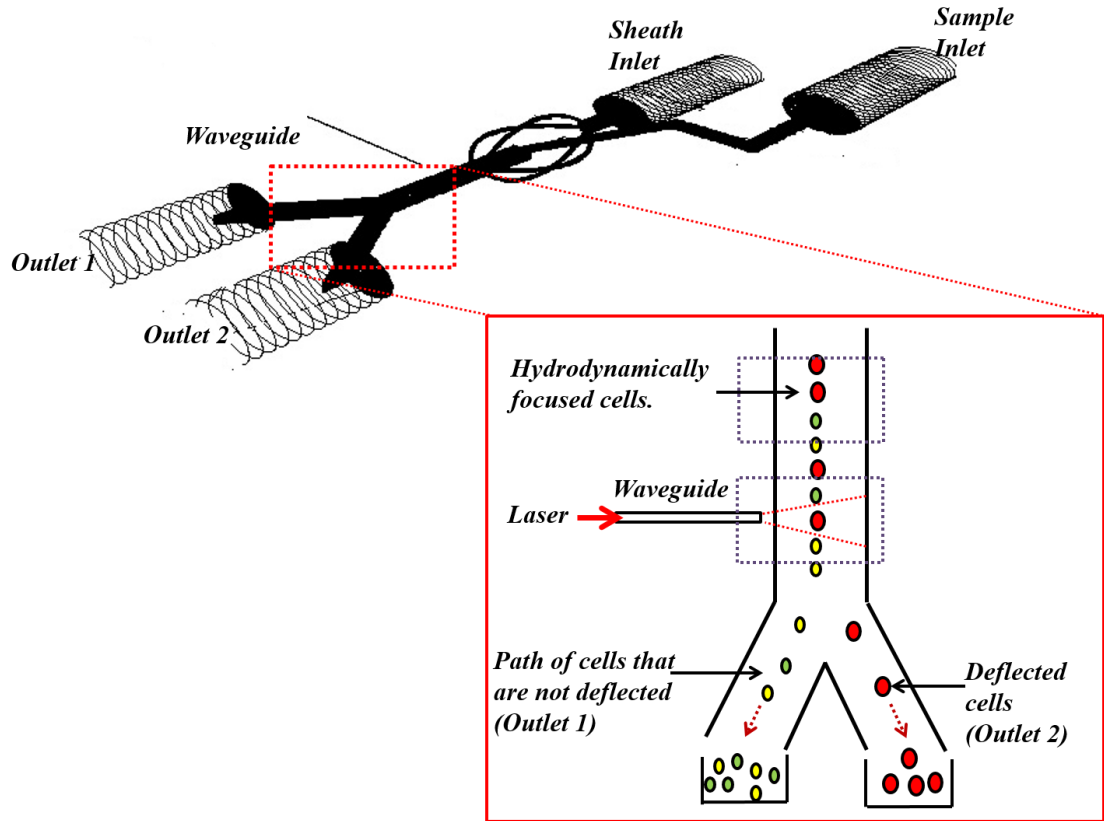


Figure 5.1 Schematic illustration of the laser trajectory of the device design plotted using N-plot software (Not to scale). After being aligned to the centre of the channel using hydrodynamic flow focusing effect, the cells pass through the optical interrogation region. Optical radiation from the laser coupled waveguide is then used to push the cells along the beam axis and directed towards the collection outlet channels 2. The undeflected cells are directed through outlet 1, which can be recirculated in principle, if necessary.

Figure 5.1 represents the design of the cell separator device along with an illustration of the working principle of the device. One of the important functionalities of the device is to confine the sample flow consisting of cells in to a narrow stream. This is achieved by introducing the focusing module that constitutes the sheath inlet port, sample inlet port, sheath inlet channel and the 4 curved sheath inlet channels. At a relative sheath to sample flow rate, the sample fluid can be hydrodynamically focused into a narrow stream constrained by the flows from 4 inlet curved channels. Optical manipulation, which is the other key functionality of the device, is achieved through the embedded laser coupled waveguide through which the optical power needed for manipulation is

delivered. The waveguides are positioned orthogonal to the main outlet channel. The optical control system here acts to rout the cells into a different outlet channel for collection and downstream analysis. Particle or cell separation based on size of the particle within the device can be achieved by applying appropriate laser power, as discussed in Chapter 4. Thus the device geometry offers to separate, sort and isolate cells and particles using optical forces. The separated cells flowing downstream are then transported through the outlet channels within the same device, enabling collection for further analysis.

## 5.4    Device fabrication

The device was fabricated using ULI followed by selective chemical etching. The inscription setup used for fabrication is as detailed in section 3.3 of chapter 3. The inscription parameters for fabricating the 3D microfluidic channel network and waveguides were adopted from that used for fabricating the device detailed in section 4.5 of chapter 4. Three different versions of the device with varying inlet and outlet geometries were fabricated for accomplishing the functionalities as proposed in the design discussed in section 5.4. The 3D microfluidic channel structures in these devices were written using laser pulse energy of 680 nJ, with polarisation perpendicular to sample translation direction. The 3D modification for all the microfluidic channel structures was achieved by modifying the outline of the structure; likewise in the device detailed in chapter 4. The waveguides were written perpendicular to the outlet channel using multiscan technique with laser pulse energy of 234 nJ and translation speed of 1.5 mm/s. The femtosecond irradiation of the microstructures and waveguides within the three devices was followed by selective chemical etching process in HF. The post etched devices were rinsed in DI water followed by acetone. The end facets of the devices were polished to optical quality for ensuring better coupling of laser.

The first version *device 1,* as shown in figure 5.2a, consists of sample focusing module, orthogonally positioned waveguides, and two outlet channels. The geometry of the focusing module that includes the sheath and sample inlet channels were adopted from the device detailed in Chapter 4, section 4.5. Of the two outlet collection channels, outlet 1 was written as an extension of the main channel, allowing the cells that are not deflected by the laser to flow through. The outlet 2 which is 0.84 mm long was written

at an angle 45° to the main channel with the aim to direct the cells that are pushed out of the sample flow for collection and downstream analysis. The flow behaviour at the outlet channels was monitored, using fluorescent dye as the sample and DI water as the sheath, for different sheath to sample input pressure ratios using the experimental setup detailed in section 3.3, chapter 3. A confined flow of sample fluid was achieved along the centreline of the channel through the outlet channel 1. However there was no observed fluid flow through the outlet channel 2. In order to overcome the fluidic resistance at the outlet channel, a second version of the device, with symmetric outlet channels was designed and fabricated. *Device 2* is as shown in figure 5.2b.
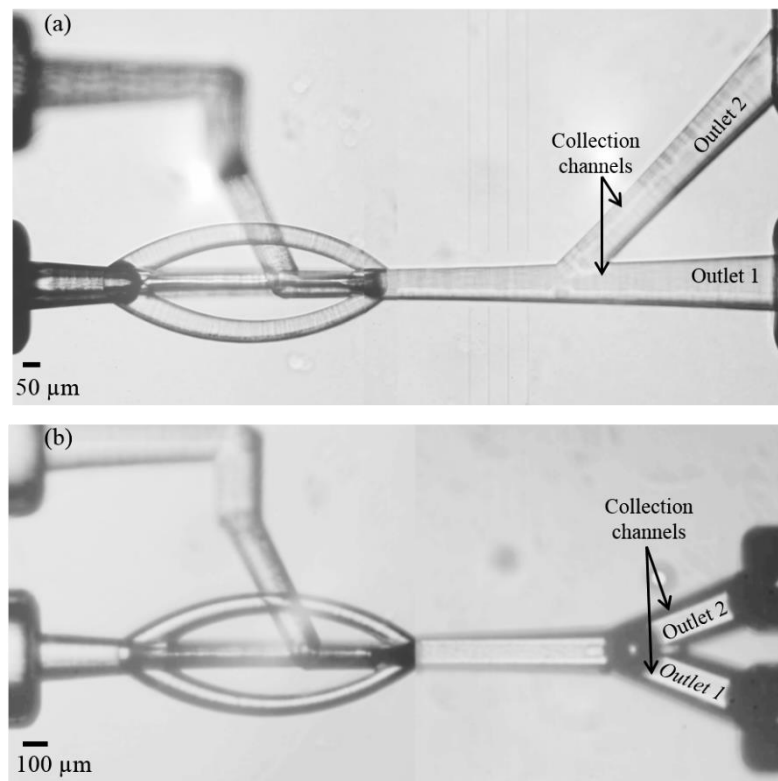


Figure 5.2 Top view microscopic images of the two versions of the device a) device 1: Outlet channel2 written at an angle 45° to outlet channel 1 b) device 2: bifurcation of outlet 1 and 2 to angle 20° from the main channel

The geometries of inlet focusing module, main outlet channel and the waveguide positions were the same as for *device 1*. The outlet collection channels were written in such a way that it bifurcates from the main channel in to 20° angled branches; outlet 1 and outlet 2. After fabrication, the device performance was monitored to ensure a

resistance-free fluid flow through both the outlet channels at different sample to sheath flow rates.

In order to clearly visualise the path of confined sample flow, fluorescent dye was used as sample with DI water as sheath fluid. At relative sheath to sample flow rates a confined flow of the sample was achieved along with a resistance free fluid flow through the outlet channels. However, the confined sample stream flowing through the centre line of the channel was directed towards the junction were the outlet channel bifurcates. This resulted in mixing of the sample with the fluid in both outlets 1 and outlet 2, which is not favourable for sorting applications. In addition, this increases the risk of sample particles sticking to the channel wall were two outlet channels meet.

In previous reported studies it was shown that the location of the focused stream can be precisely positioned and guided by adjusting the relative flow rates of the sheath flows. This has been exploited in developing various novel microfluidic devices including valveless microflow switches [119] and microarrays [120]. In these devices, the flow switching, in other words the precise positioning of the focused flow across the channel, was achieved using multiple pumps for injecting the sheath fluids at relative flow rates. The theoretical investigation of asymmetric hydrodynamic focusing in rectangular microchannels by Gwo-Bin *et al.* [121] has shown that by introducing asymmetries in the focusing module through variable volumetric flow rates of the sheath inlet fluid, the location of the hydrodynamically focus sample flow can be controlled. To address the limitation of *device 1,* the approach of introducing an asymmetric hydrodynamic focusing effect was considered. For this *device 3* was fabricated, as shown in figure 5.3. The curved sheath inlet channels of the device were designed in such a way that one of the horizontal curved channels possesses a lower cross sectional area than the other three curved channels, thereby varying the volumetric flow rate of the horizontal channel with respect to other three curved channels. The asymmetric geometry of the sheath inlet channels results in an asymmetric hydrodynamic focusing effect that enables the repositioning of the focused stream from the centreline of the channel. The top view of the fabricated device after etching in 10% HF for ~15hrs is shown in figure 5.3a. Like device 1 and 2, device 3 incorporated the inlet focusing module with sample and sheath inlet channels, the optical interrogation region that constitutes the main

channel with orthogonally positioned waveguides, and the symmetric outlet channels. The variation in the dimensions of H1 compared to H2 can be seen in figure 5.3b.
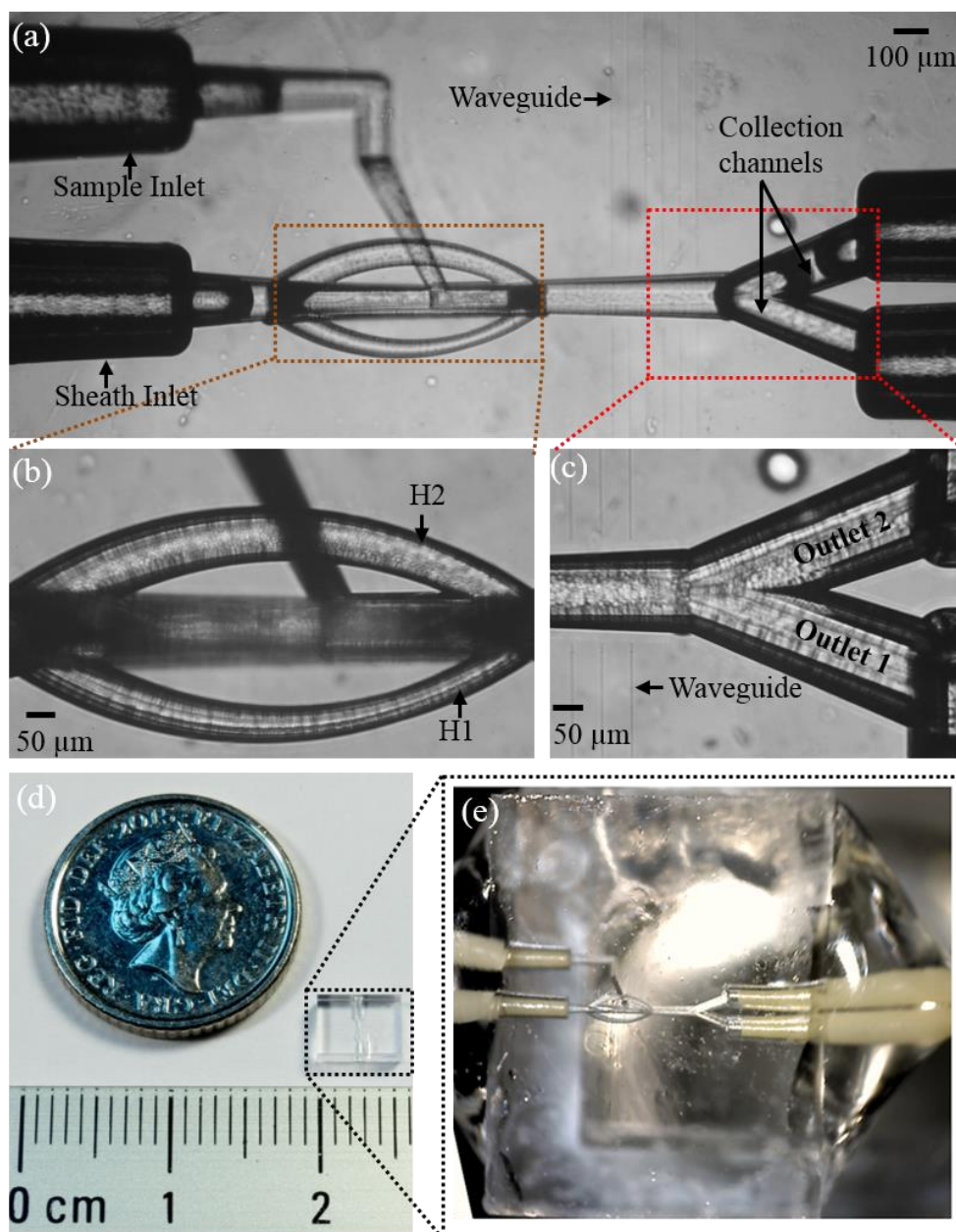


Figure 5.3 Optical microscopic images of device 3. a) Top view of the device, b) Magnified view of the asymmetric, horizontal inlet channels H1 and H2, c) Magnified view of the symmetric outlet channels 1 and 2, d) Scale of the fabricated device, comparison with a 5 pence coin, e) Device with peek tubing inserted in to the inlet and outlet ports, represents the device that is ready to be used for experiment.

The H1 curved channel was 55 µm wide and 110 µm deep. The H2 channel and the two vertical channels were 85 µm wide and 110 µm deep. The 0.56 mm long outlet main channel with a width of ~144 µm and height of ~150 µm bifurcates at an angle 20º in to outlet channels 1 and 2 with cross sections of both the channels ~200 × 200 µm. Figure 5.3 c shows a magnified view of the optical manipulation region as well as the symmetric outlet channels. The waveguides are ~95 µm away from the centre of the main channel. Figure 5.3d shows the scale of the fabricated device. The final size of the device in fused silica is 6 × 4.5 × 2 mm. The device, after post etch processes, including cleaning and polishing steps, was tested for its performance capability. The following section details the performance validation and the experimental results achieved using *device 3*.

## 5.5    Experiment Results and discussions

### 5.5.1    *Device validation*

The performance of *device 3* to laterally displace the focused flow by applying relative sheath to sample flow rates was assessed. Figure 5.3e shows device 3, with PEEK tubing's inserted and glued in to the inlet and outlet ports, thereby enabling device to pump interconnection. A pressure driven pump (Fluigent) was used for delivering sample and sheath fluid through the respective inlet channels. The clear visualization of the focused flow was achieved by using fluorescein as sample fluid and DI water as sheath fluid. The live monitoring of the experiment was performed using a USB digital microscope (Dino-Lite Premier AM4113T-GFBW). The experimental setup used for device validation is as discussed in section 3.3 of chapter 3. At a relative sheath to sample input pressure ratio of 5:0.5 mBar, a confined flow of sample with a slight displacement from the centre line of the channel was observed, as presented in figure 5.4.
.
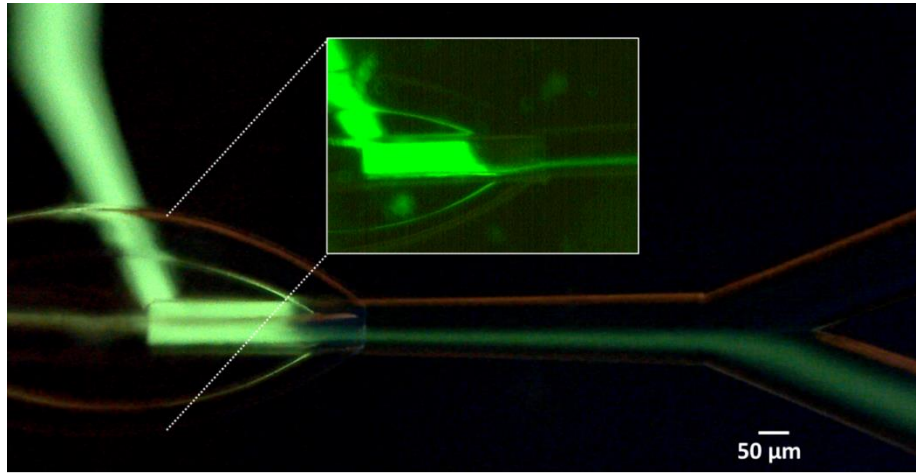
Figure 5.4 Experimental image showing focusing of fluorescein by DI water. The lateral displacement of the focused flow from the centre line was achieved using the proposed geometry. The image presented inside the frame shows the clear view of the hydrodynamically focused sample coming out of the sample inlet channel, surrounded by the sheath fluid.

The position of the focused flow was shifted laterally away from the centre a distance of $30\pm7.357$ µm. The width of the focussed flow at the same input pressure ratio was measured as $14.8\pm1.5$ µm along the horizontal plane and $23.03\pm1.9$ µm along the vertical plane. The focusing along the vertical plane was achieved at the centre line with respect to the height of the channel, as expected.

### 5.5.2  *Particle / Cell Separator: Performance Validation*

After evaluating the 3D flow focusing capability as well as the device geometry to displace the focused flow laterally, the device performance as a cell separator was assessed. In order to validate the selective sorting and cell separating capability of the device different samples including fluorescent polystyrene beads, AtT-20 cells and *E. coli* bacteria were used. A cw Nd:YAG laser, operating at a wavelength of 1064 nm with a power up to 3W was coupled to the embedded waveguide in the device, providing the optical force on the particle to be separated. The total insertion loss of 1.76 dB measured at a wavelength 1064 nm wavelength was used for estimating the power at the centre of the outlet channel. All the experiments performed with this device were monitored using the USB digital microscope connected to the computer.

This microscope is optimized for viewing objects emitting green fluorescence above 510 nm as excited by its 480 nm (blue) LED lights. The recorded images from the experiments are presented in following sections.

The key functionality of the device was first assessed using polystyrene beads before introducing biological samples into the device. To use with the USB microscope, green fluorescent microspheres of size 10 µm was chosen as sample. Microspheres were suspended in DI water along with a small amount of surfactant. This sample fluid was injected into the sample inlet and DI water that served as the sheath fluid was injected in to the sheath inlet using the pressure driven pump. At a sheath to sample input pressure ratio of 5:0.5 mBar, a narrow stream of focused flow was formed at the outlet main channel with sequentially arranged microspheres. The focused stream was successfully displaced from the centre line of the channel, in the direction opposite to the incident beam from waveguide, allowing the flow to successfully guide all the sample microspheres through outlet 1. Optical radiation from the laser was then used to push individual particles flowing past the laser coupled waveguide out of the focused flow, into the sheath flow. Figure 5.5 shows a sequence of snapshot images from the recorded video showing the path of the microspheres when laser was off and then turned on. The velocity of the particles in the focused flow was measured to be 6.03±1.49 mm/s (for around 10 beads). The two snapshot images shown in figure 5.5a, show microspheres (streaks) travelling along the main outlet channel and entering the outlet 1. In this case the laser was turned off so there was no optical pressure. With same input flow conditions and upon applying a laser power of ~1.8 W, individual particles were directed towards the outlet 2 as shown in figure 5.5b.
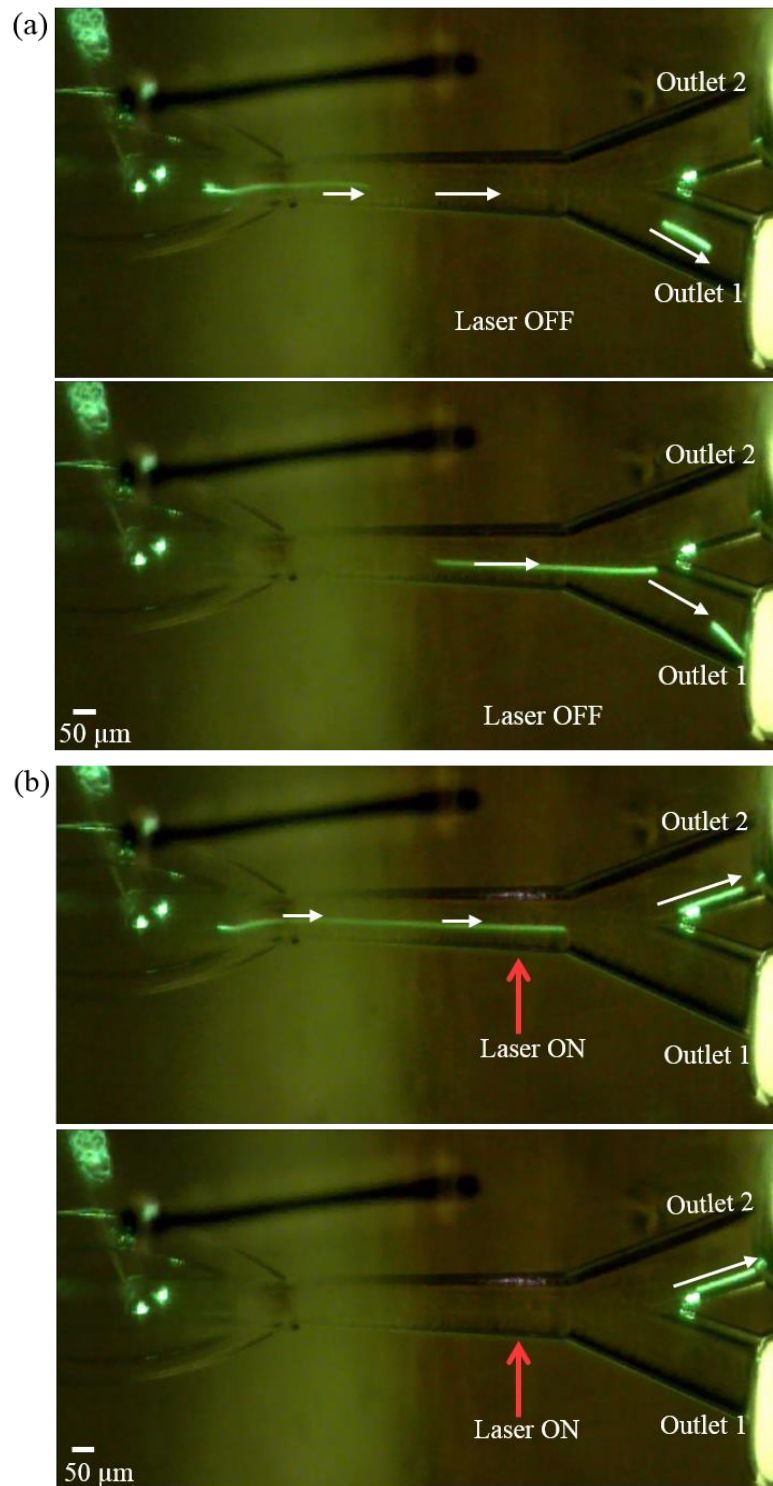
Figure 5.5 Sequence of snapshot images from the experiments performed with device 3. (a) shows the path of the microsphere with laser off, and beads are directed towards outlet 1. (b) shows the path of microspheres with laser on for an applied power ~1.8 W, and beads are directed towards outlet 2.

These results demonstrate the capability of the device in routing cells to required outlets by combining hydrodynamic and optical forces in an integrated device. The optical force here provides a switching mechanism enabling us to separate, isolate or sort desired particles or cells within the device.

Having validated the performance of the device with microspheres, the device capability for use with cells was evaluated. For this *E. coli* bacteria expressing GFP (with an average cell diameter of 1-2 µm) and cultures of AtT-20 cells (of average size 13±0.54 µm) were chosen as the samples due to accessibility, ease to make fluoresce and size difference. Live monitoring of the experiment was done using the USB fluorescent microscope. The *E. coli* cells were injected through the sample inlet and DI water through the sheath inlet channel ports at a relative sheath to sample input pressure ratio of 5: 0.2 mBar. In order to clearly visualize the flowing stream of bacteria, a highly concentrated cell suspension was used in this experiment.
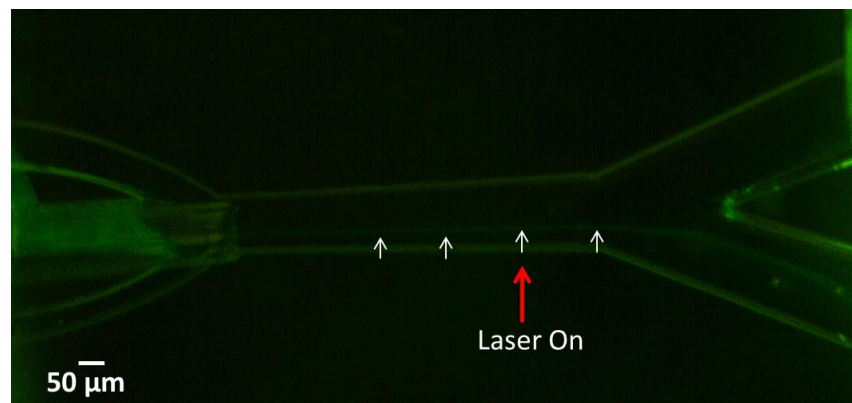


Figure 5.6 Experimental image showing the focusing of E. coli cells directed towards outlet1. Cells were found to be unaffected by the applied laser power.

A tightly focused stream of *E.coli* cells were formed in the main channel and are directed towards outlet 1, as shown in figure 5.6. In order to evaluate the routing of cells by optical force, a laser power of 1.8 W was coupled to the waveguide. However no cells were found to be deflected toward the outlet 2 on application of optical force. The reason for this can be attributed to the higher velocity and smaller size of the cells requiring higher optical power for causing any displacements.
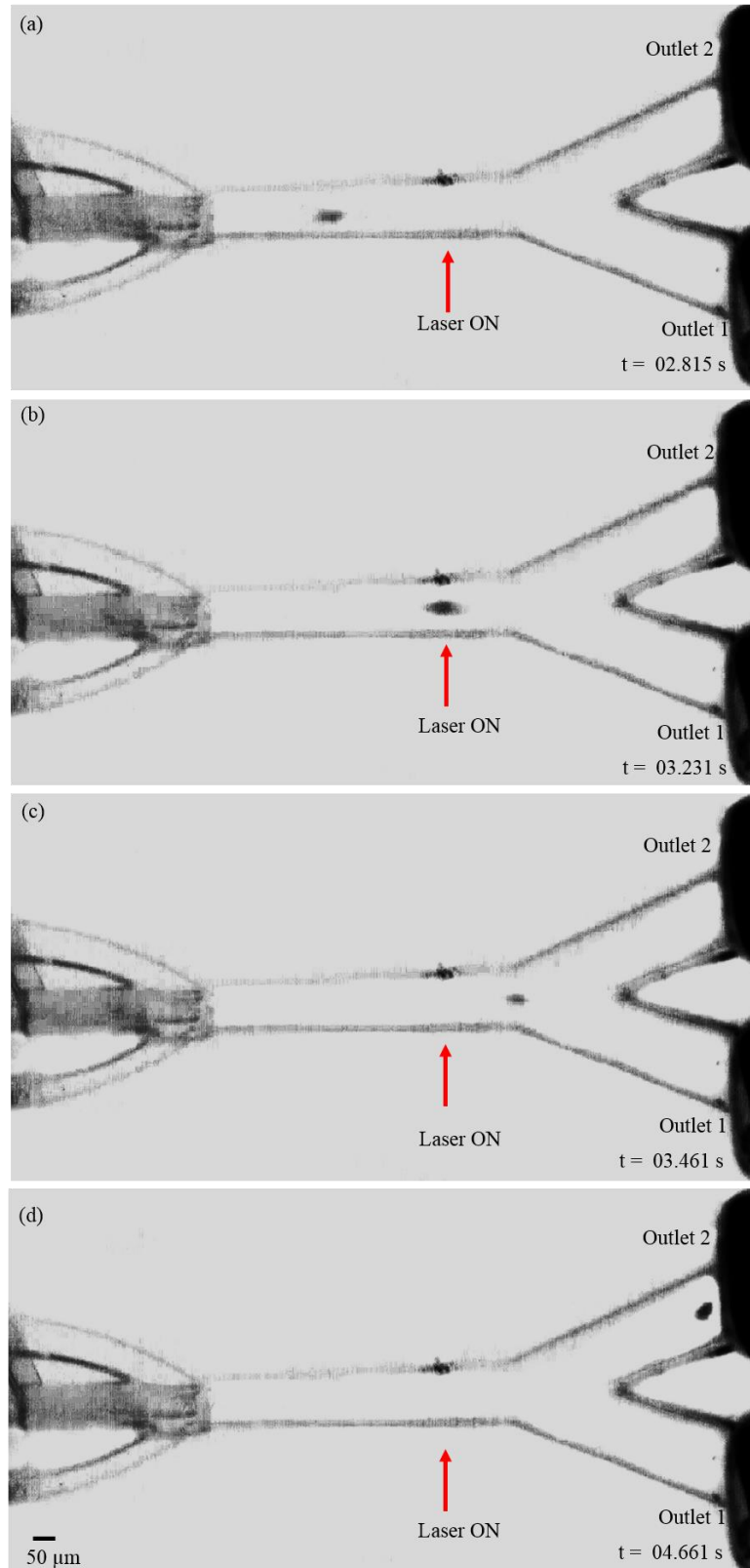
Figure 5.7 Experimental images showing the path of focused AtT-20 cells before and after deflection using optical force. a) Shows single cell before deflection, b) cell displaced along the beam axis, c) cell pushed out of the focused flow directed towards outlet 2, d) cell flowing through the outlet channel 2.

After performing the experiment with *E. coli* cells, AtT-20 cells were introduced in to the device. The cells were fixed and stained with a fluorescent marker (Calcein, AM) to enable visualisation of the cells with the USB fluorescent microscope. The protocol for staining the cells with Calcein, AM, cell-permanent is described in chapter 3. Versene buffer solution was used as sheath fluid for confining At-T20 cells. At a relative input pressure ratio of 5:3 mBar, AtT-20 cells were focussed at a distance of ~33 µm from the centre of the channel. The velocity of individual cells focussed in the main channel was measured as 0.5±0.246 mm/s. The particles in the focused flow at a sheath to sample input pressure ratio 5:3 mBar were found to move at a lower velocity compared to the particle velocity when the input pressure ratio is 5:0.5 mBar. As discussed in section 4.6.1, the width of the focused flow decreases with an increase in sheath to sample pressure ratios. The velocity of the focussed flow increases with a decrease in the width of the focussed flow [113], therefore resulting in variation in flow velocities of particles in the focussed flow for two different input pressure ratios.

The routing of cells using optical force was evaluated with laser off and on. The cells were found to be directed towards the outlet 1 with the laser off, as predicted. An optical power of ~1.7 W was then applied and the direction of individual AtT-20 cells flowing past the laser coupled waveguide was monitored and recorded. The selected frames from the recorded movie are as shown in figure 5.7. With the applied laser power of ~1.7 W a deviation of 16.32±3.9 µm from the centre of channel was observed along the direction of propagation of beam and thereafter directed towards outlet 2. At a controlled fluid flow, the integrated device thus allows us to controllably direct cells in to different collection channels. The optical control within the device serves as a switch that could potentially be used to separate or even isolate desired cells from a population and find use as an active cell sorter.

## 5.6  Summary

The work presented in this chapter exhibits the capability of ULI fabrication technology in developing 3D complex devices with integrated multifunctional components to use for cell manipulation experiments. The miniaturised optofluidic device presented in this chapter demonstrates the potential of the device for passive separation or sorting or cells

or particles. A step by step progression in the device design for achieving the proposed device functionality along with their functional validation has been detailed. The experiments performed with the devices show that the optical element integrated within the device can provide an active binary switch for separating cells and particles or can be used for passive cell or particle separation based on particle size. Although the throughputs demonstrated were on the order of only a few particles or cells per minute, the device importantly offers the potential to be used for selectively sorting cells based on their size or based on a signal that can be excited or detected by integrated waveguides or using a standard microscope.

The results obtained from the experiments reveal the possibility of using this device for multipurpose cell manipulation experiments, including isolation, separation and sorting of cells. Apart from sorting cells based on their sizes the device can be optimised for sorting based on refractive index of the cells or beads. In addition, the integration capability of ULI can be utilized to include components for fluorescence excitation and detection within the device, with the possibility to sort cells based on their fluorescence.

# Chapter 6

# Conclusions and Future Work

## 6.1 Conclusion

The work reported in this thesis has focused on developing three dimensional optofluidic devices for performing cell manipulation required for cell separation, sorting and ultimately single cell based studies. The unique features of ULI fabrication technology to fabricate 3D structures providing multifunctional capabilities and to integrate them within the same substrate have been exploited in this work. Chapter 3 details the materials and methods utilised for fabricating the different optofluidic device and for performing the validation tests. Chapter 4 presents the detailed investigation of optical separation of particles and cells in two geometrically varying optofluidic devices. Finally, chapter 5 presents an optofluidic 3D cell separator device capable of routing cells into desired outlets using optical force, thereby allowing separation of cells and particles. A summary of the work presented in each chapter is as follows.

**Chapter 3** presents the different steps involved in fabricating optofluidic devices in fused silica using ULI followed by a description of the experimental setup used for validating the fabricated devices. The parameters for achieving low loss waveguides and enhancing the selective etching in fused silica was optimised, providing the initial parameters for fabricating the optical and fluidic elements within the devices detailed in chapters 4 and 5. The experimental setup that was used for performing all the experiments detailed in this thesis is described in detail. A brief description on the samples used in this work and their preparation are detailed.

**Chapter 4** is an investigation of particle separation that can be performed in ULI fabricated microfluidic devices using optical manipulation. The potential of using the optical scattering force for controllably displacing individual particles along the beam propagation axis was first demonstrated using a simple optofluidic device. The device included a straight microfluidic channel with waveguides positioned orthogonal to the

channel. The displacement of particles and cells by the optical scattering force was measured for different laser power as well as flow velocities. A larger deflection of particles and cells from their original path was observed at slower flow rates and larger beam powers. Taking in to account the limitations of the geometry of this device and for achieving improved manipulation efficiency, a second geometry was prototyped. The device design, fabrication and validation details are presented in this chapter. Along with the ability to optically manipulate particles, the device geometry possessed the ability to hydrodynamically focus the sample fluid. This allowed particles and cells to be confined in a small, focussed volume thereby allowing the sequential arrangement of cells to pass through the manipulation/detection region (the beam exiting the waveguide) one by one. The three dimensional flow focusing, achieved by maintaining a relative sheath to sample input pressure ratio, has been validated using polystyrene microspheres, coloured dye and biological samples. A minimum width of 7 µm along horizontal and 12 µm along vertical plane of the channel was obtained, which was suitable for the validation tests performed with the device. The evaluation of change in focused flow width with regard to the input flow rate ratios shows that the device geometry is well suited for single cell based applications. Optical particle separation within the device was demonstrated for different sizes of particles. A comparative study on the displacement of 5 µm and 10 µm particles from the confined sample flow into the sheath for different incident laser powers was investigated. For the same applied laser power 10 µm beads were found to displace more than 5 µm. The results presented confirmed the potential of the device geometry for passive cell sorting, separation and isolation applications, based on particle size.

**Chapter 5** presents an upgraded version of the device detailed in Chapter 4. The ULI fabricated device was demonstrated to use as a passive cell sorter. Three different versions of the device with varying geometries were designed and fabricated as a part of optimising and analysing the cell separator functionality of the device. As discussed in the chapter 5, the three geometries were fabricated at different stages taking into consideration the limitations of the previous designs. The final version, *device 3* (as shown in figure 5.3) with its improved geometry for laterally displacing the focused flow and the ability to controllably displace particles using optical force has been demonstrated to use as a cell separator device. The integrated device, consisting of multifunctional elements, has been validated using polystyrene beads, fluorescein dye

and different biological samples. The optical element within the device delivers the power required for manipulation while the hydrodynamic focusing functionality of the device allows the cells and particles to flow through the manipulation region one at a time. The capability of the device to route particles and cells into different paths from their original trajectories upon the application of appropriate optical powers was first assessed. Initial validation tests performed using 10 µm polystyrene microspheres confirmed the working principle of the device. Biological cells including AtT-20 cells and *E.coli* cells were later introduced into the device and the functionality of the device was validated. The capability of *device 3* to direct cells in to different outlets achieved by optical switching function within the device, offers the possibility of using the device for selectively separating cells.

## 6.2  Future work

### 6.2.1  *Investigations on passive and active sorting of cells based on refractive index and fluorescence, respectively.*

Particle and cells can be separated based on the user defined parameters including size, refractive index morphology as well as fluorescence. The monolithic integrated device presented in chapter 4 with key functionalities including 3D hydrodynamic flow focusing and optical manipulation is capable of size based particle separation. The device with the same geometry can be utilised for investigating the dependence of incident laser power in displacing the cells and particles based on refractive index of the particle. Refractive index change in cells may be a marker for disease progression, for example in cancers [122].  Cell sorting based on size and refractive indices of cells avoids labelling of cells with fluorescent markers, and in some cases the surface markers for some rare cancers may not be known, so refractive index change may be the best indicator of disease. However, it remains to be seen if my 3D optofluidic devices will be sensitive enough to discriminate between these very small refractive index differences.

The device also offers potential for sorting where the sorting is performed based on fluorescence, similar to FACS on a chip. The integration capability of ULI can be used to incorporate a waveguide for guiding the fluorescence excitation light to the fluorescently labelled cells to be sorted. The fluorescent signal from the cells can be

detected using a camera. The laser can be programmed to switch on when a fluorescent particle is detected thereby pushing the desired particle out of the sample into the sheath flow for downstream analysis. Optimising these devices is important for realising high efficiency, multifunctional cell sorting.

### 6.2.2    Multifunctional cell sorter device

The device detailed in chapter 5 has been demonstrated for separating cells based on size. However the sorting efficiency of the device needed to be optimised. A known volume of cells can be injected to the device for sorting. The total number of cells collected at the outlet chambers after sorting can be then compared with the number of injected cells to estimate the sorting efficiency of the device. A cell viability assessment of the collected cells is also important to ensure that the effect of passage through the device has a minimal effect on cell viability.

The device can be further optimised to use as a cell sorter device capable of sorting cells based on multiple parameters including size, refractive index and fluorescence. The present design of the device can be extended to incorporate another waveguide for delivering fluorescent excitation light to the cells. This would allow sorting cells based on fluorescence. Furthermore, separated or sorted cells can be deposited in different microwells of a microwell plate, in conjunction with a robotically controlled stage, allowing collection and monitoring of single cells, or grouping of particular cells. In addition, the 3 capability offers recirculation of samples to provide several enrichment steps, and offers the capability of parallel processing of multiple samples. A monolithic device with these integrated functionalities thus forms a favourable platform for performing single cell manipulation and analysis that will find use in biological research labs.

### 6.2.3    ULI fabricated device with optical tweezers.

The 3D writing capability of ULI can be utilised to fabricate sample chambers in which to perform single beam optical trapping (3D optical trap, also known as optical tweezers (OT)). Reservoirs, channels and chambers, written within the fused silica substrate, can be used for on-chip cell manipulation, monitoring and cell culture applications. This will be of particular interest for studying single cells, investigating cell to cell

interaction and to monitor the growth and cultivability of isolated cells. Figure 6.1 shows the schematic illustration of an on-chip culture system. A mixed population of cells can be inserted to the large reservoir of the chip. OTs can be used in combination with such devices for picking the cells of interest from the large reservoir and to deposit them at the required micro chambers for further analysis.
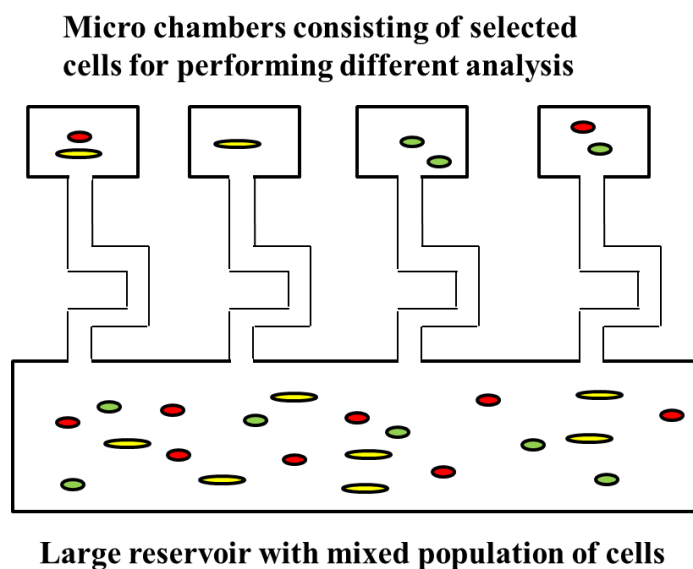


Figure 6.1 Schematic illustration of an on chip culture system that can be fabricated using ULI followed by selective chemical etching. The large reservoir can be filled with a mixed population of cells. OT can be used to pick the desired cells from the large reservoir and transport it to the micro chambers for further analysis.

A portable OT system has been designed and built during my PhD with the aim to isolate bacterial cells. The system was delivered to NCIMB in Aberdeen for testing and then to Royal Netherlands Institute for Sea Research NIOZ in Yerseke, Netherlands, allowing them to isolate marine microbe. The system was also used by students at the 'Sampling, Isolation & Cultivation of Marine Microorganisms' Summer school in Texel, Netherlands. A second OT setup was used at Heriot Watt to successfully isolate single cells of cyanobacteria, several micro algal species, yeast cells and lab cultures of bacteria.

A ULI fabricated device, as shown in figure 6.2 was tested for use with the OT system. A comparison of the ULI device, a PDMS device and a standard sample chamber (made from a borosilicate glass slide with a coverslip on top, separated by a vinyl spacer that

contained the sample) was made. The tweezing within the devices was performed with the help of Isabella McKenna (MPhys Research project). The ULI device consisted of a central straight channel which is 0.5 mm long connected to the inlet and outlet ports using two angled channels.
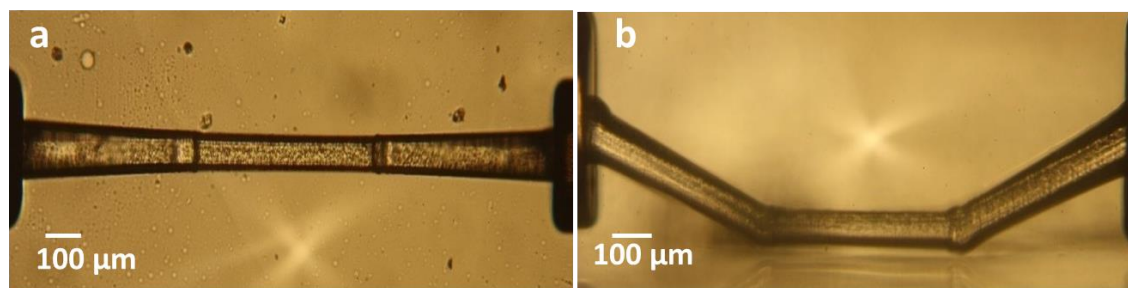


Figure 6.2 ULI fabricated device with sub surface microfluidic channel in fused silica. This device has been used for demonstrating tweezing of yeast cells within the chip. a) Top view, b) Side view image.

Yeast cells suspended in DI water were injected into the channel using a syringe. A CW laser beam operating at 975 nm was focused by the x 60 microscope objective into the device and a laser power of 40 mW was used to trap a single yeast cell in three dimensions. The quality of trapping within the fabricated device was estimated by measuring the critical velocity or maximum velocity at which trapped yeast cell could be translated without falling out of the trap. The critical velocity was measured by increasing the velocity of the sample stage incrementally until a maximum velocity was reached. A maximum velocity of 0.37 mm/s was reached using the ULI fabricated chip whereas a velocity of 0.77 mm/s was achieved for the standard chamber and 0.37 mm/s for the PDMS device. The velocity of tweezing in the PDMS device was affected by the small height of the channel (only 8 micrometers) so the boundary walls, and perhaps the undulating PDMS surface made the tweezing poorer than in the standard chamber, of 80 micron height. Tweezing in the ULI device was poorer due to the rough surface of the device. However, having demonstrated the tweezing within the ULI fabricated chip, there is an excellent scope for future work on developing the on-chip culture system as shown in figure 6.1 to use with the OT system. An on chip culture system along with an

automated portable tweezers system can be taken to biological research labs for performing single cell based studies.

## 6.3  Summary

The development of three dimensional optofluidic devices that are fabricated exploiting the unique features of ULI fabrication technology to use for biophonic applications, in particular for cell separation and ultimately for single cell based studies, form the main body of this thesis. The fabrication and functional validation details of the three different optofluidic device geometries are presented in this thesis. Of the three, first two geometries demonstrate the potential of optical manipulation techniques embedded within the device for manipulating particle and cells in a microchannel. In addition, the importance of incorporating a fluid manipulation element for achieving improved efficiency in handling cell samples and enabling single cells to be addressed by the embedded beam has been demonstrated. The third geometry of the device exploited the key functionalities of the device, to 1. hydrodynamically focus the sample flow and to 2. optically manipulate single particles and cells, to demonstrate cell separation applications. The fabricated devices exhibit excellent scope for further development to realise different functionalities using my device geometries and by introducing new elements to the device, as discussed in section 6.2. A further optimisation of the devices for refractive index and fluorescence based sorting could potentially lead to the realisation of a multifunctional, integrated cell separator device. Such miniaturised, integrated, optofluidic platforms promise to be used in biological research labs as an alternative to the conventional cell separators involving complicated bulk optics.

# References

1.      D. Di Carlo and L. P. Lee, "Dynamic single-cell analysis for quantitative biology," Anal. Chem. **78**, 7918-7925 (2006).

2.      D. K. Button, F. Schut, P. Quang, R. Martin, and B. R. Robertson, "Viability and Isolation of Marine-Bacteria by Dilution Culture - Theory, Procedures, and Initial Results," Appl Environ Microb **59**, 881-891 (1993).

3.      S. Tasoglu, U. A. Gurkan, S. Q. Wang, and U. Demirci, "Manipulating biological agents and cells in micro-scale volumes for applications in medicine," Chem. Soc. Rev. **42**, 5788-5808 (2013).

4.      H. Yun, K. Kim, and W. G. Lee, "Cell manipulation in microfluidics," Biofabrication **5**(2013).

5.      D. J. Stephens and V. J. Allan, "Light microscopy techniques for live cell Imaging," Science **300**, 82-86 (2003).

6.      K. Dholakia, P. Reece, and M. Gu, "Optical micromanipulation," Chem. Soc. Rev. **37**, 42-55 (2008).

7.      A. Ashkin, "Acceleration ans trapping of particles by radiation pressure," Physical Review Letters **24**, 156-& (1970).

8.      A. Ashkin and J. M. Dziedzic, "Optical trapping and manipulation of viruses and bacteria," Science **235**, 1517-1520 (1987).

9.      G. M. Whitesides, "The origins and the future of microfluidics," Nature **442**, 368-373 (2006).

10.     X. L. Wang, S. X. Chen, M. Kong, Z. K. Wang, K. D. Costa, R. A. Li, and D. Sun, "Enhanced cell sorting and manipulation with combined optical tweezer and microfluidic chip technologies," Lab on a Chip **11**, 3656-3662 (2011).

11.     M. M. Wang, E. Tu, D. E. Raymond, J. M. Yang, H. C. Zhang, N. Hagen, B. Dees, E. M. Mercer, A. H. Forster, I. Kariv, P. J. Marchand, and W. F. Butler, "Microfluidic sorting of mammalian cells by optical force switching," Nat. Biotechnol. **23**, 83-87 (2005).

12. L. Pang, H. M. Chen, L. M. Freeman, and Y. Fainman, "Optofluidic devices and applications in photonics, sensing and imaging," Lab Chip **12**, 3543-3551 (2012).

13. J. Godin, C. H. Chen, S. H. Cho, W. Qiao, F. Tsai, and Y. H. Lo, "Microfluidics and photonics for Bio-System-on-a-Chip: A review of advancements in technology towards a microfluidic flow cytometry chip," J. Biophotonics **1**, 355-376 (2008).

14. N. T. Huang, H. L. Zhang, M. T. Chung, J. H. Seo, and K. Kurabayashi, "Recent advancements in optofluidics-based single-cell analysis: optical on-chip cellular manipulation, treatment, and property detection," Lab on a Chip **14**, 1230-1245 (2014).

15. D. Erickson and R. Akhmechet, "Optofluidics: Techniques for fabrication and integration," in Encyclopedia of Microfluidics and Nanofluidics, D. Li, ed. (Springer US, Boston, MA, 2013), pp. 1-9.

16. K. F. Lei, "Chapter 1 Materials and fabrication techniques for nano- and microfluidic devices," in Microfluidics in Detection Science: Lab-on-a-chip Technologies (The Royal Society of Chemistry, 2015), pp. 1-28.

17. Y. N. Xia and G. M. Whitesides, "Soft lithography," Angew. Chem.-Int. Edit. **37**, 550-575 (1998).

18. C. L. Bliss, J. N. McMullin, and C. J. Backhouse, "Integrated wavelength-selective optical waveguides for microfluidic-based laser-induced fluorescence detection," Lab on a Chip **8**, 143-151 (2008).

19. D. Y. Zhang, L. Q. Men, and Q. Y. Chen, "Microfabrication and Applications of Opto-Microfluidic Sensors," Sensors **11**, 5360-5382 (2011).

20. K. Sugioka and Y. Cheng, "Current techniques for fabricating microfluidic and optofluidic devices," in Femtosecond Laser 3d Micromachining for Microfluidic and Optofluidic Applications (Springer, New York, 2014), pp. 7-17.

21. K. M. Davis, K. Miura, N. Sugimoto, and K. Hirao, "Writing waveguides in glass with a femtosecond laser," Opt. Lett. **21**, 1729-1731 (1996).

22. H. B. Zhang, S. M. Eaton, and P. R. Herman, "Single-step writing of Bragg grating waveguides in fused silica with an externally modulated femtosecond fiber laser," Optics Letters **32**, 2559-2561 (2007).

23. R. R. Thomson, H. T. Bookey, N. D. Psaila, A. Fender, S. Campbell, W. N. MacPherson, J. S. Barton, D. T. Reid, and A. K. Kar, "Ultrafast-laser inscription of a three dimensional fan-out device for multicore fiber coupling applications," Optics Express **15**, 11691-11697 (2007).

24. A. Marcinkevicius, S. Juodkazis, M. Watanabe, M. Miwa, S. Matsuo, H. Misawa, and J. Nishii, "Femtosecond laser-assisted three-dimensional microfabrication in silica," Opt. Lett. **26**, 277-279 (2001).

25. R. Osellame, V. Maselli, R. M. Vazquez, R. Ramponi, and G. Cerullo, "Integration of optical waveguides and microfluidic channels both fabricated by femtosecond laser irradiation," Applied Physics Letters **90**(2007).

26. Y. Bellouard, A. A. Said, and P. Bado, "Integrating optics and micro-mechanics in a single substrate: a step toward monolithic integration in fused silica," Optics Express **13**, 6635-6644 (2005).

27. D. J. H. Moosung Kim, Hojeong Jeon, Kuniaki Hiromatsu and Costas P. Grigoropoulos, "Single cell detection using a glass-based optofluidic device fabricated by femtosecond laser pulses," Lab on a Chip **9**, 8 (2009).

28. P. M. F. Bragheri , R. Martinez Vazquez , N. Bellini , P. Paiè , C. Mondello , R. Ramponi , I. Cristianib and R. Osellame, "Optofluidic integrated cell sorter fabricated by femtosecond lasers " Lab on a Chip **12**, 14 (2012).

29. K. V. N Bellini, F Bragheri, L Ferrara, P Minzioni, R ramponi, I Christiani, R Osellame, "Femtosecond laser fabricated monolithic chip for optical trapping and stretching of single cells," Optics Express **18**, 9 (2010).

30. D. Choudhury, D. Jaque, A. Rodenas, W. T. Ramsay, L. Paterson, and A. K. Kar, "Quantum dot enabled thermal imaging of optofluidic devices," Lab on a Chip **12**, 2414-2420 (2012).

31. F. B. Petra Paiè, Rebeca Martinez Vazquez and Roberto Osellame, "Straightforward 3D hydrodynamic focusing in femtosecond laser fabricated microfluidic channels," Lab on a Chip (2014).

32. T. H. Maiman, "Stimulated optical radiation in rubyON IN RUBY," Nature **187**, 493-494 (1960).

33. W. J. Chen, S. M. Eaton, H. B. Zhang, and P. R. Herman, "Broadband directional couplers fabricated in bulk glass with high repetition rate femtosecond laser pulses," Optics Express **16**, 11470-11480 (2008).

34. B. C. Stuart, M. D. Feit, S. Herman, A. M. Rubenchik, B. W. Shore, and M. D. Perry, "Nanosecond-to-femtosecond laser-induced breakdown in dielectrics," Phys. Rev. B **53**, 1749-1761 (1996).

35. C. B. Schaffer, A. Brodeur, and E. Mazur, "Laser-induced breakdown and damage in bulk transparent materials induced by tightly focused femtosecond laser pulses," Meas. Sci. Technol. **12**, 1784-1794 (2001).

36. L. V. Keldysh, "Ionization in the field of a strong electromagnetic wave," Soviet Physics JETP **20**, 5 (1965).

37. M. Ams, G. D. Marshall, P. Dekker, M. Dubov, V. K. Mezentsev, I. Bennion, and M. J. Withford, "Investigation of Ultrafast Laser-Photonic Material Interactions: Challenges for Directly Written Glass Photonics," IEEE J. Sel. Top. Quantum Electron. **14**, 1370-1381 (2008).

38. R. R. Gattass and E. Mazur, "Femtosecond laser micromachining in transparent materials," Nat Photon **2**, 219-225 (2008).

39. R. Taylor, C. Hnatovsky, and E. Simova, "Applications of femtosecond laser induced self-organized planar nanocracks inside fused silica glass," Laser & Photonics Reviews **2**, 26-46 (2008).

40. K. Miura, J. R. Qiu, H. Inouye, T. Mitsuyu, and K. Hirao, "Photowritten optical waveguides in various glasses with ultrashort pulse laser," Applied Physics Letters **71**, 3329-3331 (1997).

41. L. Sudrie, M. Franco, B. Prade, and A. Mysyrewicz, "Writing of permanent birefringent microlayers in bulk fused silica with femtosecond laser pulses," Opt. Commun. **171**, 279-284 (1999).

42. C. Hnatovsky, R. S. Taylor, P. P. Rajeev, E. Simova, V. R. Bhardwaj, D. M. Rayner, and P. B. Corkum, "Pulse duration dependence of femtosecond-laser-fabricated nanogratings in fused silica," Applied Physics Letters **87**(2005).

43. S. Juodkazis, K. Nishimura, S. Tanaka, H. Misawa, E. G. Gamaly, B. Luther-Davies, L. Hallo, P. Nicolai, and V. T. Tikhonchuk, "Laser-induced microexplosion confined in the bulk of a sapphire crystal: Evidence of multimegabar pressures," Physical Review Letters **96**(2006).

44. K. Itoh, W. Watanabe, S. Nolte, and C. B. Schaffer, "Ultrafast processes for bulk modification of transparent materials," MRS Bull. **31**, 620-625 (2006).

45. J. W. Chan, T. Huser, S. Risbud, and D. M. Krol, "Structural changes in fused silica after exposure to focused femtosecond laser pulses," Opt. Lett. **26**, 1726-1728 (2001).

46. R. Bruckner, "Properties and structure of vitreous silica. I," Journal of Non-Crystalline Solids **5**, 52 (1970).

47. K. Hirao and K. Miura, "Writing waveguides and gratings in silica and related materials by a femtosecond laser," Journal of Non-Crystalline Solids **239**, 91-95 (1998).

48. A. M. Streltsov and N. F. Borrelli, "Study of femtosecond-laser-written waveguides in glasses," Journal of the Optical Society of America B-Optical Physics **19**, 2496-2504 (2002).

49. V. R. Bhardwaj, E. Simova, P. B. Corkum, D. M. Rayner, C. Hnatovsky, R. S. Taylor, B. Schreder, M. Kluge, and J. Zimmer, "Femtosecond laser-induced refractive index modification in multicomponent glasses," J. Appl. Phys. **97**(2005).

50. P. G. Kazansky, H. Inouye, T. Mitsuyu, K. Miura, J. Qiu, K. Hirao, and F. Starrost, "Anomalous anisotropic light scattering in Ge-Doped silica glass," Physical Review Letters **82**, 2199-2202 (1999).

51. Y. Shimotsuma, P. G. Kazansky, J. R. Qiu, and K. Hirao, "Self-organized nanogratings in glass irradiated by ultrashort light pulses," Physical Review Letters **91**(2003).

52. V. R. Bhardwaj, E. Simova, P. P. Rajeev, C. Hnatovsky, R. S. Taylor, D. M. Rayner, and P. B. Corkum, "Optically produced arrays of planar nanostructures inside fused silica," Physical Review Letters **96**(2006).

53. P. P. Rajeev, M. Gertsvolf, V. R. Bhardwaj, E. Simova, C. Hnatovsky, R. S. Taylor, D. M. Rayner, and P. B. Corkum, "Memory and nanostructure formation in the intense field ionization of fused silica," in Ultrafast Phenomena XV, P. Corkum, D. Jonas, R. J. D. Miller, and A. M. Weiner, eds. (Springer-Verlag Berlin, Berlin, 2007), pp. 680-682.

54. C. Hnatovsky, R. S. Taylor, E. Simova, P. P. Rajeev, D. M. Rayner, V. R. Bhardwaj, and P. B. Corkum, "Fabrication of microchannels in glass using focused femtosecond laser radiation and selective chemical etching," Applied Physics a-Materials Science & Processing **84**, 47-61 (2006).

55. E. N. Glezer, M. Milosavljevic, L. Huang, R. J. Finlay, T. H. Her, J. P. Callan, and E. Mazur, "Three-dimensional optical storage inside transparent materials," Optics Letters **21**, 2023-2025 (1996).

56. S. Juodkazis, S. Matsuo, H. Misawa, V. Mizeikis, A. Marcinkevicius, H. B. Sun, Y. Tokuda, M. Takahashi, T. Yoko, and J. Nishii, "Application of femtosecond laser pulses for microfabrication of transparent media," Appl. Surf. Sci. **197**, 705-709 (2002).

57. S. M. Eaton, H. B. Zhang, and P. R. Herman, "Heat accumulation effects in femtosecond laser-written waveguides with variable repetition rate," Optics Express **13**, 4708-4716 (2005).

58. R. R. Thomson, N. D. Psaila, H. T. Bookey, D. T. Reid, and A. K. Kar, "Controlling the Cross-section of Ultrafast Laser Inscribed Optical Waveguides," in Femtosecond Laser Micromaching: Photonic and Microfluidic Devices in Transparent Materials, R. Osellame, G. Cerullo, and R. Ramponi, eds. (Springer-Verlag Berlin, Berlin, 2012), pp. 93-125.

59.     J. R. Macdonald, R. R. Thomson, S. J. Beecher, N. D. Psaila, H. T. Bookey, and A. K. Kar, "Ultrafast laser inscription of near-infrared waveguides in polycrystalline ZnSe," Optics Letters **35**, 4036-4038 (2010).

60.     S. Rajesh and Y. Bellouard, "Towards fast femtosecond laser micromachining of fused silica: The effect of deposited energy," Optics Express **18**, 21490-21497 (2010).

61.     S. M. Eaton, H. Zhang, M. L. Ng, J. Z. Li, W. J. Chen, S. Ho, and P. R. Herman, "Transition from thermal diffusion to heat accumulation in high repetition rate femtosecond laser writing of buried optical waveguides," Optics Express **16**, 9443-9458 (2008).

62.     J. A. Dharmadhikari, R. Bernard, A. K. Bhatnagar, D. Mathur, and A. K. Dharmadhikari, "Axicon-based writing of waveguides in BK7 glass," Optics Letters **38**, 172-174 (2013).

63.     M. Ams, G. D. Marshall, D. J. Spence, and M. J. Withford, "Slit beam shaping method for femtosecond laser direct-write fabrication of symmetric waveguides in bulk glasses," Optics Express **13**, 5676-5681 (2005).

64.     R. Osellame, G. Cerullo, S. Taccheo, M. Marangoni, D. Polli, P. Laporta, and R. Ramponi, "Femtosecond lasrwriting of symmetrical optical waveguides by astigmatically shaped beams," in Integrated Optics and Photonic Integrated Circuits, G. C. Righini and S. Honkanen, eds. (Spie-Int Soc Optical Engineering, Bellingham, 2004), pp. 360-368.

65.     R. R. Thomson, A. S. Bockelt, E. Ramsay, S. Beecher, A. H. Greenaway, A. K. Kar, and D. T. Reid, "Shaping ultrafast laser inscribed optical waveguides using a deformable mirror," Optics Express **16**, 12786-12793 (2008).

66.     Y. Nasu, M. Kohtoku, and Y. Hibino, "Low-loss waveguides written with a femtosecond laser for flexible interconnection in a planar light-wave circuit," Optics Letters **30**, 723-725 (2005).

67.     C. B. Schaffer, A. Brodeur, J. F. Garcia, and E. Mazur, "Micromachining bulk glass by use of femtosecond laser pulses with nanojoule energy," Optics Letters **26**, 93-95 (2001).

68. R. R. Thomson, S. Campbell, I. J. Blewett, A. K. Kar, and D. T. Reid, "Optical waveguide fabrication in z-cut lithium niobate (LiNbO3) using femtosecond pulses in the low repetition rate regime," Appl. Phys. Lett. **88** (2006).

69. D. Jaque, N. D. Psaila, R. R. Thomson, F. Chen, L. M. Maestro, A. Rodenas, D. T. Reid, and A. K. Kar, "Ultrafast laser inscription of bistable and reversible waveguides in strontium barium niobate crystals," Applied Physics Letters **96** (2010).

70. S. Sowa, W. Watanabe, T. Tamaki, J. Nishii, and K. Itoh, "Symmetric waveguides in poly(methyl methacrylate) fabricated by femtosecond laser pulses," Optics Express **14**, 291-297 (2006).

71. Y. Cheng, K. Sugioka, K. Midorikawa, M. Masuda, K. Toyoda, M. Kawachi, and K. Shihoyama, "Control of the cross-sectional shape of a hollow microchannel embedded in photostructurable glass by use of a femtosecond laser," Optics Letters **28**, 55-57 (2003).

72. A. F. A Ruiz de la Cruz, W Gawelda, D Puerto, M Galv an Sosa, J Siegel, and J Solis, "Independent control of beam astigmatism and ellipticity using a SLM for fs-laser waveguide writing," Optics Express **17**, 7 (2009).

73. G. Spierings, "Wet chemical etching of silicate-glasses in hydrofluoric-acid based solutions," J. Mater. Sci. **28**, 6261-6273 (1993).

74. Y. Bellouard, A. Said, M. Dugan, and P. Bado, "Fabrication of high-aspect ratio, micro-fluidic channels and tunnels using femtosecond laser pulses and chemical etching," Optics Express **12**, 2120-2129 (2004).

75. C. Hnatovsky, R. S. Taylor, E. Simova, V. R. Bhardwaj, D. M. Rayner, and P. B. Corkum, "Polarization-selective etching in femtosecond laser-assisted microfluidic channel fabrication in fused silica," Optics Letters **30**, 1867-1869 (2005).

76. S. Matsuo, H. Sumi, S. Kiyama, T. Tomita, and S. Hashimoto, "Femtosecond laser-assisted etching of Pyrex glass with aqueous solution of KOH," Appl. Surf. Sci. **255**, 9758-9760 (2009).

77. S. Kiyama, S. Matsuo, S. Hashimoto, and Y. Morihira, "Examination of etching agent and etching mechanism on femotosecond laser microfabrication of channels inside vitreous silica substrates," J. Phys. Chem. C **113**, 11560-11566 (2009).

78. A. Crespi, Y. Gu, B. Ngamsom, H. Hoekstra, C. Dongre, M. Pollnau, R. Ramponi, H. H. van den Vlekkert, P. Watts, G. Cerullo, and R. Osellame, "Three-dimensional Mach-Zehnder interferometer in a microfluidic chip for spatially-resolved label-free detection," Lab on a Chip **10**, 1167-1173 (2010).

79. V. Maselli, J. R. Grenier, S. Ho, and P. R. Herman, "Femtosecond laser written optofluidic sensor: Bragg grating waveguide evanescent probing of microfluidic channel," Optics Express **17**, 11719-11729 (2009).

80. Z. Wang, K. Sugioka, and K. Midorikawa, "Fabrication of integrated microchip for optical sensing by femtosecond laser direct writing of Foturan glass," Applied Physics a-Materials Science & Processing **93**, 225-229 (2008).

81. W. Watanabe, S. Sowa, T. Tamaki, K. Itoh, and J. Nishii, "Three-dimensional waveguides fabricated in poly(methyl methacrylate) by a femtosecond laser," Jpn. J. Appl. Phys. Part 2 - Lett. Express Lett. **45**, L765-L767 (2006).

82. D. Choudhury, A. Rodenas, L. Paterson, F. Diaz, D. Jaque, and A. K. Kar, "Three-dimensional microstructuring of yttrium aluminum garnet crystals for laser active optofluidic applications," Applied Physics Letters **103**(2013).

83. D. J. Little, M. Ams, P. Dekker, G. D. Marshall, J. M. Dawes, and M. J. Withford, "Femtosecond laser modification of fused silica: the effect of writing polarization on Si-O ring structure," Optics express **16**, 20029-20037 (2008).

84. D. Choudhury, "Femtosecond laser microfabricated devices for biophotonic applications," Heriot Watt University (2013).

85. B. del Rosal, C. Sun, Y. Yan, M. D. Mackenzie, C. Lu, A. A. Bettiol, K. Kar, and D. Jaque, "Flow effects in the laser-induced thermal loading of optical traps and optofluidic devices," Optics Express **22**, 23938-23954 (2014).

86. C. Q. Yi, C. W. Li, S. L. Ji, and M. S. Yang, "Microfluidics technology for manipulation and analysis of biological cells," Analytica Chimica Acta **560**, 1-23 (2006).

87. D. Choudhury, W. T. Ramsay, R. Kiss, N. A. Willoughby, L. Paterson, and A. K. Kar, "A 3D mammalian cell separator biochip," Lab on a Chip **12**, 948-953 (2012).

88. L. A. Herzenberg, R. G. Sweet, and L. A. Herzenberg, "Fluorescence-actvated cell sorting," Scientific American **234**, 108-117 (1976).

89. L.-M. Fu, R.-J. Yang, C.-H. Lin, Y.-J. Pan, and G.-B. Lee, "Electrokinetically driven micro flow cytometers with integrated fiber optics for on-line cell/particle detection," Analytica Chimica Acta **507**, 163-169 (2004).

90. R. W. Applegate Jr, J. Squier, T. Vestad, J. Oakey, D. W. M. Marr, P. Bado, M. A. Dugan, and A. A. Said, "Microfluidic sorting system based on optical waveguide integration and diode laser bar trapping," Lab on a Chip **6**, 422-426 (2006).

91. T. P. Forbes and S. P. Forry, "Microfluidic magnetophoretic separations of immunomagnetically labeled rare mammalian cells," Lab on a chip **12**, 1471-1479 (2012).

92. L. Ren, Y. Chen, P. Li, Z. Mao, P.-H. Huang, J. Rufo, F. Guo, L. Wang, J. P. McCoy, S. J. Levine, and T. J. Huang, "A high-throughput acoustic cell sorter," Lab on a Chip **15**, 3870-3879 (2015).

93. J. Voldman, "Electrical forces for microscale cell manipulation," Annu Rev Biomed Eng **8**, 425-454 (2006).

94. T. Kolb, S. Albert, M. Haug, and G. Whyte, "Optofluidic rotation of living cells for single-cell tomography," Journal of biophotonics **8**, 239-246 (2015).

95. S. J. Hart and A. V. Terray, "Refractive-index-driven separation of colloidal polymer particles using optical chromatography," Applied Physics Letters **83**, 5316-5318 (2003).

96.  A. Ashkin, J. M. Dziedzic, J. E. Bjorkholm, and S. Chu, "Observation of a single-beam gradient force optical trap for dielectric particles," Optics Letters **11**, 288-290 (1986).

97.  S. B. Kim, J. H. Kim, and S. S. Kim, "Theoretical development of in situ optical particle separator: cross-type optical chromatography," Appl. Optics **45**, 6919-6924 (2006).

98.  K. H. Lee, S. B. Kim, K. S. Lee, and H. J. Sung, "Enhancement by optical force of separation in pinched flow fractionation," Lab on a chip **11**, 354-357 (2011).

99.  A. Ashkin, "Forces of a single-beam gradient laser trap on a dielectric sphere in the ray optics regime," Biophysical journal **61**, 569-582 (1992).

100. S. B. Kim, S. Y. Yoon, H. J. Sung, and S. S. Kim, "Cross-type optical particle separation in a microchannel," Analytical Chemistry **80**, 2628-2630 (2008).

101. D. Di Carlo, D. Irimia, R. G. Tompkins, and M. Toner, "Continuous inertial focusing, ordering, and separation of particles in microchannels," Proceedings of the National Academy of Sciences of the United States of America **104**, 18892-18897 (2007).

102. D. Di Carlo, "Inertial microfluidics," Lab on a Chip **9**, 3038-3046 (2009).

103. D. Huh, W. Gu, Y. Kamotani, J. B. Grotberg, and S. Takayama, "Microfluidics for flow cytometric analysis of cells and particles," Physiol. Meas. **26**, R73-R98 (2005).

104. M. Frankowski, J. Theisen, A. Kummrow, P. Simon, H. Ragusch, N. Bock, M. Schmidt, and J. Neukammer, "Microflow Cytometers with Integrated Hydrodynamic Focusing," Sensors **13**, 4674-4693 (2013).

105. L. Martin-Banderas, M. Flores-Mosquera, P. Riesco-Chueca, A. Rodriguez-Gil, A. Cebolla, S. Chavez, and A. M. Ganan-Calvo, "Flow focusing: A versatile technology to produce size-controlled and specific-morphology microparticles," Small **1**, 688-692 (2005).

106. H. Gu, M. H. Duits, and F. Mugele, "Droplets formation and merging in two-phase flow microfluidics," International journal of molecular sciences **12**, 2572-2597 (2011).

107. C. Simonnet and A. Groisman, "Two-dimensional hydrodynamic focusing in a simple microfluidic device," Applied Physics Letters **87**(2005).

108. I. R. P.-N. G. Goranovic, U.D. Larsen, A. Wolff, J.P.Kutter, P.Telleman, "Three-dimensional single step flow sheathing in microcell sorter in Modelling and Simulation of Microsystems 2001," Computational Publications (2001).

109. N. Sundararajan, M. S. Pio, L. P. Lee, and A. A. Berlin, "Three-dimensional hydrodynamic focusing in polydimethylsiloxane (PDMS) microchannels," J. Microelectromech. Syst. **13**, 559-567 (2004).

110. Y. J. Chiu, S. H. Cho, Z. Mei, V. Lien, T. F. Wu, and Y. H. Lo, "Universally applicable three-dimensional hydrodynamic microfluidic flow focusing," Lab on a Chip **13**, 1803-1809 (2013).

111. R. Scott, P. Sethu, and C. K. Harnett, "Three-dimensional hydrodynamic focusing in a microfluidic Coulter counter," Rev. Sci. Instrum. **79**(2008).

112. C. C. Chang, Z. X. Huang, and R. J. Yang, "Three-dimensional hydrodynamic focusing in two-layer polydimethylsiloxane (PDMS) microchannels," Journal of Micromechanics and Microengineering **17**, 1479-1486 (2007).

113. C. I. Hung, B. J. Ke, G. R. Huang, B. H. Hwei, H. F. Lai, and G. B. Lee, "Hydrodynamic focusing for a micromachined flow cytometer," J. Fluids Eng.-Trans. ASME **123**, 672-679 (2001).

114. (http://www.physics.emory.edu/faculty/weeks//idl/).

115. K. C. Neuman, E. H. Chadd, G. F. Liou, K. Bergman, and S. M. Block, "Characterization of photodamage to Escherichia coli in optical traps," Biophysical Journal **77**, 2856-2863 (1999).

116. F. Wetzel, S. Ronicke, K. Muller, M. Gyger, D. Rose, M. Zink, and J. Kas, "Single cell viability and impact of heating by laser

absorption," European biophysics journal : EBJ **40**, 1109-1114 (2011).

117. H. M. Shapiro, "Practical flow cytometry," Wiley-Liss **4th edition**(2003).

118. M. Roederer, S. De Rosa, R. Gerstein, M. Anderson, M. Bigos, R. Stovel, T. Nozaki, D. Parks, L. Herzenberg, and L. Herzenberg, "8 color, 10-parameter flow cytometry to elucidate complex leukocyte heterogeneity," Cytometry **29**, 328-339 (1997).

119. L. Gwo-Bin, I. H. Chen, K. Bin-Jo, H. Guan-Ruey, and H. Bao-Herng, "Micromachined pre-focused 1× N flow switches for continuous sample injection," Journal of Micromechanics and Microengineering **11**, 567 (2001).

120. B. Regenberg, U. Kruhne, M. Beyer, L. H. Pedersen, M. Simon, O. R. T. Thomas, J. Nielsen, and T. Ahl, "Use of laminar flow patterning for miniaturised biochemical assays," Lab on a Chip **4**, 654-657 (2004).

121. L. Gwo-Bin, C. Chih-Chang, H. Sung-Bin, and Y. Ruey-Jen, "The hydrodynamic focusing effect inside rectangular microchannels," Journal of Micromechanics and Microengineering **16**, 1024 (2006).

122. P. Y. Liu, L. K. Chin, W. Ser, H. F. Chen, C. M. Hsieh, C. H. Lee, K. B. Sung, T. C. Ayi, P. H. Yap, B. Liedberg, K. Wang, T. Bourouina, and Y. Leprince-Wang, "Cell refractive index for cell biology and disease diagnosis: past, present and future," Lab on a Chip **16**, 634-644 (2016).